Investigation of Lateral Phenomenon in Flight Control System Design

ENRIQUE DAVAZE

A Thesis

in

The Department

of

Mechanical and Industrial Engineering

Presented in Partial Fulfillment of the Requirements

For the Degree of Master of Applied Science at

Concordia University

Montreal, Quebec, Canada

August 2004

Your file Votre référence
ISBN: 0-612-94725-4
Our file Notre référence
ISBN: 0-612-94725-4

ABSTRACT

Investigation of Lateral Phenomenon in Flight Control System Design

Enrique Davaze

Modern flight control systems are analyzed and certified to meet the requirements of the Federal Aviation Administration (FAA) and the Joint Aviation Association (JAA). However, discrepancies in the performance of the hydro-mechanical flight control systems may appear during the life of the aircraft, and analyses must be performed to track and solve these anomalies.

A number of airplanes of different types and manufacturers have exhibited small and uncommanded yaw shudders or "kicks". Concordia University and Bombardier Aerospace collaborated to understand the yaw activity and to track the root causes of lateral phenomena through numerical simulation.

The objective of this thesis is to study more closely the hydro-mechanical power control unit, which seems to be in most cases the suspected part of the rudder control system for yaw activity. The performance of the power control unit was evaluated to track any discrepancies in this system. Three hydraulically independent servo-actuators actuate the rudder control surface. Backlash, deadband or friction is present in the three servoactuators assembly, and each actuator may not take the same load when the aircraft is in flight. Therefore, a load sharing analysis between these actuators is performed in this thesis. The flow forces acting on the servovalve are also presented; and the pressure relief valves that regulate the pressure in the power control unit manifold are also modeled and simulated in detail. Conclusions and recommendations will be made based on the simulation findings and results.

ACKNOWLEDGEMENTS

The author wishes to express his gratitude to his supervisors Dr. J. Svoboda and Dr. H. Hong for their guidance, support and patience in completing this project and for their precious help in correcting this thesis.

The invaluable assistance of the simulation group at Bombardier Aerospace (BA) including Antonio D'Amore and Claude Tessier for their advises and help is greatly appreciated. Last but not the least, the author wishes to thank Carlos Trindade, BA Stategic Technology group, and Jacques Thibaudeau, BA Flight Operations, for their advises in coordinating the Concordia University project.

I wish to thank my friends Nicolas Ulysse, Nathalie Gratton, and my brother Mickaël for their support when needed. This would be incomplete without a word for my parents and my family in France and in Canada: without them, I would not have gone this far in my studies. I also wish to thank my wife Sandrine; for her love and great understanding.

TABLE OF CONTENTS

LIST OF FIGURES

LIST OF TABLES

NOMENCLATURE

Symbol	Description	Unit(s)
a	Lever arm	[in]
A	Effective piston area of both chambers	[in^2]
A_1	Effective actuator area of chamber 1	[in^2]
A_2	Effective actuator area of chamber 2	[in^2]
A_C	Cross section area of the control valve chamber	[in^2]
A_{check}	Check valve orifice area	[in^2]
A_{CV}	Area per unit port opening X_v	[in^2]
A_P	Pressure relief valve inlet area	[in^2]
A_{PRV}	Pressure relief valve area	[in^2]
b	Lever arm	[in]
B	Structural damping coefficient	[lb.in.sec/rad]
B_c	Backup structure strutural damping	[lb.sec/in]
c	Lever arm	[in]
C_d	Orifice discharge coefficient	[--]
C_D	Drag coefficient	[--]
C_{hR}	Hinge moment coefficient	[--]
C_{L0}	Lift coefficient for zero angle of attack	[--]
C_L	Lift coefficient	[--]
C_R	Lift coefficient	[--]
d	Lever arm	[in]

d_{act}	diameter of the PCU actuator rod	[in]
d_V	Distance between the control valve entry and exit ports	[in]
d_{V1}	Distance between the control valve entry and exit ports in chamber 1	[in]
d_{V2}	Distance between the control valve entry and exit ports in chamber 2	[in]
D	Drag Force	[lb]
D_{act}	diameter of the PCU actuator	[in]
D_p	Pressure relief valve inlet diameter	[in]
e	Lever arm	[in]
f	Lever arm	[in]
$\vec{F}$	Force per unit area (aerodynamic and/or thrust)	[lb/ft^2]
F_0	Bias spring preload	[lb]
F_{Ax}	Aerodynamic force component along X-Axis of the Body Axis System	[lb]
F_{Ay}	Aerodynamic force component along Y-Axis of the Body Axis System	[lb]
F_{Az}	Aerodynamic force component along Z-Axis of the Body Axis System	[lb]
F_C	Coulomb friction force	[lb]
f_{cv}	Control valve damping coefficient	[lb/in/sec]
F_{ext}	Force created by surrounding	[lb]
$F_{friction}$	Friction force	[lb]

F_m	Momentum force in pressure relief valve	[lb]
F_{mp}	Axial momentum force in pressure relief valve	[lb]
F_{press}	Pressure force acting on the poppet	[lb]
f_{PRV}	Pressure relief valve poppet damping coefficient	[slug/in/sec]
$F_{spring\ preload}$	Force of the spring against the pressure relief valve poppet	[lb]
F_{SR}	Fluid momentum force	[lb]
F_{TR}	Transient reaction force	[lb]
F_{TR1}	Transient reaction force in control valve chamber 1	[lb]
F_{TR2}	Transient reaction force in control valve chamber 2	[lb]
F_{Tx}	Thrust force component along X-Axis of the Body Axis System	[lb]
F_{Ty}	Thrust force component along Y-Axis of the Body Axis System	[lb]
F_{Tz}	Thrust force component along Z-Axis of the Body Axis System	[lb]
g	gravitational acceleration	[in/sec^2]
I_R	Moment of inertia of the rudder	[lb. in^2]
I_{xx}	Airplane Moment of Inertia about X-Axis of the Body Axis System	[slug.ft^2]
I_{xz}	Airplane Product of Inertia about X-Axis of the Body Axis System	[slug.ft^2]
I_{yy}	Airplane Moment of Inertia about Y-Axis of the Body	[slug.ft^2]

	Axis System	
I_{zz}	Airplane Moment of Inertia about Z-Axis of the Body Axis System	[slug.ft^2]
K_c	Equivalent backup structure stiffness along the PCU line of action	[lb/in]
K_f	PCU feedback gain	[in/in]
K_H	Linear attachment stiffness	[lb/in]
K_{in}	Input gain	[in/in]
K_{in}	Input gain	[in/in]
K_{oil}	Oil stiffness in actuator chamber	[lb/in]
k_{spring}	Control valve bias spring stiffness	[lb/in]
K_{sv}	Control valve static gain	[in/in]
K_T	Torsional stiffness of the control surface	[lb.in/rad]
K_v	Valve flow coefficient	[--]
L	Lift Force	[lb]
L_1	Length between the PCU attachment point and the rudder panel rotation point	[in]
L_2	Length of the PCU actuator at neutral	[in]
L_3	Length of the PCU actuator at a given position	[in]
L_A	Aerodynamic moment component about X-Axis of the Body Axis System	[lb.ft]
L_T	Thrust moment component about X-Axis of the Body Axis System	[lb.ft]

m	Pressure relief valve poppet mass	[slug]
M_A	Aerodynamic moment component about Y-Axis of the Body Axis System	[lb.ft]
M_{aero}	Hinge Moment (aerodynamic loads)	[lb.in]
$m_{airplane}$	Aircraft Mass	[slug]
m_c	Mass of PCU casing	[slug]
M_p	PCU actuator mass	[slug]
M_T	Thrust moment component about Y-Axis of the Body Axis System	[lb.ft]
m_v	Spool valve mass	[slug]
N_A	Aerodynamic moment component about Z-Axis of the Body Axis System	[lb.ft]
N_T	Thrust moment component about Z-Axis of the Body Axis System	[lb.ft]
p	Angular Velocity along X-Axis of the Body Axis System	[rad/sec]
$\dot{p}$	Angular acceleration along X-Axis of the Body Axis System	[rad/sec^2]
P_1	Actuator chamber 1 pressure	[psi]
P_2	Actuator chamber 2 pressure	[psi]
P_{cv}	Pressure at the check valve exit	[psi]
P_L	Load pressure	[psi]
P_s	Supply pressure	[psi]
P_{ret}	Return pressure	[psi]

q	Angular Velocity along Y-Axis of the Body Axis System	[rad/sec]
$\dot{q}$	Angular acceleration along Y-Axis of the Body Axis System	[rad/sec^2]
Q_{01}	Flow rate through the control valve	[in^3/sec]
Q_{02}	Flow rate through the control valve	[in^3/sec]
Q_1	Flow rate through chamber 1	[in^3/sec]
Q_2	Flow rate through chamber 2	[in^3/sec]
Q_c	Center flow rate	[in^3/sec]
Q_{cv}	Flow rate across the check valve	[in^3/sec]
Q_L	Load flow rate	[in^3/sec]
Q_{oil}	Volumetric flow rate	[in^3/sec]
Q_{PRV1}	Pressure relief valve flow rate connected to chamber 1	[in^3/sec]
Q_{PRV2}	Pressure relief valve flow rate connected to chamber 2	[in^3/sec]
r	Angular Velocity along Z-Axis of the Body Axis System	[rad/sec]
$\dot{r}$	Angular acceleration along Z-Axis of the Body Axis System	[rad/sec^2]
$\vec{r}$	Vector that connects the center of gravity with a mass element	[ft]
r_c	radial clearance between the spool and the sleeve	[in]
R_p	Pressure relief valve inlet radius	[in]
R_{pcu}	Distance between the line of action of the PCU and the rudder hinge line when the PCU actuator is at neutral	[in]
$R(X_a)$	PCU moment arm	[in]

S	Wing Area	[in^2]
u	Linear Velocity along X-Axis of the Body Axis System	[ft/sec]
$\dot{u}$	Linear acceleration along X-Axis of the Body Axis System	[ft/sec^2]
v	Linear Velocity along Y-Axis of the Body Axis System	[ft/sec]
$\dot{v}$	Linear acceleration along Y-Axis of the Body Axis System	[ft/sec^2]
V	Aircraft airspeed	[ft/sec]
$\vec{V}$	Aircraft velocity (true airspeed)	[ft/sec]
V_{01}	Volume of chamber 1 when actuator is at neutral	[in^3]
V_{02}	Volume of chamber 2 when actuator is at neutral	[in^3]
V_1	Volume of chamber 1	[in^3]
V_2	Volume of chamber 2	[in^3]
V_{oil}	Velocity of oil	[in/sec]
V_{PRV}	Velocity of the fluid at the pressure relief valve exit	[in/sec]
w	Linear Velocity along Z-Axis of the Body Axis System	[ft/sec]
$\dot{w}$	Linear acceleration along Z-Axis of the Body Axis System	[in/sec^2]
w_c	area gradient of control valve	[in^2/in]
w_p	Width of valve ports	[in]
X	Aircraft X coordinate in the Earth axis system	[ft]
X_a	Actuator position	[in]
$\dot{X}_a$	Actuator rate	[in/sec]

$\ddot{X}_a$	Actuator acceleration	[in/sec^2]
X_B	Aircraft X coordinate in the body axis system	[ft]
X_c	PCU casing position	[in]
$\dot{X}_c$	PCU casing rate	[in/sec]
$\ddot{X}_c$	PCU casing acceleration	[in/sec^2]
X_i	Input differential lever position	[in]
X_S	Aircraft X coordinate in the stability axis system	[ft]
X_v	Spool valve position	[in]
X_w	Aircraft X coordinate in the Wind axis system	[ft]
y	Pressure relief valve poppet position	[in]
Y	Aircraft Y coordinate in the Earth axis system	[ft]
Y_B	Aircraft Y coordinate in the body axis system	[ft]
Y_S	Aircraft Y coordinate in the stability axis system	[ft]
Y_w	Aircraft Y coordinate in the Wind axis system	[ft]
Z	Aircraft Z coordinate in the Earth axis system	[ft]
Z_B	Aircraft Z coordinate in the body axis system	[ft]
Z_S	Aircraft Z coordinate in the stability axis system	[ft]
Z_w	Aircraft Z coordinate in the Wind axis system	[ft]
α	Aircraft angle of attack	[rad]
$\alpha_{critical}$	Critical angle of attack	[rad]
β	Sideslip angle	[rad]
β_f	Effective bulk modulus of fluid	[psi]

β_{f1}	Effective bulk modulus of fluid in chamber 1	[psi]
β_{f2}	Effective bulk modulus of fluid in chamber 2	[psi]
Δp	Differential pressure	[psi]
Δp_1	Pressure drop in control valve chamber 1	[psi]
Δp_2	Pressure drop in control valve chamber 2	[psi]
ε	PCU lever arm angle	[rad]
γ	Jet flow angle	[rad]
μ	Oil absolute viscosity	[lb-sec/in^2]
Φ	PCU lever arm angle	[rad]
ψ	Airplane heading angle	[rad]
σ	Viscous friction coefficient	[lb/in/sec]
δ_{xa}	Angular position of actuator (commanded position to the rudder control surface)	[rad]
$\delta_{xa}(up)$	Angular position of the upper actuator	[rad]
$\delta_{xa}(mid)$	Angular position of the middle actuator	[rad]
$\delta_{xa}(low)$	Angular position of the lower actuator	[rad]
δ_R	Angular position of the rudder control surface	[rad]
$\dot{\delta}_R$	Angular velocity of the rudder control surface	[rad/sec]
$\ddot{\delta}_R$	Angular velocity of the rudder control surface	[rad/sec^2]
θ	Airplane pitch attitude angle	[rad]
θ_{crank}	Angle of the rudder control surface with the line created by the two attachment points of the PCU and rudder surface with the	[rad]

	structure when the rudder is at neutral	
θ_{PRV}	Pressure relief valve poppet angle	[rad]
τ	Time lag	[sec]
ρ	Mass density of fluid	[lb/in^3]
ρ_{air}	Air density	[slug/ft^3]

CHAPTER 1

INTRODUCTION

This section presents the background of the thesis project, the problem definition and the approach that was used to troubleshoot and find the possible causes to cure the anomaly in the lateral control system.

1.1 Previous Work

During their development or in sustaining, airplanes from different manufacturers have experienced lateral phenomena. The delivery of an aircraft can be significantly delayed due to an unacceptable level of yaw activity. Analyses to such a specific phenomenon are usually not published. However, in the literature, many studies exist on aircraft limit-cycle oscillations such as the wing-rock and dutch roll (refer to section 1.3). Troubleshooting of the phenomenon was experimentally performed on the aircraft (refer to section 1.2). The investigation is however very costly to the aircraft manufacturer and customer, since the customer has to leave its aircraft few days for testing. Most of the time, aircraft manufacturers have been able to either eliminate this phenomenon or the oscillations were unnoticeably small to the customer. Consequently, this issue usually remains low level priority and does not generate a deep investigation. Although this yaw activity is not a safety issue, it is annoying to the people onboard the aircraft.

Putting the problems and costs associated with current resolution methods aside for the moment, the most significant issue that yaw oscillations create is the discomfort of

passengers and crew. Passenger expectations, especially with regard to the business aircraft, are high. This reality is further complicated by the growing list of activities passengers wish to do during flight. This list includes walking, reading, writing, typing, eating, drinking and sleeping [1]. The frequency of the oscillations in question has been stated to be within the region of 0.9 to 1.1 Hertz [2]. This rather low frequency is difficult to measure. It falls within the kinetosis (i.e. motion sickness) region [1]. Even though yaw oscillations do not occur in all aircraft, the manufacturer must ensure that all of its products is comfortable and pleasant to the flying public. The authorities do not regulate yaw accelerations. However, the International Standards Organization (ISO) have gathered vast amounts of data and information on human comfort and perception to vibrations that can be used as a guideline to ensure adequate ride qualities are built in the aircraft.

The standard that is the root of a chain of standards relating to human tolerance to vibration is ISO 2631-1 Mechanical vibration and shock – Evaluation of human exposure to whole-body vibration – Part 1: General requirements [3]. This standard defines the methods for the measurement of periodic, random and transient whole body vibration. The standard also describes the principal factors that are combined to determine the acceptability of an exposure and suggests possible effects, recognizing the large variations in responses between individuals [4]. From this measurement specification document arises a string of others, which are directly related to lateral accelerations of seated humans. This includes:

- ISO 2631-2: Vibrations measurement in buildings (0.063 to 1 Hz) [5]

- ISO 2631-4: Guidelines for the evaluation of the effects of vibration and rotational motion on passenger and crew comfort of fixed guideway transport systems [5].
- ISO 6897-1984: Guidelines for the evaluation of the response of occupants of fixed structures, especially buildings and off-shore structures to low frequency horizontal motion (0.063 to 1 Hz). [5]

It is the last of the three documents that is of most interest here. It deals with lateral accelerations at a low frequency. It assumes that the perception of motion comes from proprioceptive cues or vestibular organs rather than through visual cues [6]. These perfectly describe the motion resulting from yaw oscillations and their perception mechanism. The available data indicates that the lower threshold of perception of horizontal motion by humans is represented by the lower curve in Figure 1.1. These magnitudes are appropriate for areas expected to be stationary. The average threshold of perception represents the mean threshold of perception of horizontal motion for a normal adult population. The magnitudes suggested by the upper curve in Figure 1.1 are appropriate for special buildings where precision work is carried out. These magnitudes are four times those given the activities covered by the lower curve.

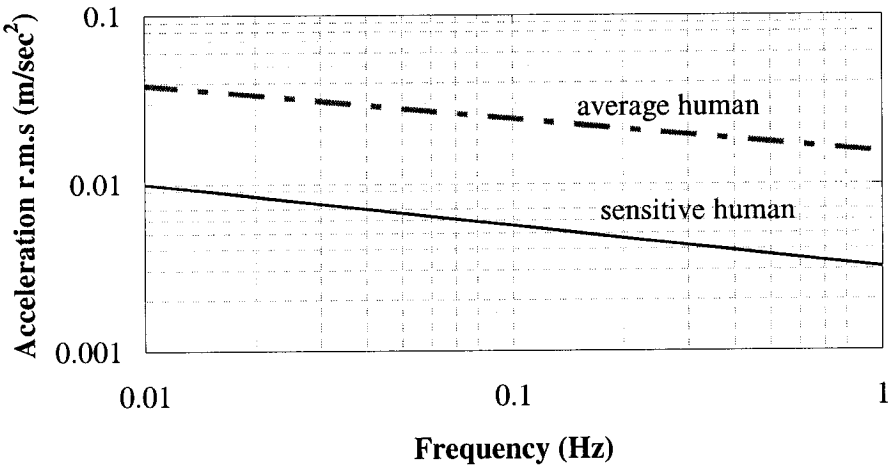

Figure 1.1: Perception of Horizontal Motion by Humans [5]

Therefore, the yaw activity creates oscillations at the frequency of one hertz, which is not acceptable for high-class commercial and business jets. To understand the root cause and eventually eliminate the yaw activity, Concordia University has been asked by Bombardier Aerospace to investigate the yaw activity phenomenon, which might appear on their aircraft. The aircraft aerodynamics was investigated for years, and improvements were made but it did not cure the phenomenon. The goal of this thesis was to understand the yaw activity, recreate the phenomenon as seen on the aircraft through system modeling and simulation and find possible causes to the phenomenon. During the write-up of this thesis, Concordia University has developed a detailed model of the rudder control system, encompassing mechanical linkages, cables, and hydraulic servo-actuators to investigate non-linear phenomena such as backlash and friction [7].

1.2 Problem Definition

One of the Bombardier Aerospace jets was chosen to be the sample aircraft for this analysis. Yaw kicks and yaw oscillations are two different types of yaw activity as illustrated in Figure 1.2. Both types of yaw activity occur at relatively high indicated airspeeds, approximately between 250 and 300 knots, and at medium altitudes, from 10,000 feet to 30,000 feet [2]. Yaw kicks often appear when cruising straight, and most of the time yaw oscillations appear during a turn. The yaw kick can be viewed as a sudden abrupt lurch of the aircraft from right to left or vice-versa. It does not necessarily repeat itself immediately and no frequency can be detected. In flight, yaw oscillations create a sinusoidal movement of the aircraft and can be temporary or continuous (i.e. limit-cycle oscillations) depending on atmospheric conditions and aircraft maneuvering. As previously stated, yaw activity is not dangerous for the crew, but the human body is very sensitive to yaw motion. Regulations for yaw motion are not clear, and it is usually up to the aircraft manufacturer to decide on the tolerances. In fact, most airplane manufacturers avoid to give requirements of yaw oscillations because of the difficulty to measure them and demonstrate compliance. Up to now, since the aircraft manufacturers do not want to publicize this annoying phenomenon, not many studies exist on this subject. The only available studies are limited experimental data where the engineers tried to troubleshoot the phenomenon.

A yaw kick on the aircraft initiates oscillations for a short period of time. The oscillations created by the yaw activity look like typical limit cycle oscillations. Wing-rock is a known lateral limit cycle oscillation that can be used as an example to present

the principal causes of the yaw oscillations. The next section describes the phenomenon, and presents the root causes of wing-rock.

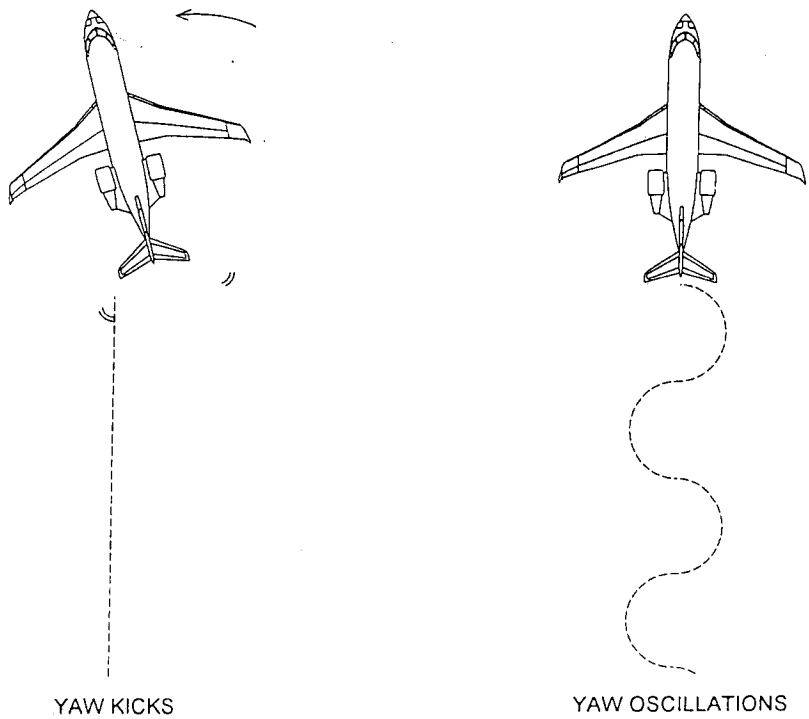

Figure 1.2: Yaw Activity Phenomena

1.3 Limit-Cycle Oscillations

A nonlinear system supplied with a constant source of energy can achieve sustained oscillation. If a cycle is formed and the cyclic behavior of the system operates independent of precise starting conditions in spite of moderate disturbances that tend to slow the process down or speed it up, then it is said to be a limit cycle [8]. The phenomenon of limit-cycle-oscillation (LCO) in flight control systems is a common occurrence. It is believed to be due to the numerous non-linearities found in these systems such as: in the aerodynamics of the aircraft itself, or the mechanical deadband,

backlash, friction and hysteresis of the flight control system. However, it is not well understood, and no satisfactory design procedures have been developed to eliminate or even reduce it.

Limit cycle oscillations in aircraft lateral dynamics is called wing-rock [9]. Wing-rock is an uncommanded roll-yaw with low frequency and constant amplitude (0.3 to 0.7 Hertz, 0.1 to 0.5 deg) [10]. It may be initiated either with a sideslip or during zero-sideslip flight with some aerodynamic flow asymmetry over the aircraft such as vortices normal to the wing surface or other flow disturbances [11]. Once the asymmetric flow starts, the amplitude of a roll oscillation keeps building up if the roll damping is negative. The transient amplitude of wing-rock will grow gradually over some oscillation cycles. This phenomenon cannot be attenuated or prevented by dihedral as this effect is negligible dihedral effect at low roll angle. Although the roll damping is negative at small roll angles, it is positive at larger roll angles for a sustained wing-rock. At large roll angles, both the effective dihedral effect and positive roll damping will gradually reduce the roll rate. Therefore, as these restoring moments become stronger, the aircraft reaches a maximum roll angle and finally the rolling direction is inverted. Thus, wing-rock is constrained to a finite-amplitude oscillation through nonlinear roll damping [12]. There are two distinct sources that can individually lead to wing-rock: aerodynamic flow asymmetry [10] and mechanical non-linearities.

Aerodynamic flow asymmetry is by far the most highly investigated source of wing-rock. The type of wing-rock of interest is due to the formation of vortices by the airplane that

interfere with the proper operation of lift. However, the vortices can be created by one of two mechanisms. The first mechanism is the formation of vortices normal to the wing surface or other flow disturbances as eluded to earlier. This alternating detachment and reattachment of the vortices is the culprit for aircraft oscillations [13]. The periodic changes are determined by the strength and size of these disturbances [14]. This condition is dependent on the leading edge sweep, aircraft angle of attack and sideslip [15,16].

The second source of vortices leading to initiation of wing-rock is the aircraft forebody. The forebody creates vortices that propagate to the wing section of the aircraft and interact with the airflow over the lifting surfaces [17,18]. This has a similar effect as the leading edges vortices. This phenomenon is entirely dependent on the vehicle configuration. In fact, the slender the forebody, and the smaller the distance between the aircraft nose and the wing, the greater the chance that wing-rock will occur. It is important to note that the aircraft angle of attack plays a significant role in this phenomenon.

Mechanical components do substantially contribute to wing-rock. Through non-linearities such as backlash in the system as a whole, cable stretch, dry friction (stiction), servomechanism non-linearities or changes in properties of the hydraulic oil. Any of the aforementioned mechanical sources would appear as hysteresis in the system. These mechanical non-linearities all lead to wing-rock and could potentially be found within the flight control system mechanism and are thus suspects.

Bombardier Aerospace has studied the aerodynamics of the aircraft for years to find possible causes of yaw activity. The thesis objective was to explore the mechanical non-linearities in the system that can lead to yaw activity through simulation modeling and analyses.

1.4 Thesis Approach

The study of yaw activity leads to analyzing independently yaw kicks and yaw oscillations. In fact, flight testing demonstrate that yaw oscillations may appear only when the yaw dampers are turned on. The yaw controller seems to play a major role in the apparition of these limit-cycle oscillations. Note that the internal logic of the yaw damper is the proprietary of the supplier, and Concordia University cannot have access to it. Therefore, yaw oscillations phenomenon cannot be investigated without the collaboration and permission of the supplier.

Flight test data also state that yaw kicks do not depend on the yaw damper settings. This statement made by Bombardier Aerospace engineering is the key of this thesis. The thesis will cover only yaw kick phenomenon since it seems to be related to mechanical non-linearities in the rudder control system. Bombardier Aerospace, with their expertise in the mechanical non-linearities in flight control system, proposes to deeply investigate the hydraulic power control units that actuate the rudder control surface.

Moreover, Bombardier Aerospace provided a six degrees of freedom flight model of one of their airplanes to investigate the phenomenon. This model was validated against flight

test data, and represents the actual performance of the aircraft. To run this model faster, a simplified model of the power control unit was used. Therefore, Bombardier Aerospace proposes that the study should be concentrated on the modeling of a more sophisticated power control unit to better understand its non-linearity effects on the flight control system. This detailed model may also become a useful tool to investigate all kinds of failures of the power control unit sub-components.

CHAPTER 2

AIRCRAFT MODEL

This section presents the aircraft model provided by Bombardier Aerospace. This model was used as a platform to investigate the yaw kick phenomenon by simulation.

2.1 Introduction to the Flight Model

Figure 2.1 presents the model of a typical Bombardier aircraft. The engine and landing gear blocks are not covered in this thesis, however they are simplified models that provide inputs to generate the aircraft equations of motion. This model was validated against flight test data, and it is the platform of this thesis to study the aircraft behavior when a yaw kick occurs.

The aerodynamics block provides to the equations of motion block the forces and moments affecting the aircraft. The equations of motion calculates the behavior of the aircraft when maneuvering (takeoff, turning, landing, ...). The flight control systems block calculates the deflections of all the control surfaces commanded by the pilot. The atmospheric data block calculates corrected values for some parameters such as airspeed and altitude. It permits also for example to introduce wind gusts into the model. The autopilot block was turned off during the investigation since the yaw kicks appear with and without the autopilot. Therefore, it was agreed to isolate the problem, and therefore not to use the autopilot.

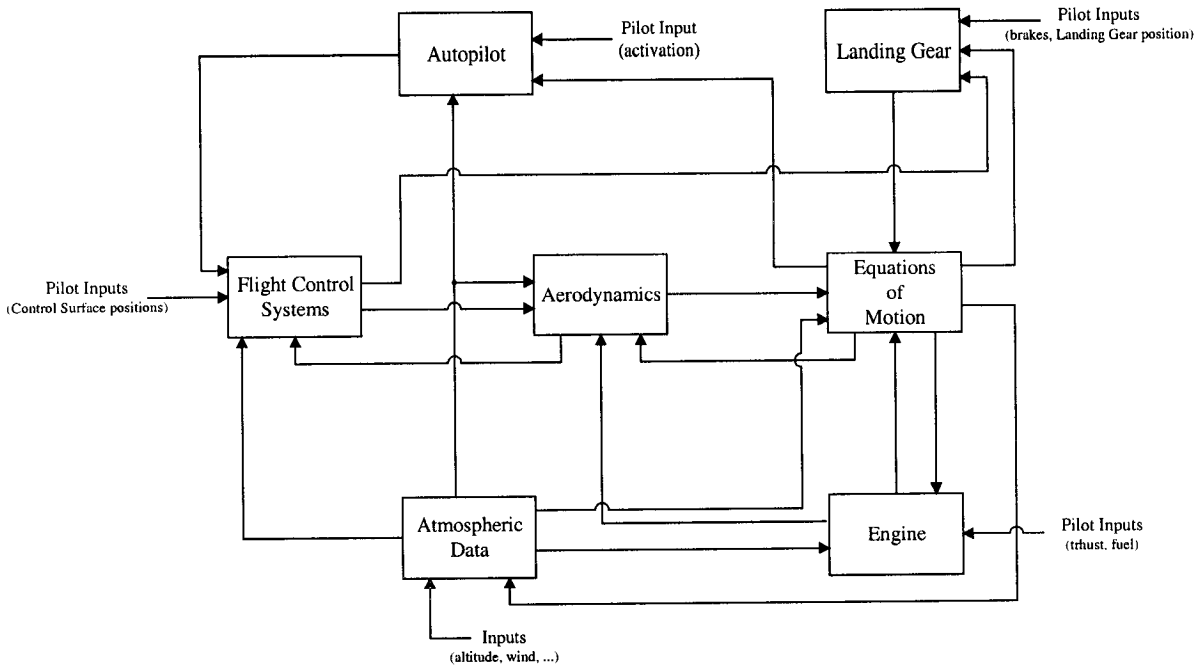

Figure 2.1: Six Degrees of Freedom Aircraft Model Architecture [19]

The next sections will present the aerodynamics, equations of motion and flight control systems blocks. An understanding of the four basic axis systems used to describe aircraft motion in space is necessary to generate aircraft equations of motion and for the reader to interpret the flight test data, since the recorded measurements may refer to different axis systems.

2.2 Axis Systems

There are four axis systems of interest in this thesis [20]; they are:

- Earth fixed axis system
- Body axis system
- Stability axis system
- Wind axis system

The following sections provide a brief description of the axis systems.

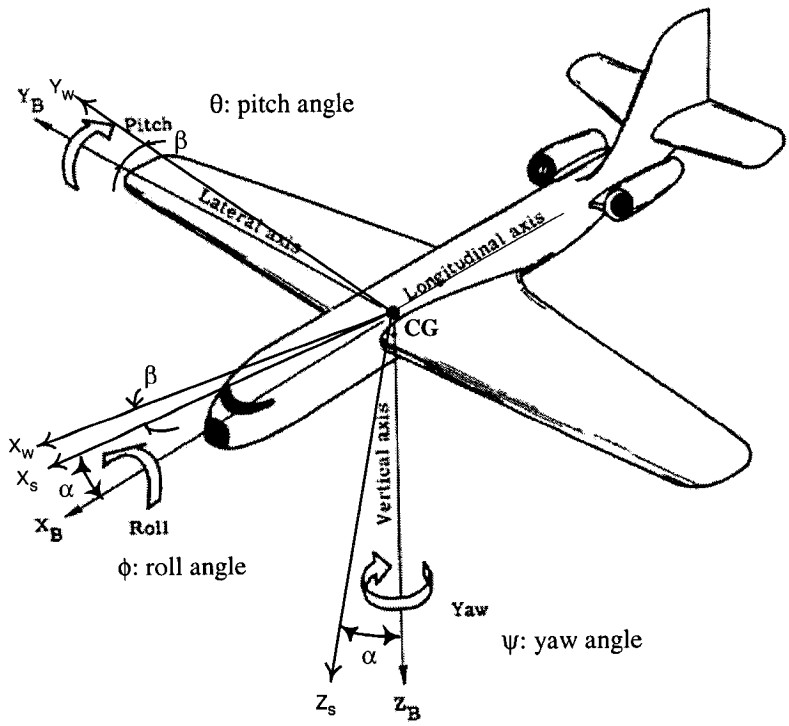

Figure 2.2: Body, Stability and Wind Axes Systems

2.2.1 Earth Axis System

The Earth axis system is used as a basic reference frame. It is used to express gravitational effects, altitude, horizontal distance, and the orientation of the aircraft. The X and Y axes lie in the local horizontal plane of the Earth. The direction of X axis is chosen to point north, and the Y axis direction is pointing east. The Z axis is parallel to the local gravity.

2.2.2 Body Axis System

This set of body axes is chosen to coincide with the principal axes of the aircraft. The three axes intersect at the aircraft center of gravity that defines the body axis system

origin. In this thesis, the aircraft equations of motion are only presented in the body axis system. As shown in Figure 2.2, the X_B-axis is directed out of the nose of the aircraft and is coincident with the longitudinal axis of the aircraft. The Y_B -axis points out of the right wing of the aircraft. Consistent with the right hand rule, the Z_B-axis is perpendicular to X_B and Y_B and points downward.

In aircraft dynamics, the most common set of transformations is that between the Earth axis system which incorporates the gravity vector g, as one axis, and the body fixed axes, X_B, Y_B and Z_B. The orientation of the airplane fixed body coordinate system relative to the earth reference frame can be obtained through the sequence of Euler angle rotations by yaw ψ, pitch θ and roll ϕ (refer to Figure 2.2).

2.2.3 Stability Axis System

With reference to Figure 2.2, the lateral axes of both stability and body axis systems are the same, i.e. $Y_S = Y_B$. The aircraft is considered in a steady level flight, so that the relative wind is seen from a constant direction by the aircraft. The axis Xs is taken as the projection of the velocity vector of the aircraft relative to the air mass parallel to the X_B-Y_B plane of symmetry. Therefore, between the X_s axis and X_B axis, there is the aircraft angle of attack (α). From a mathematical point of view, the stability axis system is defined as:

$$\begin{bmatrix} X_S \\ Y_S \\ Z_S \end{bmatrix} = \begin{bmatrix} \cos\alpha & 0 & \sin\alpha \\ 0 & 1 & 0 \\ -\sin\alpha & 0 & \cos\alpha \end{bmatrix} \begin{bmatrix} X_B \\ Y_B \\ Z_B \end{bmatrix} \tag{2.1}$$

The origin of this axis system is the aircraft center of gravity.

2.2.4 Wind Axis System

The X_W-axis points in the direction of the incoming free-stream velocity vector. The Z_W-axis is chosen to lie in the plane of symmetry of the aircraft. If the relative wind changes, the orientation of the wind-axes changes too, but Z_W-axis always lies in the plane of symmetry as defined. Therefore, between the X_W axis and X_B axis, there is the sideslip angle (β). The mathematical relations between wind axis system, stability axis system and body axis system are:

$$\begin{bmatrix} X_W \\ Y_W \\ Z_W \end{bmatrix} = \begin{bmatrix} \cos\beta & \sin\beta & 0 \\ -\sin\beta & \cos\beta & 0 \\ 0 & 0 & 1 \end{bmatrix} \begin{bmatrix} X_S \\ Y_S \\ Z_S \end{bmatrix} \tag{2.2}$$

Therefore,

$$\begin{bmatrix} X_W \\ Y_W \\ Z_W \end{bmatrix} = \begin{bmatrix} \cos\alpha\cos\beta & \sin\beta & \sin\alpha\cos\beta \\ -\sin\beta\cos\alpha & \cos\beta & -\sin\alpha\sin\beta \\ -\sin\alpha & 0 & \cos\alpha \end{bmatrix} \begin{bmatrix} X_B \\ Y_B \\ Z_B \end{bmatrix} \tag{2.3}$$

2.3 Forces and Moments Affecting an Aircraft in Flight

The airplane displacements resulting from the various movements of the flight control surfaces are those set up by the pilot in order to maneuver the aircraft into required flight attitudes such as straight and level flight, climbing, descending or rolling. As shown in Figure 2.3, there are four principal forces affecting an aircraft in flight: Lift, Drag, Weight and Thrust [21].

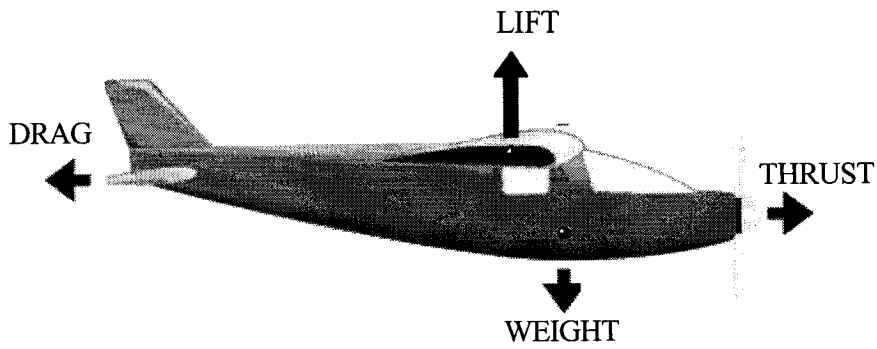

Figure 2.3: Forces Affecting an Aircraft in Flight

For example, in a steady level flight at constant airspeed, the sum of the forces applied on the aircraft is equal to zero. This implies that the weight is equal to the lift, and the drag is equal to the thrust. In level flight, if thrust is greater (lower) than drag, the aircraft will accelerate (decelerate). This acceleration is in accordance with Newton's second law of motion. However, a steady level flight is a very specific case, and if these forces do not cancel each other, they will create moments relative to the airplane centre of gravity is called pitching, rolling or yawing moments.

2.3.1 Lift

The resulting aerodynamic force on the airplane is perpendicular to flow contributions from the horizontal stabilizer, elevator control surface, wings and aircraft body. Taking the example of the wing, the lift is produced by a lower pressure created on the upper surface of an airplane's wing compared to the pressure on the wing's lower surface, causing a net upward force. Considering air flowing over an airfoil with an angle of attack (α), the pressure difference between the bottom and the top of the airfoil increases as the angle of attack increases (refer to Figure 2.4). The lift force (L) and the lift

coefficient (C_L) increase with the pressure difference. The relationship of the lift force is [22]:

$$L = \frac{1}{2} C_L \rho_{air} V^2 S \tag{2.4}$$

where ρ_{air} is the air density, V is the aircraft speed, and S is the wing area.

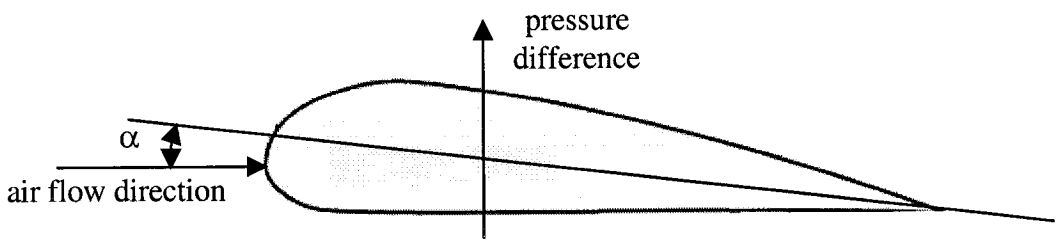

Figure 2.4: Lift Generation

The lift coefficient of an airfoil is estimated by wind tunnel tests. The typical curve is shown in Figure 2.5. The lift coefficient (or pressure difference) increases until a critical angle of attack is reached, where the air flow breaks away from the upper wing surface that results in a drop in lift and the wing stalls.

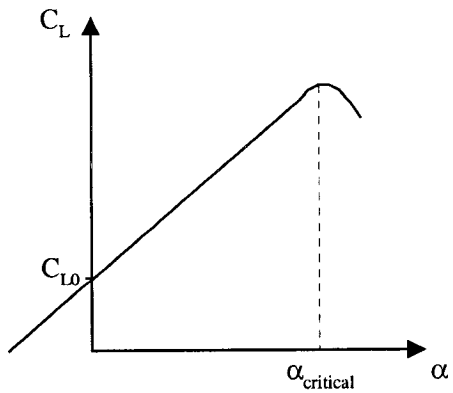

Figure 2.5: Lift Coefficient Curve

2.3.2 Drag

Drag is the aerodynamic force that opposes the aircraft motion through the air. Therefore, when designing an aircraft, the drag force should be minimum in order to reduce the size of the engines. The relationship between the drag force (D) and the drag coefficient (C_D) is:

$$D = \frac{1}{2} C_D \rho_{air} V^2 S \tag{2.5}$$

where ρ_{air} is the air density, V is the aircraft speed, and S is the wing area.

For subsonic airplanes, the total drag has two main components: the parasite drag coefficient and the induced drag. The parasite drag includes the effects of the skin friction and the shape (form) of the body. Form drag is caused by the pressure differential due to airflow around a body as shown in Figure 2.6. Skin friction drag depends on the roughness of the airplane's surfaces [23].

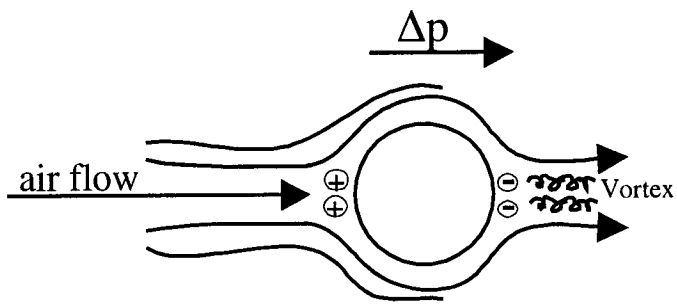

Figure 2.6: Form Drag

When a wing produces lift, the airflow over both the upper and lower surfaces join at the trailing edge, and leaves it in the form of a vortex motion, the direction of which imparts

a downward velocity component to the air. This downwash, as it is called, has the effect of inclining the lift force rearwards so that it will have a component acting in the direction of the drag force. This additional drag component is called the induced (or vortex) drag.

2.3.3 Weight

Weight is the force generated by the gravitational attraction of the earth on the airplane. For an airplane, weight is a force that is always directed towards the center of the earth. The magnitude of this force depends on the mass of all of the parts of the airplane, plus the amount of fuel, plus any payload on board (including the occupants). The weight is distributed throughout the airplane and is acting through a single point called the center of gravity. The direction of the weight always remains toward the center of the earth. During a flight the aircraft burns up its fuel, so the weight of the airplane constantly changes. Also, the distribution of the weight and the center of gravity can change, so the pilot must constantly adjust the controls to keep the airplane balanced.

2.3.4 Thrust

Thrust is the forward-acting force, which opposes drag and propels the airplane. The propulsion is based on Newton's Third Law: "For every action, there is an equal and opposite reaction" [24]. Basically, the propulsion unit pushes on a fluid (air), and the fluid pushes back on the propulsion unit, creating thrust. The piston engine and the gas turbine develop thrust by burning a combustible mixture of fuel and air. Both convert the energy of the expanding gases into propulsive force. The piston engine does this by

changing the energy of combustion into mechanical energy that is used to turn a propeller. The piston engine was the first power plant used for aircraft. To reduce the weight of the aircraft and to improve the performance, the aircraft manufacturers now often use gas turbine engines.

2.3.5 Moments

In a similar manner, the moments on the airplane can be divided into moments created by the aerodynamic load distribution and the thrust force not acting through the airplane center of gravity [25]. The moments about the three axes are the pitching moment, the rolling moment, and the yawing moment.

The major contributors to the pitching moments are the lift force applied on the wing, the horizontal stabilizer surface, and the elevator control surfaces. The pitching moment arm is the distance from the force centre of pressure to the aircraft centre of gravity. The engine contribution to the pitching moment is also not negligible when the thrust force is not acting at the aircraft centre of gravity.

The yawing and rolling moment are closely coupled, and will be produce by the deflection of aileron and rudder control surfaces. Indeed, there is a cross effect when deflecting the aileron control surfaces. The wing producing more lift also produces more drag, which will create a yawing moment in the opposite direction to the roll. This effect is known as adverse yaw [26].

The aerodynamic loads applied to the flight control systems should be computed accurately, as they define the stability of the airplane in flight. The next sections will present the flight control systems of the airplane.

2.4 Aircraft Equations of Motion

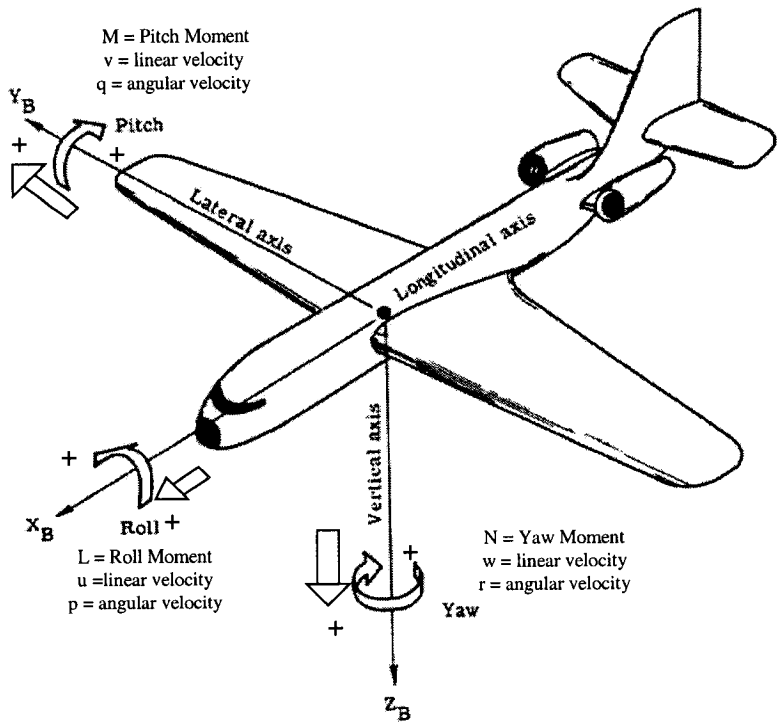

Figure 2.7: Definitions of Vector Components in the Airplane Equations of Motion

The equations of motion of the aircraft are expressed in the body axis system. Having defined the Euler angles in section 2.2.2, the relation between the earth axes velocity components and the body axes velocity components of the airplane is the following [27]:

$$\begin{bmatrix} dX/dt \\ dY/dt \\ dZ/dt \end{bmatrix} = \begin{bmatrix} \cos\theta\cos\psi & \sin\varphi\sin\theta\cos\psi - \cos\varphi\sin\psi & \cos\varphi\sin\theta\cos\psi + \sin\varphi\sin\psi \\ \cos\theta\sin\psi & \sin\varphi\sin\theta\sin\psi + \cos\varphi\cos\psi & \cos\varphi\sin\theta\sin\psi - \sin\varphi\cos\psi \\ -\sin\theta & \sin\varphi\cos\theta & \cos\varphi\cos\theta \end{bmatrix} \begin{bmatrix} X_B \\ Y_B \\ Z_B \end{bmatrix} \tag{2.6}$$

Integration of the previous equation yields the airplane's position relative to the earth axes. The relationship between the angular velocities in the body frame (p,q,r), and the Euler rates are also determined mathematically (refer to Figure 2.7):

$$\begin{bmatrix} p \\ q \\ r \end{bmatrix} = \begin{bmatrix} 1 & 0 & -\sin\theta \\ 0 & \cos\varphi & \cos\theta\sin\varphi \\ 0 & -\sin\varphi & \cos\varphi\cos\theta \end{bmatrix} \begin{bmatrix} X_B \\ Y_B \\ Z_B \end{bmatrix} \tag{2.7}$$

The rigid body equations of motion are obtained from Newton's second law, which states that the summation of all external forces $\left(\sum \vec{F}\right)$ acting on a body is equal to the time rate of change of the momentum of the body; and the summation of the external moments $\left(\sum \vec{M}\right)$ acting on the body is equal to the time rate of change of the moment of momentum.

$$\sum \vec{F} = \frac{d(m_{airplane}.\vec{V})}{dt} \tag{2.8}$$

$$\sum \vec{M} = \frac{d(\vec{H})}{dt} \tag{2.9}$$

These equations lead to the following general airplane equations of motion.

Force along X:

$$m_{airplane} \cdot (\dot{u} - vr + wq) = -m_{airplane} g \sin\theta + F_{Ax} + F_{Tx} \tag{2.10}$$

Force along Y:

$$m_{airplane} \cdot (\dot{v} + ur - wp) = m_{airplane} g \cos\theta \sin\varphi + F_{Ay} + F_{Ty} \tag{2.11}$$

Force along Z:

$$m_{airplane} \cdot (\dot{w} - uq + vp) = m_{airplane} \cdot g \cos\varphi \cos\theta + F_{Az} + F_{Tz} \tag{2.12}$$

Rolling Moment about X:

$$I_{xx}\dot{p} - I_{xz}\dot{r} - I_{xz}pq + (I_{zz} - I_{yy})rq = L_A + L_T \tag{2.13}$$

Rolling Moment about Y:

$$I_{yy}\dot{q} - (I_{xx} - I_{zz})pr + I_{xz}(p^2 - r^2) = M_A + M_T \tag{2.14}$$

Rolling Moment about Z:

$$I_{zz}\dot{r} - I_{xz}\dot{p} + (I_{yy} - I_{xx})pq + I_{xz}qr = N_A + N_T \tag{2.15}$$

2.5 Primary Flight Control Systems

This section presents the flight control systems of the aircraft as part of the six degrees of freedom model. This review will help to localize the investigated system (i.e. power control units of the rudder control system) in the aircraft model architecture. For each of the axes, the design, the corresponding mechanical modelling, and the high-level characteristics will be reviewed and described.

A pilot must be able to keep the flight of an aircraft under control. When flying, the pilot commands different control surfaces that are called primary flight control systems to control the aircraft attitude. Conventionally, these include elevators, ailerons, and the rudder, as illustrated in Figure 2.8.

Until the early forties, manual activation was used for airplane control surfaces. Push-pull rods or cables or a combination of both were and are still used. Then, the assistance of hydraulics was used to develop powered flight control systems in order to overcome the aerodynamic loads on the control surfaces as the airplanes became larger. Figure 2.9 presents the Boeing 757 powered flight control systems, and their respective location on the aircraft. The gradual introduction of fly-by-wire types of control systems since these times, especially for fighters and large aircraft, has improved considerably the controllability and the performance of the aircraft.

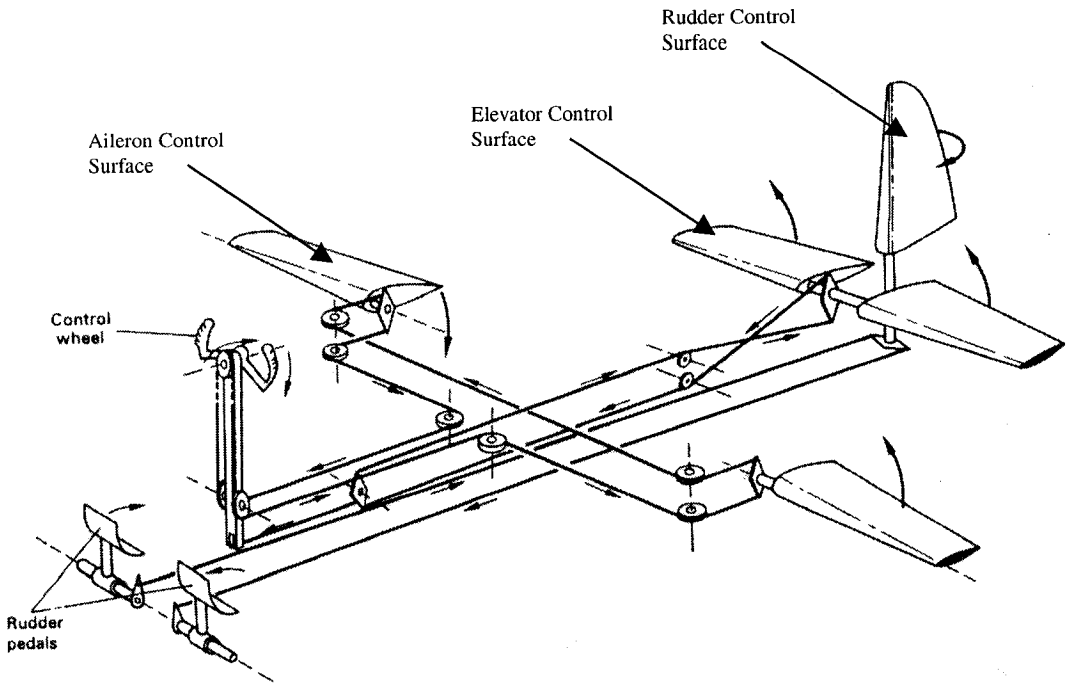

Figure 2.8: Simple Primary Flight Control Systems [28]

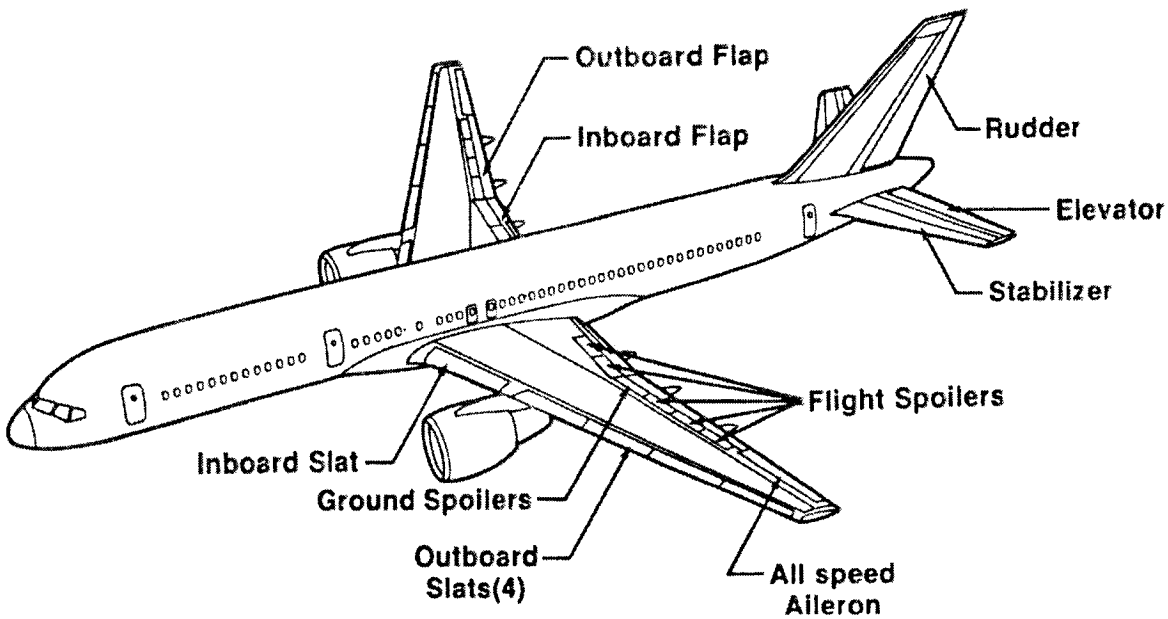

Figure 2.9: Boeing 757, Powered Flight Control Systems [29]

2.5.1 Elevators

Elevator control system controls pitch about the lateral axis of the aircraft. The elevator control surfaces are hinged to the rear spar of the horizontal stabilizer. A simple elevator control system may be all mechanical as shown in Figure 2.10. The elevator control surfaces are moved manually through pulleys and cables by deflecting the pilot control stick fore and aft.

Figure 2.10 presents the elevator control system of the Bombardier Challenger. This type of control system is typical of many conventional elevator control systems used in the aircraft industry. By pulling or pushing control columns, the pilots can adjust the position of the elevators over their operating ranges. For Bombardier aircraft, elevators are mechanically operated and hydraulically powered. A column torque tube links the two control columns to each other, and a disconnect mechanism allows the two columns to separate in case of failure such as when a mechanical jam on one side of the circuit occurs. Displacement of the control column creates a rotation of the forward pulley (also called as "forward quadrant"). The aft quadrant, which is linked to the forward quadrant by cables, also rotates and gives an input to the servoactuators (hydraulic power control units, PCU). The aft quadrant refers to the pulley located in the aft section of the airplane. The actuators are attached to the control surfaces, and a displacement of the actuators cause the deflection of the elevator surfaces. For safety issues, the flight control system has to be redundant, therefore two servoactuators operate one elevator panel.

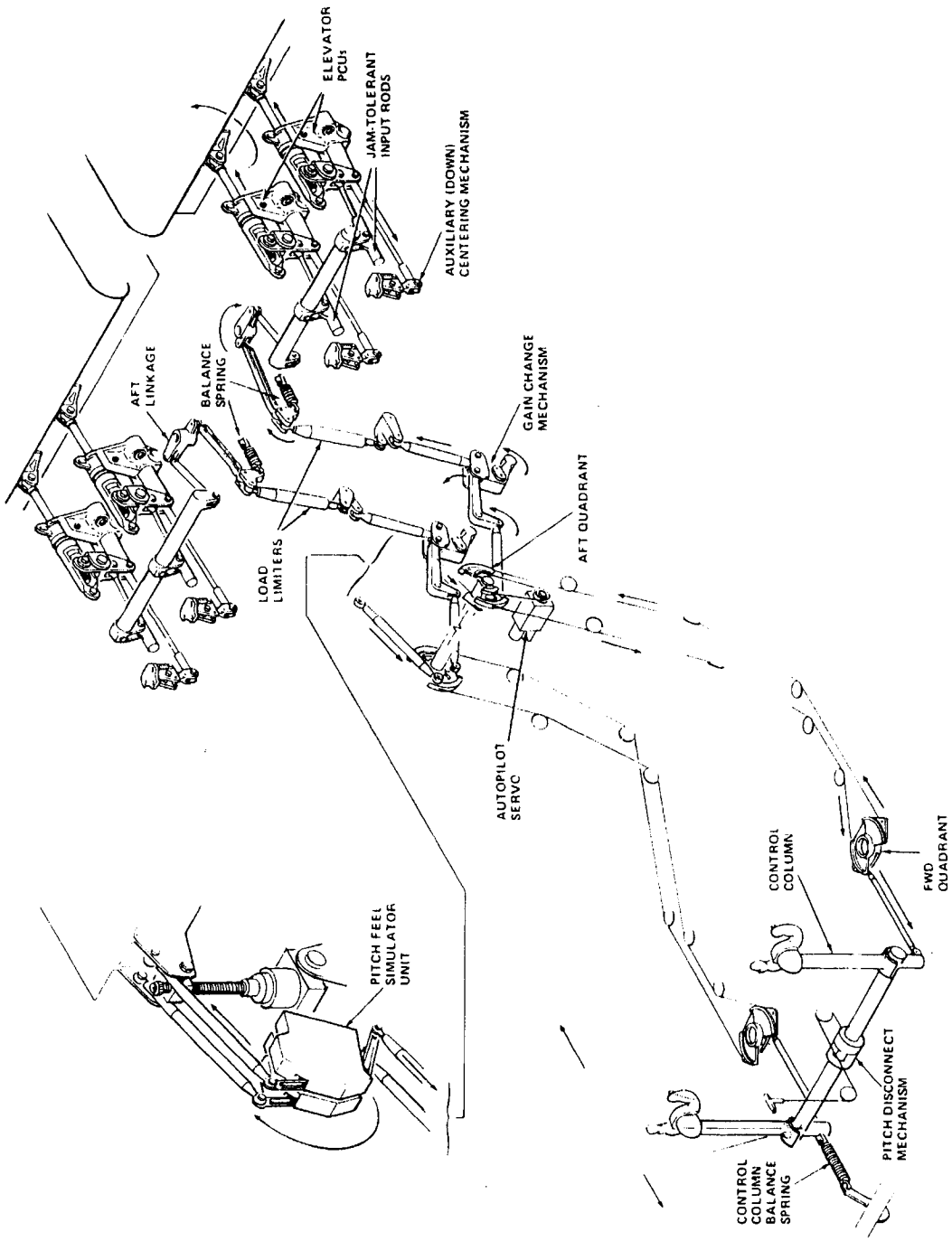

Figure 2.10: Bombardier Challenger Elevator Control System [30]

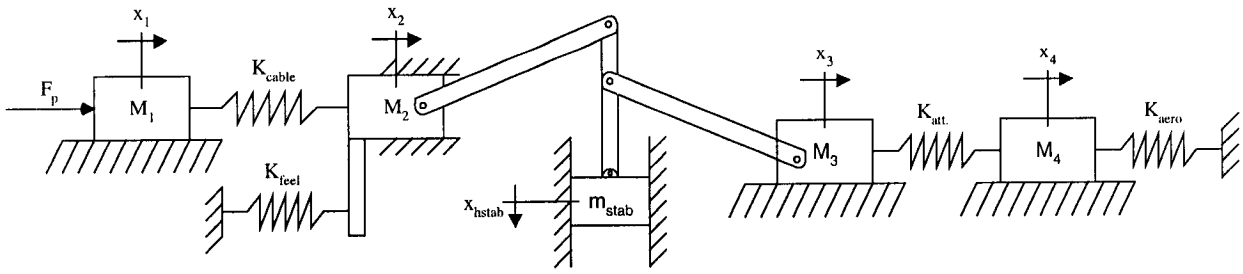

Figure 2.11: Elevator Control System Schematic

Figure 2.11 presents a general system model of a typical elevator control system that can be used for different types of airplanes such as the Bombardier Challenger. In this thesis, this schematic is only used to clarify the principles of the elevator control system presented in Figure 2.10. The elevator control panels are attached to the horizontal stabilizer, and there is a mechanical relationship between them (refer to section 2.6.2). The effects of the horizontal stablizer on the elevator control surface is illustrated in the Figure 2.11. The horizontal stabilizer is a secondary flight control surface that helps to control the aircraft about its longitudinal axis (pitch). It provides a trim capability to the system. The horizontal stabilizer will be described in detail in the secondary flight control systems section (refer to section 2.6.2). The nomenclature used in Figure 2.11 is provided in Table 2.1 below.

Table 2.1: Elevator Schematic Nomenclature

Symbol	Description
M_1	control columns + forward quadrant mass
M_2	aft quadrant mass
M_{stab}	horizontal stabilizer mass
M_3	PCU actuator mass
M_4	elevator surface mass
x	position of the respective mass
Fp	pilot force
K_{cable}	stiffness of cables
K_{feel}	stiffness of feel unit
K_{att}	attachment stiffness
K_{aero}	aerodynamic stiffness

The linkage assembly between the PCU mass and the elevator surface mass is modelled by a spring representing the stiffness of the mechanical assembly. A pitch feel unit, which is usually a function of the horizontal stabilizer and flaps positions, provides an artificial force to the pilot. Since the servoactuators take care of the aerodynamic loads applied on the elevator surfaces, this pitch feel unit produces a force feedback proportional to the load applied to the surface, which varies as a function of its rotation. Bombardier's feel gradient design is quite different from Airbus and Boeing designs. Bombardier uses a non-linear component in the elevator control system to obtain a flat feel gradient at neutral as shown in Figure 2.12, whereas the other aircraft manufacturers use a more linear gradient. The flat feel gradient is a deadband the pilot feels at the neutral column position.

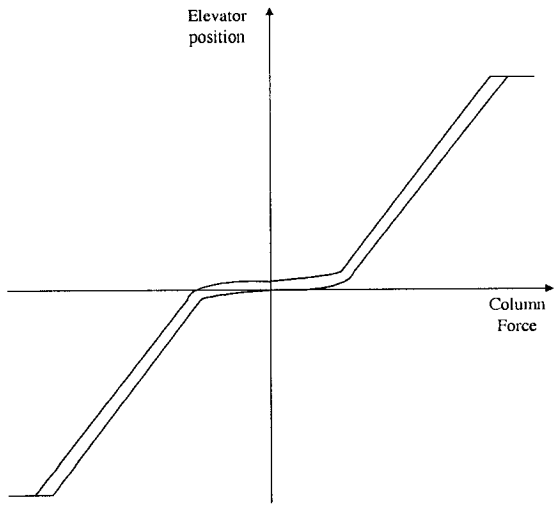

Figure 2.12: Bombardier Typical Non-Linear Gradient on the Elevator Control System

The left and right sides of the elevator control system are symmetrical, except that a servomotor is attached by a cable to the pilot side aft quadrant. The function of the autopilot is to provide automatic control of the aircraft. With the autopilot engaged, the pilot no longer directly controls the aircraft but selects the flight conditions that the autopilot has to maintain. In this mode, the task of the pilot is the monitoring of operation of the autopilot.

A load limiter is a control rod with a spring-loaded rod end. Its purpose is to protect the mechanical part to which it is connected from excessive loads, i.e when the system is operating without hydraulic power or overtravel is induced. As shown in Figure 2.10, a balance spring prevents the weight unbalance created by the failure of a component in the system.

2.5.2 Ailerons

The aileron flight control system controls roll about the longitudinal axis of the aircraft. A simple aileron control system was presented in Figure 2.8. The aileron control surfaces are hinged on the rear spar of the wings. For light aircraft, a system with only cables, push-rods and pulleys is sufficient to provide lateral control because the aerodynamic loads are small enough and can be overcome by the pilot.

Figure 2.13 presents the aileron control system of the Bombardier Challenger. The roll control is provided by two hydraulically actuated ailerons that operate in unison. Two handwheels enable the pilot and co-pilot to command the ailerons. Like the elevator system, a rotation of the pilot handwheel rotates the forward and aft quadrants and gives an input to the servoactuators, which rotate the aileron panels. For this system, an artificial feel unit located on the aft pulley gives feedback of the actual aerodynamic loads to the pilot. The autopilot is attached to an aft quadrant on one side of the aircraft. Dampers are attached to the aileron control surfaces to prevent flutter. Each aft quadrant (also called "splitter") uses an artificial feel mechanism to give control feel to the handwheel.

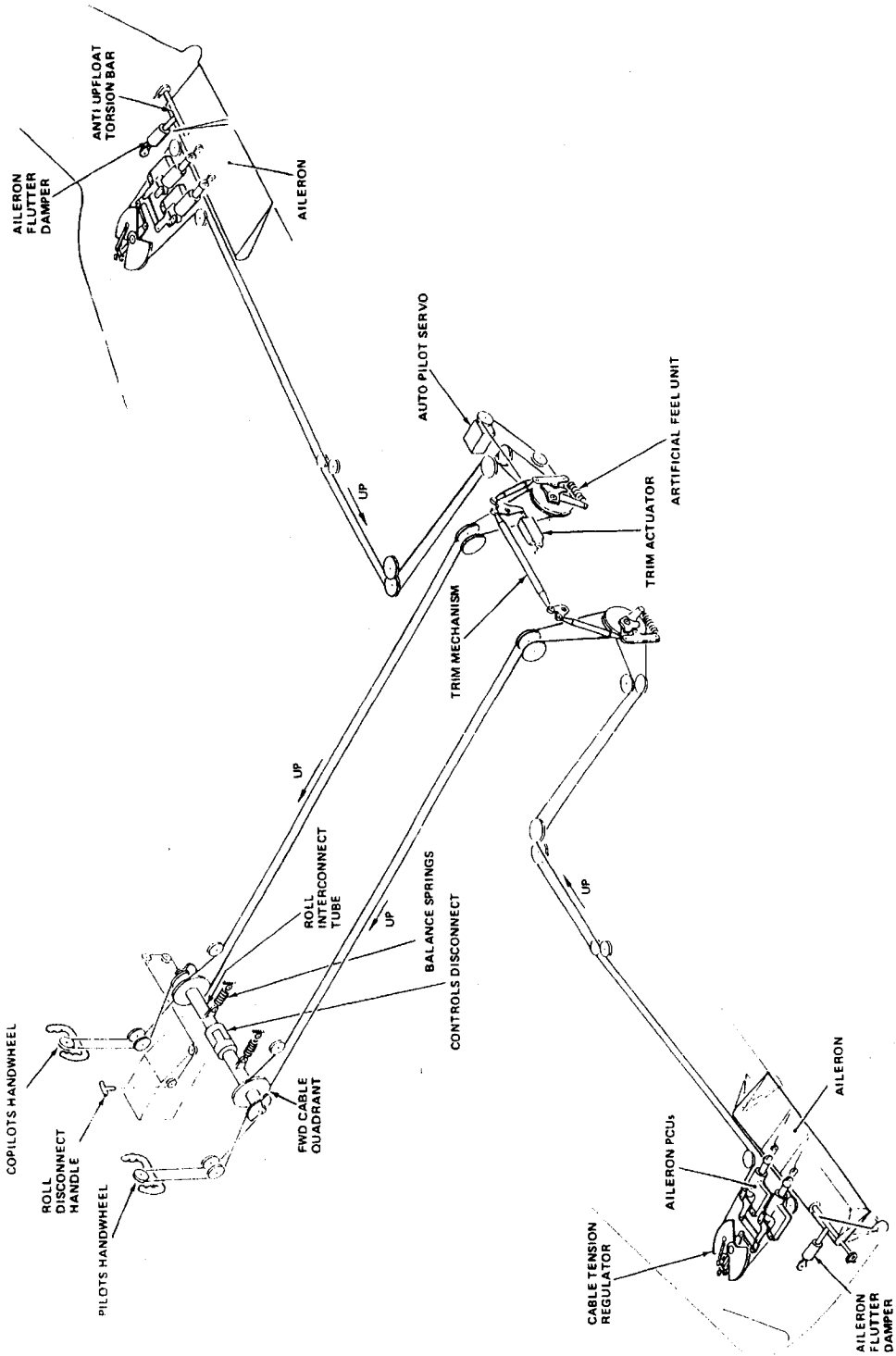

Figure 2.13: Bombardier Challenger Aileron Control System [30]

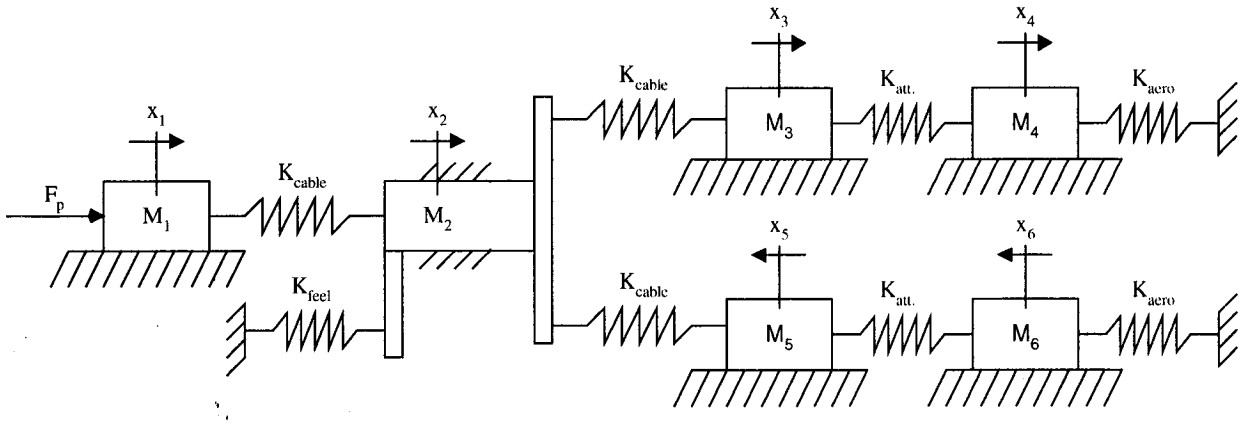

Figure 2.14: Aileron Control System Schematic

Figure 2.14 presents the general system model of the aileron control system that can be used to illustrate the Bombardier Challenger aileron control system. The nomenclature used in Figure 2.14 is provided in Table 2.2.

Table 2.2: Aileron Schematic Nomenclature

Symbol	Description
M_1	control handwheels mass + forward quadrant mass
M_2	aft quadrant mass
M_3, M_5	PCU actuator masses
M_4, M_6	aileron control surface masses
X	position of the respective mass
Fp	pilot force
K_{cable}	stiffness of cables
K_{feel}	stiffness of feel unit
K_{att}	attachment stiffness
K_{aero}	aerodynamic stiffness

2.5.3 Rudder

A rudder surface hinged on the rear spar of the vertical stabilizer provides a yawing moment on the aircraft. The displacement of the rudder is controlled by foot pedals, which are located in the cockpit of the aircraft (Figure 2.15). The rudder control system of the Bombardier Challenger will be explained in detail later in this thesis (refer to Chapter 3).

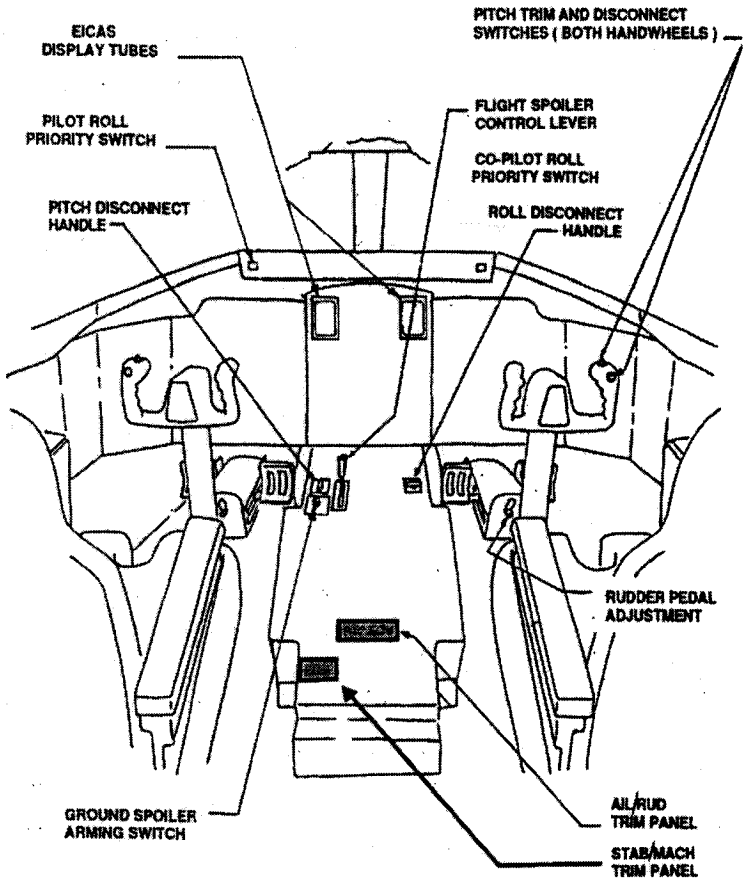

Figure 2.15: Typical cockpit of an Aircraft [30]

Figure 2.15 describes typical flight control inceptors that are found in a standard cockpit. Disconnect handles for all axes allow the pilot or co-pilot to separate the right and left

flight control mechanisms in case of failures such as a jam. For example, if a cable jam occurs on the right side of the aircraft (co-pilot side), the pilot can retain half control authority of the aircraft by pulling the disconnect handle. Trim switches assist the pilots when flying by reducing the forces required at inceptors. Trimming control systems will be explained in detail as part of the secondary flight control systems (refer to section 2.6).

To cater to pilots with a variety of leg-reaches, each set of pedals is provided with an adjusting mechanism (shown on Figure 2.15), which consists of a hand-crank located between and aft of the pedals. The flight spoiler control lever (shown on Figure 2.15) commands the deflection of the flight spoiler surfaces, which are described in the following section. As shown on Figure 2.15, the system status messages are displayed on the Engine Indication Crew Alerting System (EICAS) tubes. EICAS is the interface between the pilots and the avionic systems.

2.6 Secondary Flight Control Systems

The secondary flight controls supplement the primary controls by helping the pilot in controlling the aircraft. Various types are used on aircraft, but only the most common are discussed here. They are the following: trim tabs, horizontal stabilizer, wing flaps, slats, and the spoilers.

2.6.1 Trim Tabs

A trim tab is a small airfoil fitted to the trailing edge of a primary control surface, especially on the elevator and rudder control systems. Their purpose is to enable the pilot

to neutralize any unbalanced load on the surface that might exist during flight, without exerting any pressure on the control stick or rudder pedals. Each trim tab is hinged to its parent control surface, but is operated independently by a separate control.

The pilot moves the trim tab using a cockpit control. The tab on the control surface is normally moved in a direction opposite to the desired control surface movement. The airflow striking the trim tab causes the larger surface to move to a position that will correct the unbalanced condition of the surface moment. For example as shown in Figure 2.16, by moving the trim tab from its initial position, a trim force is generated to compensate for aerodynamic load on the control surface [31]. Then, the elevator surface is trimmed to the desired position with no pilot force input.

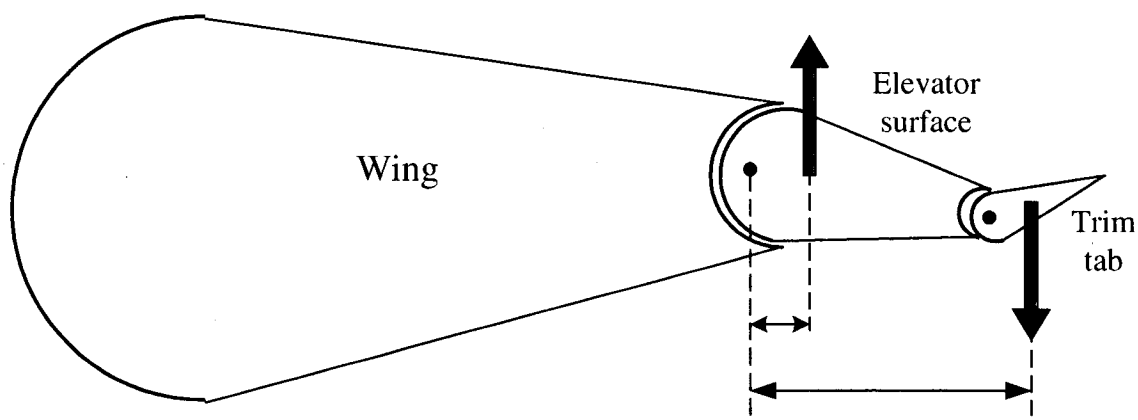

Figure 2.16: Effect of Trim Tabs

Primary control surface trimming may be achieved manually or by an electro-mechanical trim actuator located in the aft part of the primary flight control system. The systems are normally designed such that the trimming of the aircraft is achieved without back-driving of the rudder pedals or control sticks.

2.6.2 Horizontal Stabilizer

The horizontal stabilizer (HSTAB) allows trimming of the aircraft in pitch. This is achieved by varying its angle of incidence. By trimming the aircraft with the horizontal stabilizer, no significant forces need to be applied to the elevators to maintain the balance conditions. By moving the horizontal stabilizer surface, the elevator control surfaces are deflected as shown in Figure 2.17. Therefore, trimming the horizontal stabilizer shifts the elevator position versus column position. With the same position of the column (x_{column}), the pilot will command more deflection of the elevator panel. Moreover, in a hydraulic powered elevator control system, the force gradient is also changed when moving the horizontal stabilizer. This is generated by the pitch feel simulator to provide feedback to the pilot of the change of aerodynamic loads on the control surfaces.

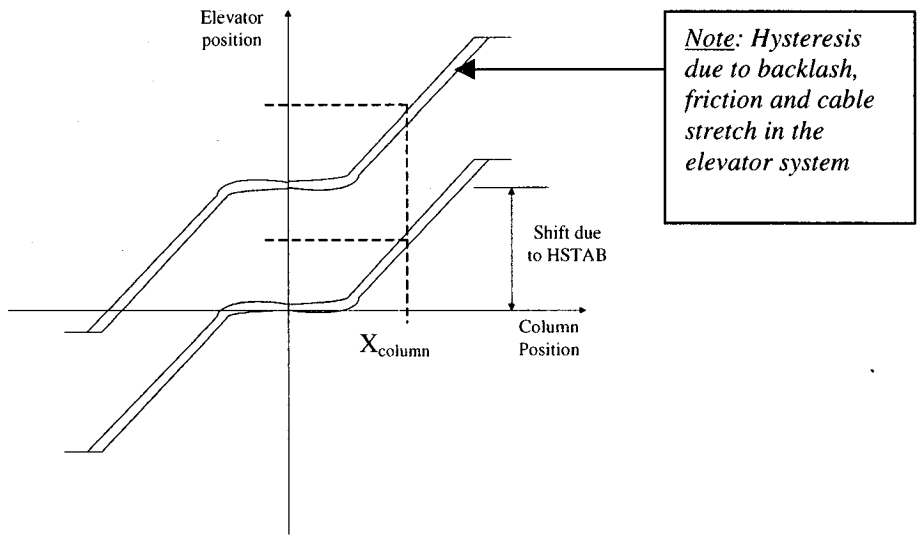

Figure 2.17: Effect of the Horizontal Stabilizer on the Elevator Position

2.6.3 Wing Flaps

The wing flaps are movable surfaces on the rear part of the wings, and they increase lift of the aircraft during takeoff and landing. When landing, by providing an increase C_L the flaps allow the aircraft to be flown at a lower airspeed, therefore shortening the landing distance. The flaps shift the lift coefficient versus the angle of attack curve upwards as shown in Figure 2.18 [32].

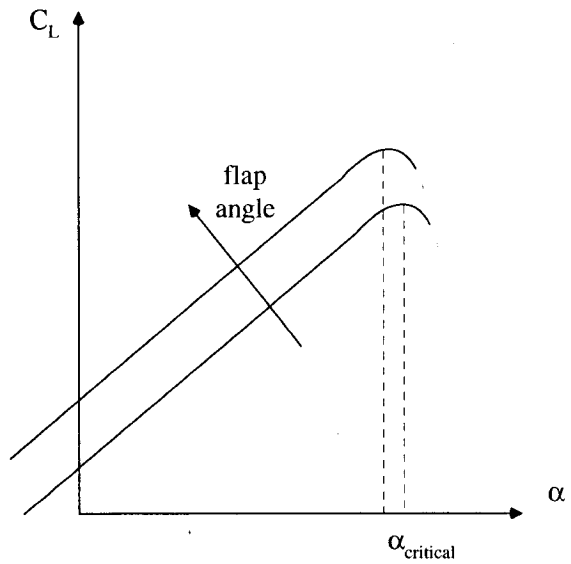

Figure 2.18: Effect of Wing Flaps

2.6.4 Slats

The slats are movable surfaces attached to the leading edges of the wings. They are used during takeoff and landing to increase the aircraft lift coefficient. As shown in Figure 2.19, as the slat angle increases, the critical angle of attack (stall angle) increases.

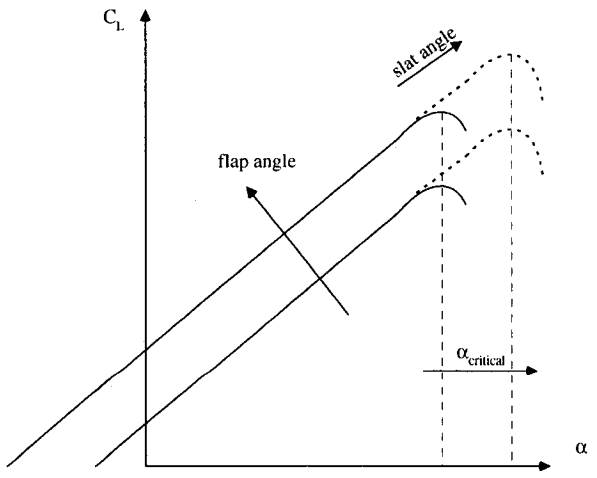

Figure 2.19: Effect of Slats on Lift Coefficient

2.6.5 Spoilers

Spoilers are located on the trailing edge of the wings (refer to Figure 2.9). They are essentially used for wing lift reduction and to provide roll assistance; however, their specific design, function, and use vary with different aircraft [33]. With deployed spoilers, the pilot can make a descent without having to lower the nose of the aircraft. Upon touchdown the spoilers deploy automatically, creating a firm downward pressure on the landing gear, which makes braking more effective. There are different types of spoilers according to their functions. Typically, two types of spoilers are used: the multi-function spoilers and the ground spoilers. The multi-function spoilers provide roll assistance to the aileron control surfaces, drag increase, proportional lift dumping and ground lift dumping. After touchdown, the ground spoilers in conjunction with the multi-function spoilers are extended to destroy lift and increase drag to assist in aircraft braking. The pilot commands the spoiler systems through a spoiler control lever located in the cockpit (refer to Figure 2.15).

2.7 Preliminary Study of Yaw Kicks

The first approach of systems engineers to cure this anomaly was to investigate the aerodynamic behavior of the airplane. No clear relation between the aerodynamic behavior of the aircraft and the yaw activity was found. The rudder control system was investigated next. By looking at the mechanical aspects of the problem, the backlash and hysteresis in the joints of the flight control system may be the source of the problem. Backlash and hysteresis in a mechanical system can create undesired outputs such as deadband. The backlash effects from cables and linkage joints before the aft pulleys of

the rudder system are reduced considerably by the second artificial mechanism composed of a cam, a follower and a spring for centering (refer to section 3.2.2). Therefore, up to now, no clear procedure to eliminate the yaw kick exists.

By using a MATRIXx mathematical model of the entire aircraft [34], the behavior of the aircraft due to a yaw kick could be reproduced by applying a displacement step input on the rudder of half a degree. It has to be noted that this value corresponds to a theoretical 0.024 inch displacement of the servo-actuator. This value was obtained by kinematic analysis between the rudder deflection and the servo-actuator displacement (refer to section 3.4.1 to see the mechanical arrangement). The reproduced yaw kick characteristics by Concordia University are shown in Figure 2.20. Yaw dampers from the autopilot were completely disabled during the flight test. This is unusual to disconnect the yaw dampers during a flight, but the engineers wanted to verify the effect of the yaw dampers. Simulation data indicate that the aircraft begins to roll, but no correction was provided by the ailerons to bring the aircraft back to its horizontal position. However, during the flight test, the aircraft rolling was corrected by the ailerons. It seems that the pilot corrected the rolling motion by "instinct". Moreover, the rudder displacement was not visible on flight test results because of the vibration noise and the accuracy of the sensors.

Figure 2.20a shows a command of 0.5-degree step displacement of the rudder control surface to induce yaw motion of the aircraft. The rudder is returned back to its initial position after 10 seconds. The yaw damper from the autopilot has been disabled as

explained earlier. As a result, Figure 2.20b indicates an oscillating sideslip of the aircraft (0.8 degree maximum). Figure 2.20d shows that the maximum angular acceleration is 1.7 deg/sec^2, and the Figure 2.20c indicates that the maximum angular velocity is about 1.5 deg/sec; all respectively about the aircraft Z-axis. Figure 2.20e shows that the maximum lateral acceleration is 0.045g. Due to yaw kick, the frequency of the oscillations is approximately 0.3 Hz and is constant. At 10 seconds in the simulation, the rudder is returned back to its zero position. Again, a decaying constant 0.3 Hertz frequency oscillation is induced in all the variables.

The simulation results were compared to one available flight test [2]. The aerodynamic characteristics of the yaw kick were therefore reproduced by simulation using the flight model.

When trying to reproduce the yaw kick phenomenon by simulation, a simplified servo-actuator model was used in the flight model. Bombardier Aerospace proposed to create a detailed model of the three parallel servo-actuators, because the non-linearities from the servo-actuators may be the source of yaw kicks. Analysis of force fight of the servo-actuators will be also performed and studied. Three actuators that do not command the same output will fight, and may create undesirable outputs. All possible sources of non-linearitites in the servo-actuator should be taken into account to track the yaw activity. The next section will present the methodology used to create the servo-actuator model.

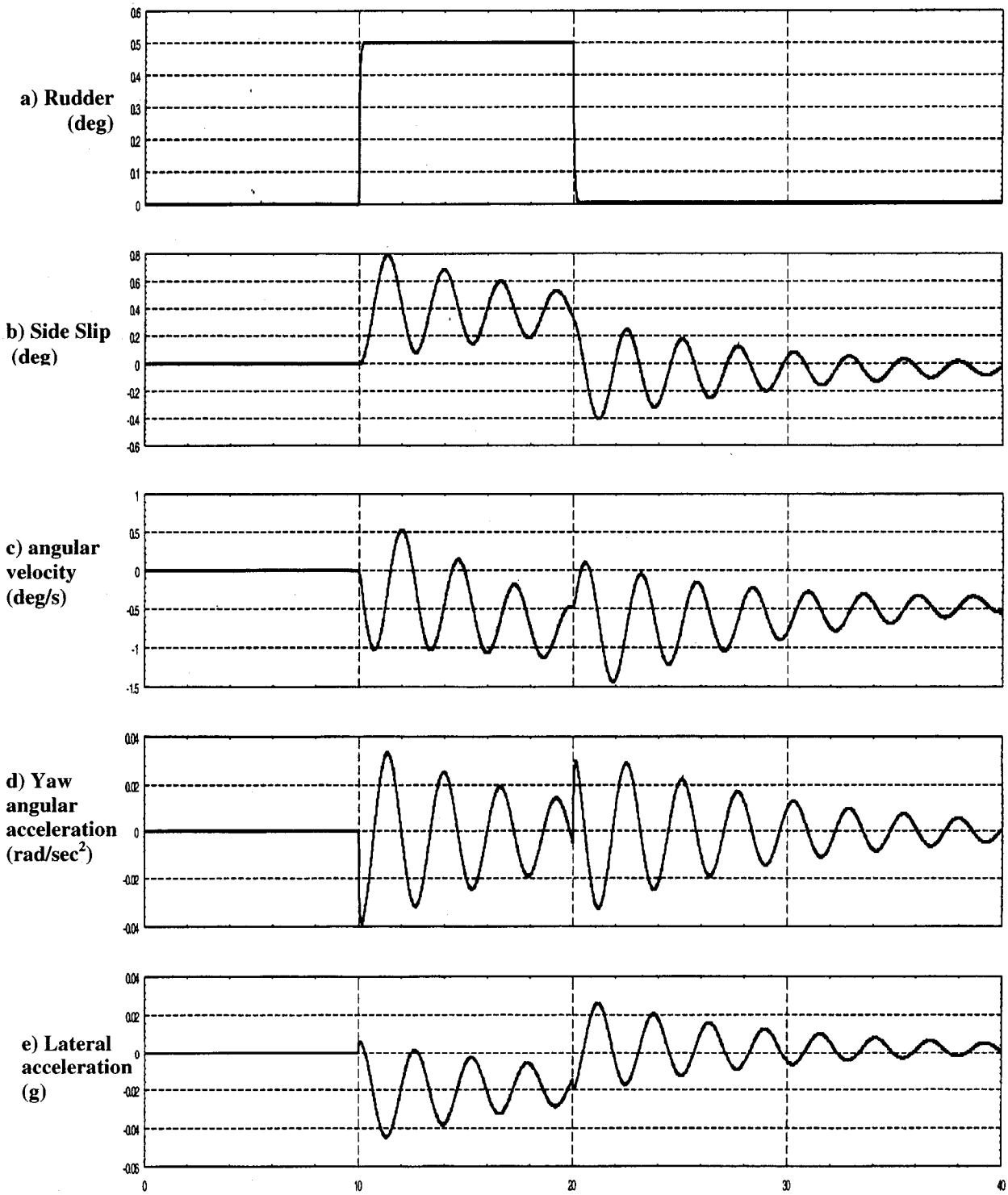

Figure 2.20: Simulation of a Yaw Kick by Using Matrix$_x$

CHAPTER 3

RUDDER CONTROL SYSTEM PRESENTATION AND SERVO-ACTUATOR MODELING

Experimental investigation of yaw kicks leads to model and analyze in detail the power control units that actuate the rudder control surface. This section presents the rudder control surface components. It describes also in detail the power control unit mechanism, and defines the mathematical equations used to build the model.

3.1 Introduction

The angular position of the rudder may vary continuously over its operating range by means of conventional dual foot pedals. That is, the pilot and co-pilot can control the rudder position by using foot pedals (also called "rudder pedals"), which are interconnected and work in unison. The rudder is mechanically operated and hydraulically powered by three hydraulic servomechanisms, all operating in an active configuration. The hydraulic power is supplied by three fully independent hydraulic systems. Each hydraulic system is designed to be sufficient for maintaining normal operation, in case of loss of the other two hydraulic systems.

3.2 Mechanical Arrangement

3.2.1 Overview

The pilot pedal movement is transmitted by push-pull rods to the forward quadrants as shown in Figure 3.1. The cables attached to the forward quadrant transmit the motion to the aft quadrants. The cables are guided by idler pulleys attached to the aircraft structure. The transmission of the movement from the aft pulleys to the input torque tube is done through load limiters and rods. Load limiters are used to balance the rudder mechanical system in case one fails. They act in normal operation as push-pull rods, and are used to limit the load applied to the PCU input tube in case of failure. The input torque tube commands the power control unit servovalve and the resulting movement of the actuator creates a feedback that stops the actuator at the desired position. The displacement of the actuators creates a deflection of the rudder within its operating range.

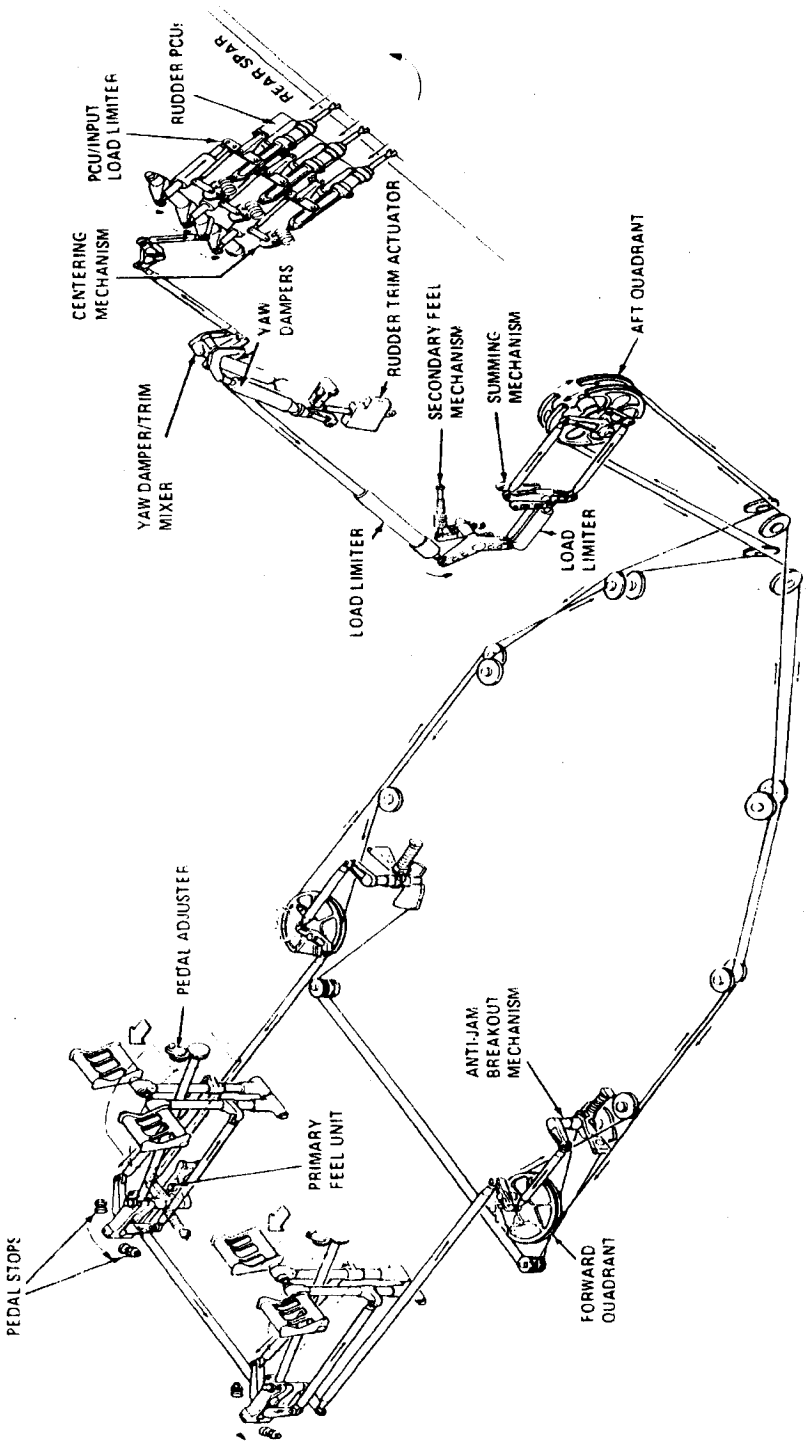

Figure 3.1: Rudder Control System [30]

Figure 3.2 presents a general system model of a typical rudder control system such as the Bombardier Challenger aircraft. The objective of this schematic is to visualize the principles of the rudder control system. The yaw damper and trim assembly will be presented in section 3.2.3. The operating principles in Figure 3.2 are valid only for trim and yaw damper actuators at their neutral positions.

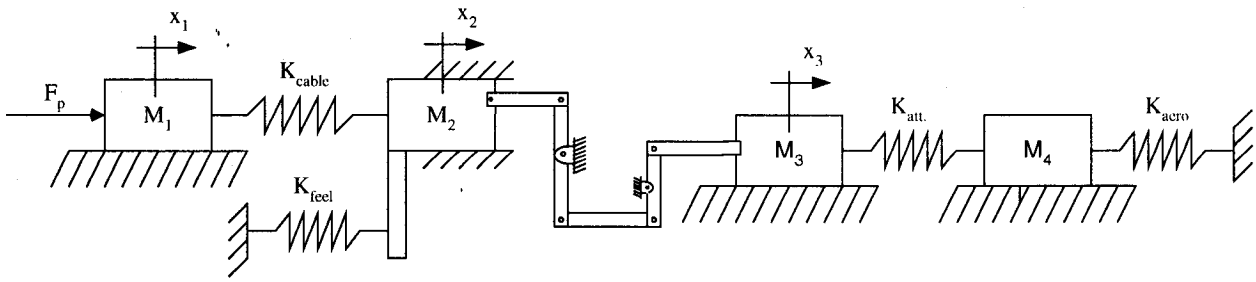

Figure 3.2: Rudder Control System Schematic

The nomenclature used in Figure 3.2 is provided in Table 3.1 below.

Table 3.1: Rudder Schematic Nomenclature

Symbol	Description
M_1	pedal assemblies + forward quadrant masses
M_2	aft quadrant mass
M_3	PCU actuator mass
M_4	rudder control surface mass
x	position of the respective mass
Fp	pilot force
K_{cable}	stiffness of cables
K_{feel}	stiffness of feel unit
K_{att}	attachment stiffness
K_{aero}	aerodynamic stiffness

3.2.2 Primary / Secondary Feel Mechanism

The rudder control system is comprised of two feel mechanisms. The primary feel mechanism consists of a centering cam and a spring-loaded roller that rides on the cam.

The design principle is illustrated in Figure 3.3. A force applied on the pedal forces the roller on the cam, and induces an increasing artificial force feeling. When releasing the force on the pedals, the cam comes back to its neutral position, which is the centering of the rudder pedals. Similar to the primary feel mechanism, the secondary feel mechanism, located after the aft quadrant, provides additional assistance for centering of the rudder and preventing backlash.

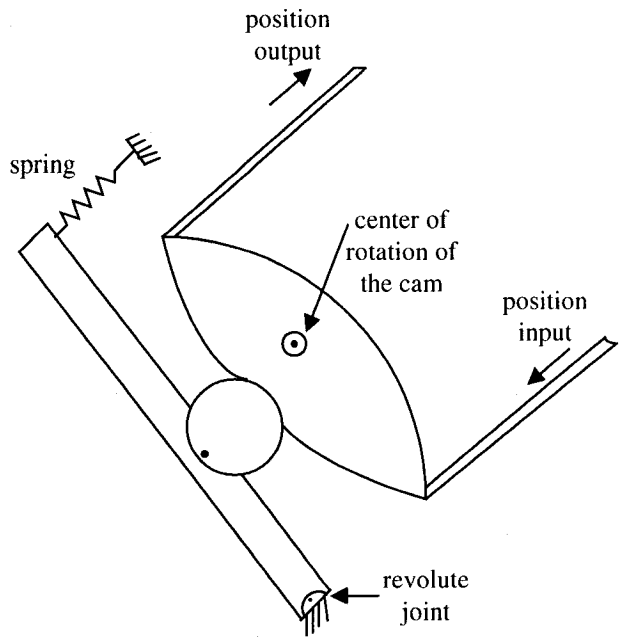

Figure 3.3: Feel Mechanism Principle

3.2.3 Yaw Damper / Trim Assembly

The trim assembly is used to generate input from yaw dampers and trim actuator without pedal motion feedback. Two yaw dampers are attached to the mixer assembly and the walking beam. A yaw damper is an actuator mechanically linked to the rudder control system and driven by a yaw controller. The purpose of the yaw damper (two independent yaw dampers for the Challenger for redundancy) is to improve the damping and stability characteristics of the aircraft, especially those associated with the Dutch Roll mode, i.e.

combined yawing-rolling oscillations. Figure 3.4 presents the principle of the trim assembly. The walking beam can be raised or lowered by using the trim actuator, which is controlled by the pilot. The trim actuator is used to offset the equilibrium point of the rudder control surface. The purpose of the balance springs is to maintain the system in equilibrium in case of a disconnect of one of the mechanical system components.

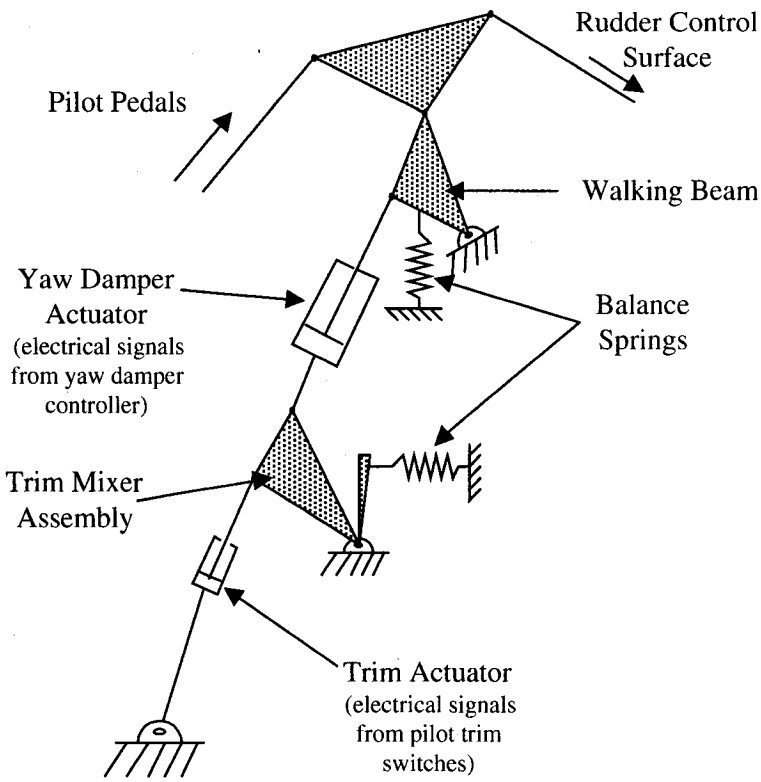

Figure 3.4: Trim / Yaw Damper Assembly Principle

3.3 Power Control Unit (PCU)

3.3.1 Overview of the PCU

Three identical rudder hydraulic power control units accomplish the actuation of the rudder. A PCU is a position hydro-mechanical servoactuator with negative feedback that is powered by a single hydraulic system. Three parallel servoactuators are similarly attached to the aft torque tube, i.e. they receive the same input (refer to Figure 3.1). The rudder PCU schematic is shown in Figure 3.5. It consists of an equal area, double-ended piston and hydraulic cylinder, a manifold housing, and inter-connecting linkages with a differential lever. Inside the manifold housing, there are bypass and relief valves, a check valve and an overlapped spool valve.

Basically, input lever motion opens the control valve and the hydraulic flow goes through the piston chamber. The differential lever provides mechanical feedback. Therefore, when the actuator position corresponds to the pilot's input, the control valve closes, and the desired position is maintained.

As shown in Figure 3.5, the aircraft hydraulic system pump supplies the servo-actuator with a hydraulic fluid at a nominal pressure of 3,000 psi. Hydraulic flow is controlled to the actuator chambers through the control valve. The flow rate in one chamber, and the outflow in the other chamber, creates the piston displacement. The flow rate depends on the pressure differential across the piston.

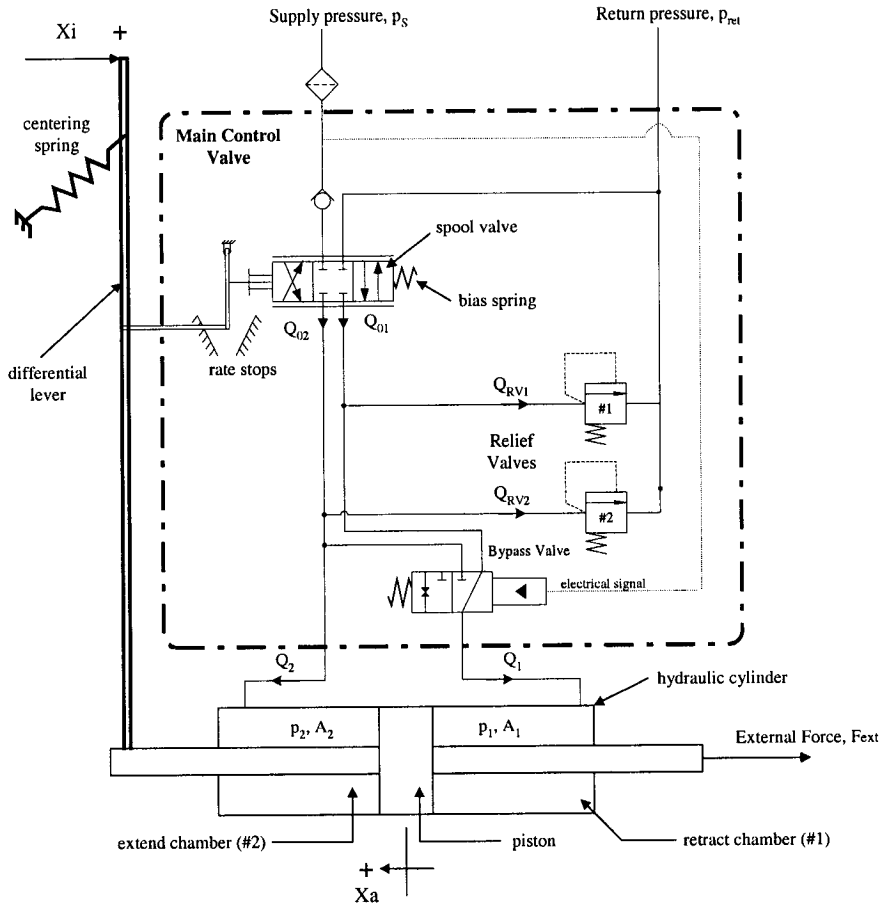

Figure 3.5: Hydraulic PCU Schematic

In this section, the PCU attachment on the aircraft structure is considered rigid. The stiffness of the attachment will be considered when attaching the PCU actuators to the rudder control surface.

3.3.2 Principle of Operation

To illustrate the principles of operation of the PCU, Figure 3.6 presents two snapshots illustrating the actuator displacement. In Figure 3.6a, a position command has just been applied by the pilot; the differential lever has essentially rotated around point C. At this

instant of time, the control valve is fully opened and the hydraulic flow enters to chamber 1; an equal amount of fluid exits chamber 2 to the return lines. The actuator will move and the control valve will gradually be brought back to its neutral position (refer to Figure 3.6b). During motion of the piston, the differential lever rotates about point A until the control valve closes at the point where the actuator has reached its commanded position.

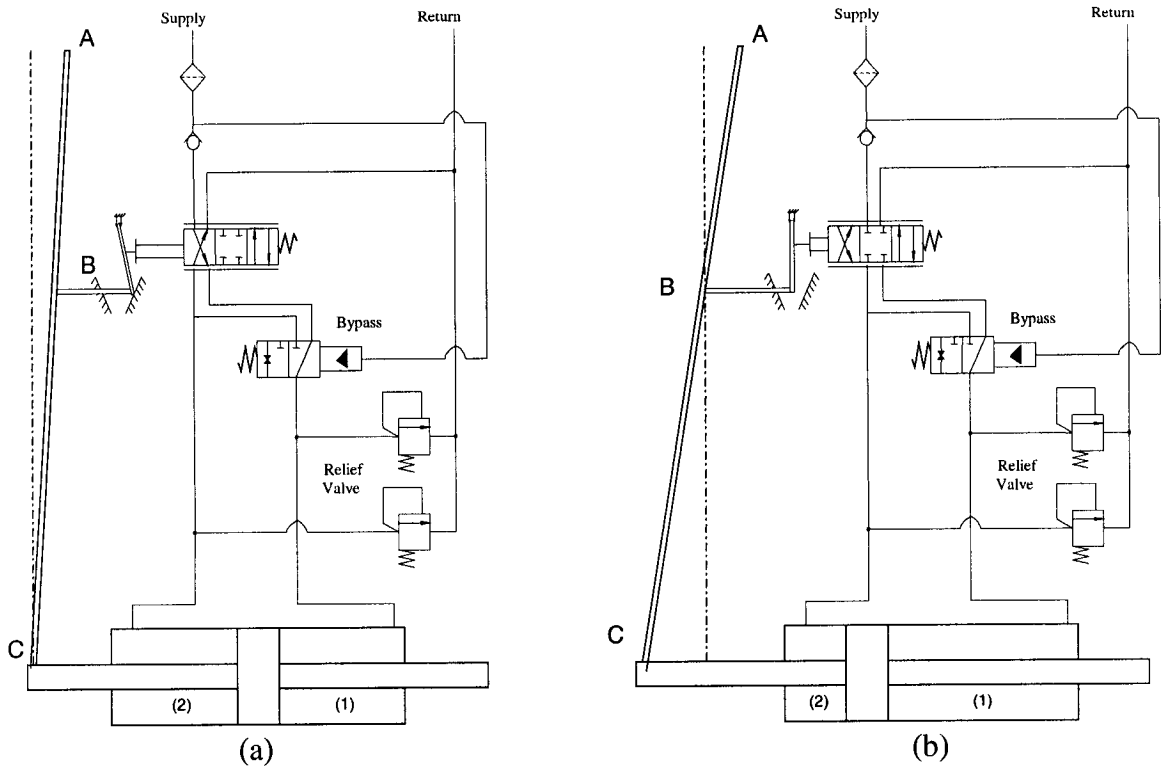

Figure 3.6: Hydraulic PCU Principle

The check valve prevents reverse flow of the hydraulic fluid back to the system pump, i.e. without the check valve and with the hydraulic system pump inoperative, the servoactuator will lose its stiffness since all the fluid will flow into the hydraulic system. This is the case when the pressure inside the inoperative pump is less than the pressure inside the PCU chamber. Without hydraulic fluid, the PCU will no longer maintain external forces and the pilot will lose control of the aircraft; i.e. the rudder surface will be

free to rotate around its hinge line. A bypass valve permits the flow between the cylinder chambers to circulate in close-loop in case of hydraulic system failure. If one PCU fails, it will follow the two other PCU actuators because of the bypass valve. In this case, the failed PCU provides damping to the system.

Anti-cavitation valves on the return line are often used to replace the bypass valve in order to provide retained stiffness. The retained stiffness is the ability of the servomechanism to maintain an external force with small displacement of the actuator when hydraulic systems are off. Anti-cavitation valves are check valves connected to the return line, and they are designed such that the minimum pressure in the PCU hydraulic system is the return pressure (between 75 to 160 psi) so as to avoid cavitation. Cavitation occurs when a liquid (such as oil) moves within tubing or pipes at very fast speeds causing the absolute pressure of the liquid to drop drastically. This process occurs with little loss of heat. If the absolute pressure drops below the vapor pressure of the liquid, cavitation will form. Bubbles appear from dissolved air and the bulk modulus of the hydraulic fluid greatly reduces. The collapse of these bubbles at high pressure may damage the hydraulic system components when exploding. Anti-cavitation valves are often preferred over bypass valves for elevator and aileron control systems because the size of their actuators is normally smaller than the rudder actuator size. Proper sizing of actuators are required to prevent control surfaces from flutter [35,36]. The flutter of a control surface is one of the most dangerous events that can occur in flight. This phenomenon is an aerodynamically induced vibration of the control surface that can result in a total structural failure.

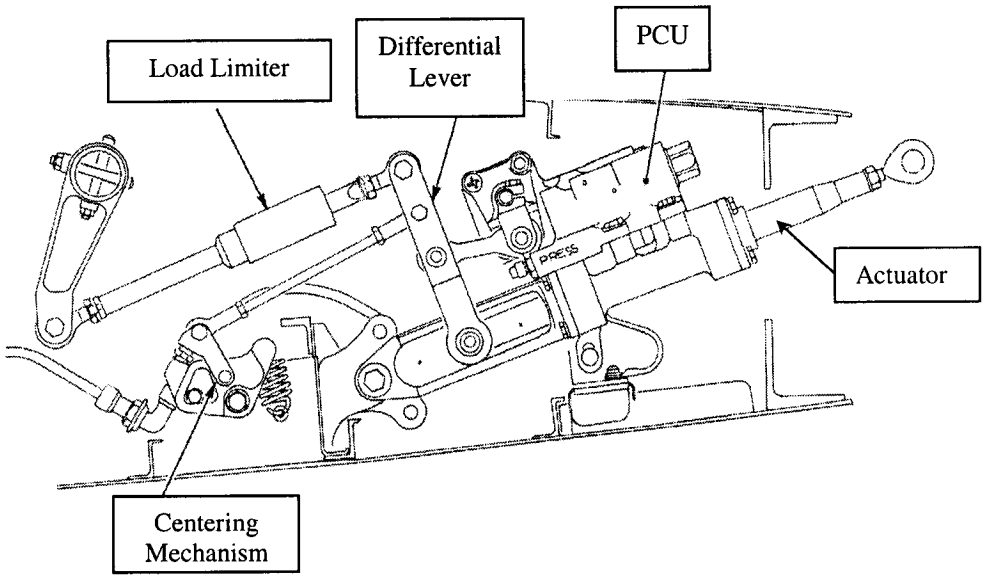

Figure 3.7: Installed Power Control Unit [37]

Various springs in the power control unit are used to reduce backlash in the system by providing centering to the control valve. As shown in Figure 3.5, the bias spring, which is attached to the spool valve, pushes the control valve against the rate stop. The centering spring (centering mechanism in Figures 3.5 and 3.7) fights the bias spring and re-centers the spool valve at its neutral position. Moreover, the centering springs tend to avoid instability of the PCU due to the control valve oscillations. In fact, because of the internal leakages of the control valve, the spool valve always oscillates at very small amplitudes when the system is active. The preload of a spring is the force that the pilot has to be overcome to start to compress the spring. The input load limiter, illustrated in Figure 3.7, is acting as a simple rod in normal operation. If one part of the mechanical system before the torque tube assembly breaks, the load limiter maintains the actuator at its neutral position.

3.3.3 Simplified Power Control Unit Models

Depending on the objective of the analysis, various sophistications of the model may be created for the power control unit. The next sections presents the basic linearized PCU model at no load condition, the linearized PCU model considering the loads on the rudder control surface, and finally a more detailed PCU model developed for this project.

3.3.3.1 Linearized Power Control Unit at No Load

This model shown in Figure 3.8 is necessary to evaluate quickly the performance of the servoactuator. The hydro-mechanical servoactuator is acting like a closed-loop first order system with a fast response. The objective is to evaluate how fast is the PCU response at the no load condition. A simplified model of the servoactuator has the following form:

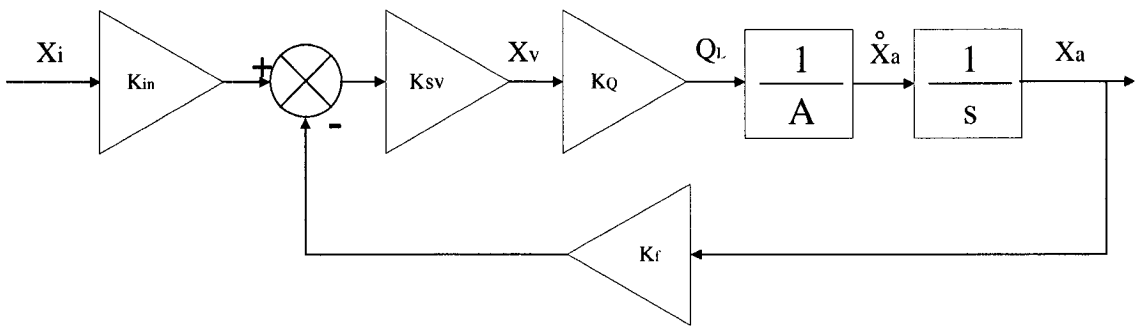

Figure 3.8: Linearized PCU Model at No Load Condition

This model is built from the following equations.

The control valve position (X_v) is (refer to section 3.3.4.1 for detailed derivation):

$$X_v = K_{sv}(K_{in}X_i - K_f X_a) \tag{3.1}$$

Then, the flow rate through the control valve is:

$$Q_L = K_Q \cdot X_v = A \cdot \dot{X}_a \tag{3.2}$$

Therefore the first order Laplace transfer function of the system is:

$$\frac{X_a}{X_i} = \frac{K_{sv} \cdot K_{in} \cdot K_Q}{A \cdot s + K_{sv} \cdot K_f \cdot K_Q} \tag{3.3}$$

The performance of the system is characterized by its frequency response. Figure 3.9 presents the bode plots of the linearized servoactuator.

For a first order system, the system bandwidth based on either 3db gain loss or 45 degrees phase lag is 35.5 rad/sec. This corresponds to a 0.028 seconds time constant.

From the general expression of the first order system, the linearized model can be written as follows:

$$\frac{X_a}{X_i} = \frac{K}{\tau s + K} \tag{3.4}$$

where τ =0.028 seconds, and K=1 since $K_{in}=K_f$. However, the linearized model does not take into account the loads applied on the control surface. The model used for the flight model should consider the aerodynamic loads on the control surfaces.

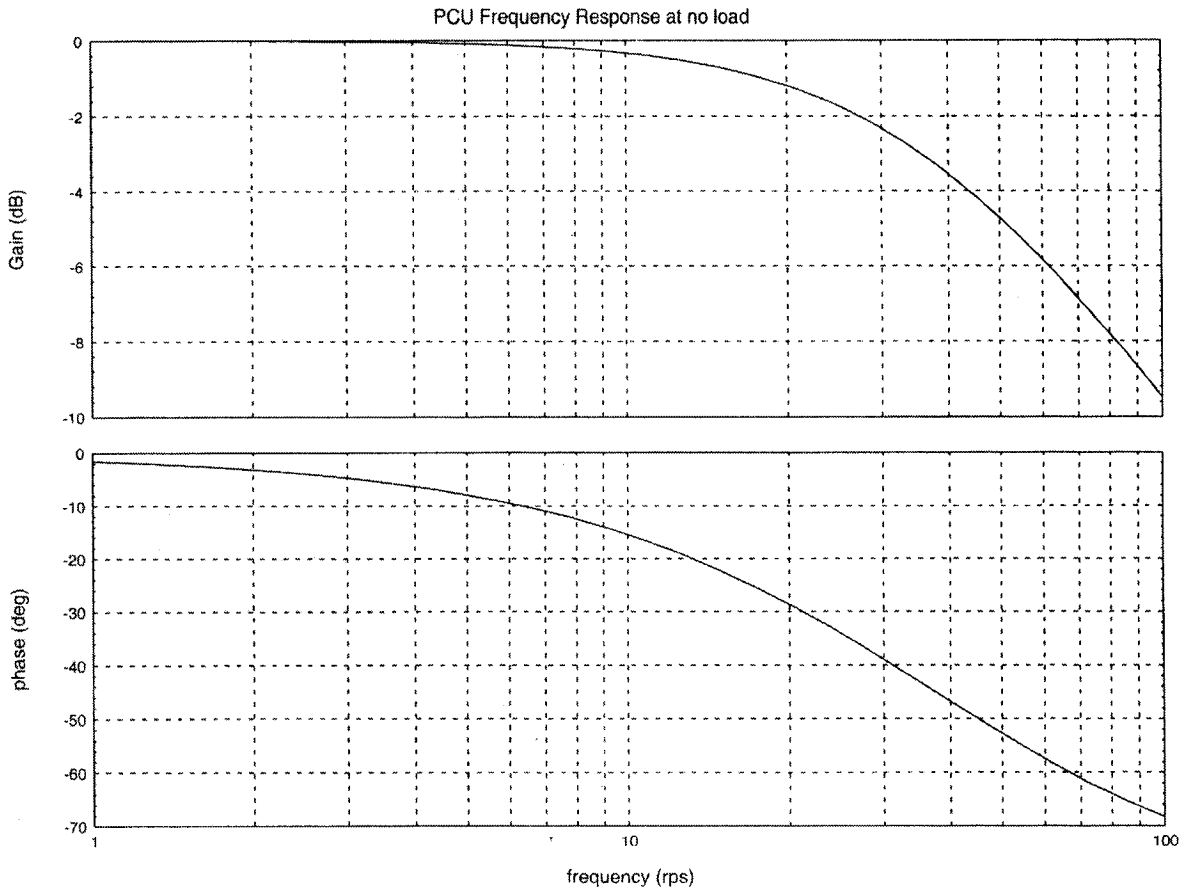

Figure 3.9: Bode Plot of Linearized PCU at no Load

3.3.3.2 Simplified Model Considering the Aerodynamic Loads

Figure 3.10 presents the simplified model that considers the aerodynamic loads on the rudder control surface. In this model, the aerodynamic loads are equally distributed amongst the three servoactuators. The moment arm $R(X_a)$ depends on the position of the actuator relative to the hinge line of the rudder control surface (refer to section 3.4.1 for the formula derivation).

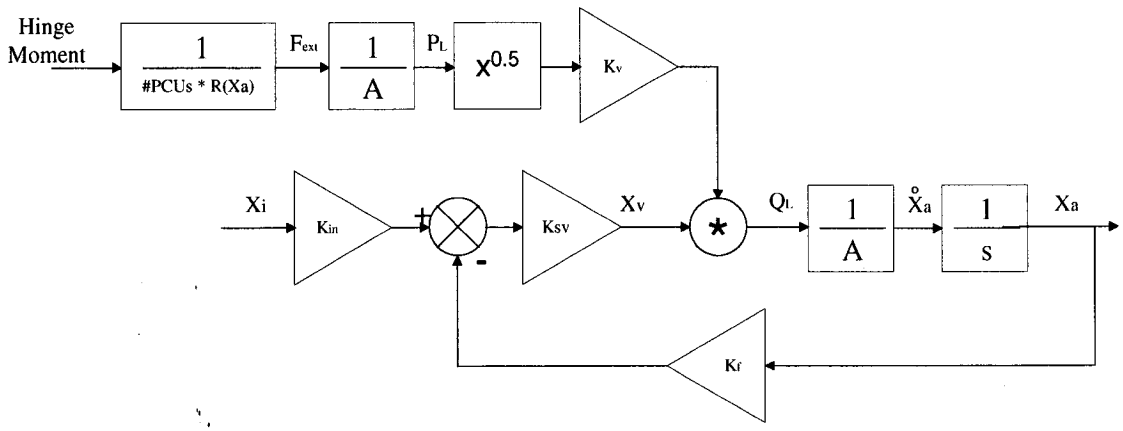

Figure 3.10: Simplified PCU Model Considering Aerodynamic Loads

The hydraulic flows through the control valve are considered as turbulent, and the flow calculation is as follows:

$$Q_L = C_d \cdot w_p \cdot X_v \cdot \sqrt{\frac{2 \cdot \Delta p}{\rho}} \tag{3.5}$$

or

$$Q_L = K_v \cdot X_v \cdot \sqrt{\Delta p} \tag{3.6}$$

where $X_v \cdot w_p$ is the total flow area of the servovalve port. X_v is the stroke of the spool valve, and w is the width of the slot.

However, the servoactuator analysis may be limited to analyze the components of the hydraulic system failures, and a detailed model is preferred to see the effects of the compressible fluid in the system, the friction of the piston seal on the cylinder, the pressure relief valves and so on. Presented in the following sections, is the development of the governing equations for each component of the servoactuator hydraulic circuit.

3.3.4 Detailed Description of the PCU Components

The PCU modeling architecture is shown in Figure 3.11, and presents the methodology followed to develop the power control unit.

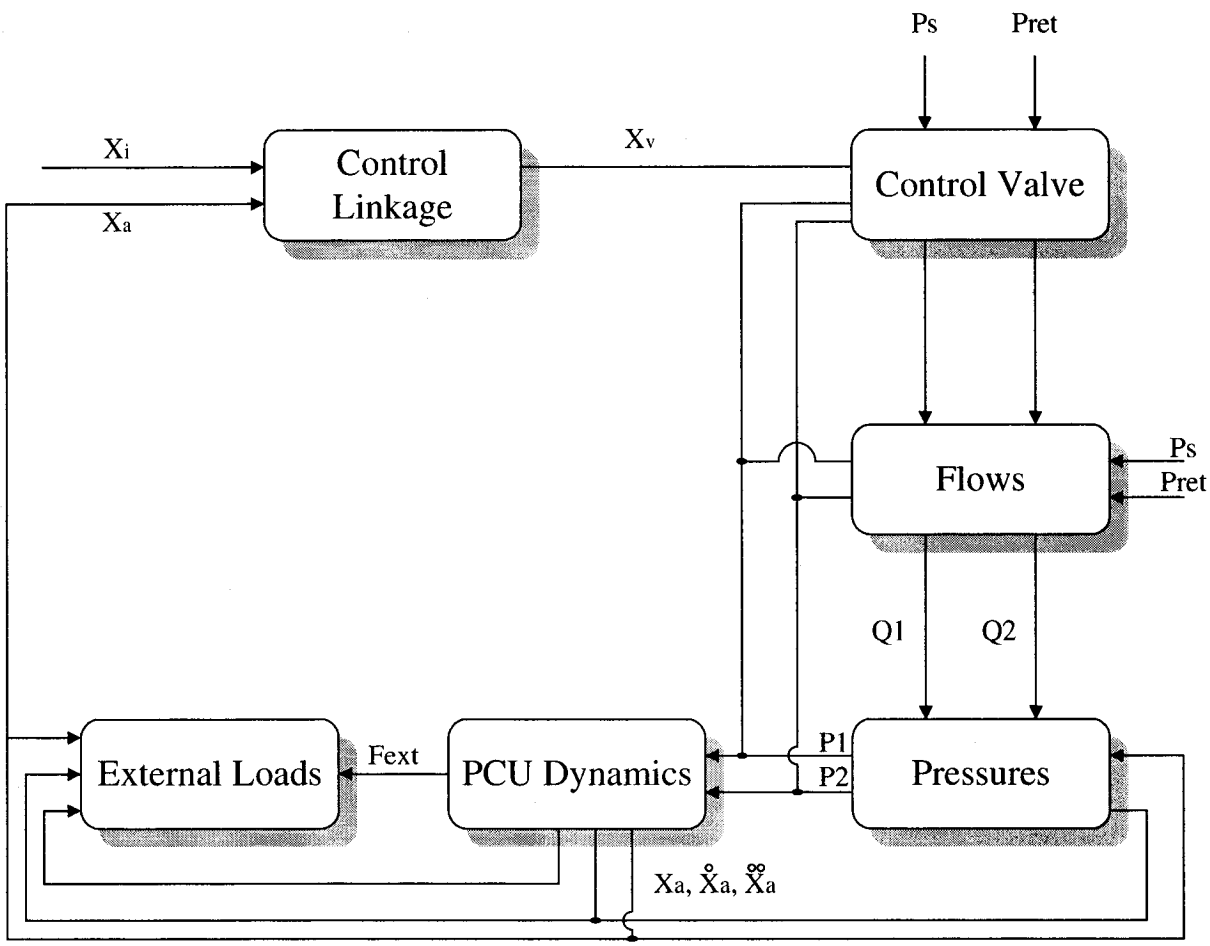

Figure 3.11: Detailed PCU Model

Following the principle of PCU operation (section 3.3.2), the *control linkage* block calculates the kinematic error between the commanded position and the actual position. The *control valve* block calculates the position of the control valve, which distributes the flow through the chambers. The *flows* block calculates the flow rates that enter and exit the hydraulic cylinder chambers. The chamber pressures are calculated in the block

pressures. Then, the dynamics of the actuator is calculated, and depends also on the loads applied on it. The next sections will present each block in detail.

3.3.4.1 Control Linkage:

The PCU linkage provides control valve displacement through a differential lever, also called a summing lever. Piston motion is subtracted from the linkage commanded motion to control the spool valve. The position of the control valve is assumed to be proportional to the error between the input and actuator positions. Figure 3.12 presents the kinematic diagram of the power control unit. For small motion of the differential lever, the control valve position (X_v) is defined as follows:

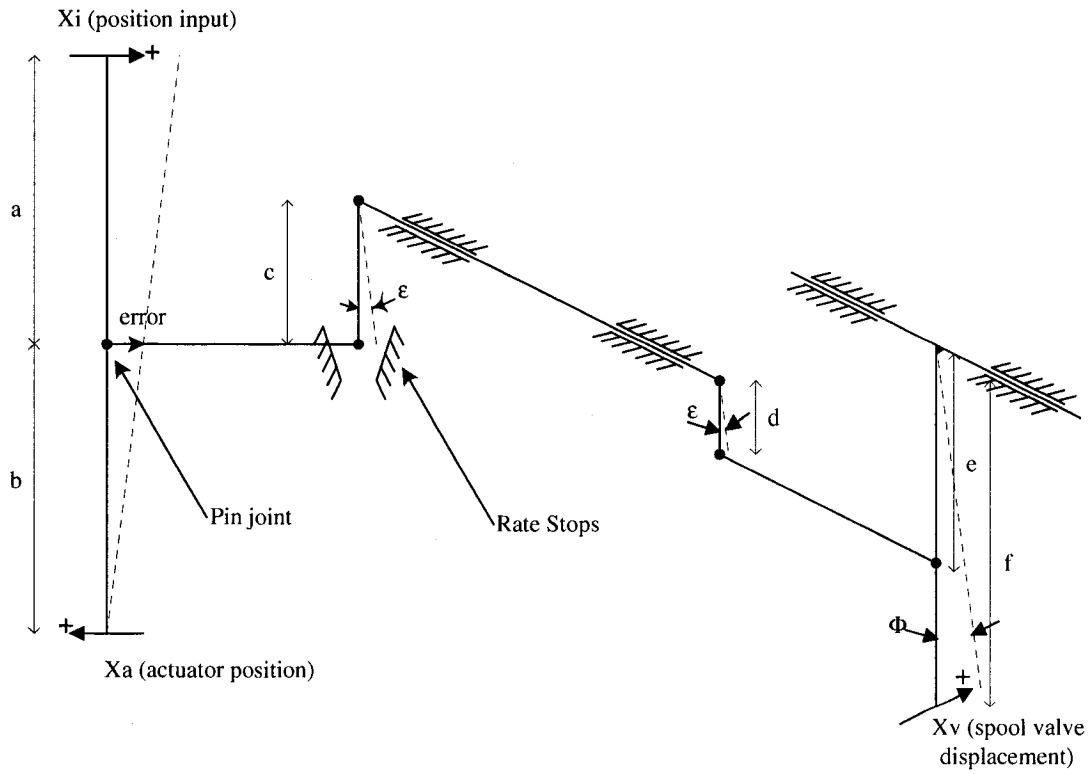

Figure 3.12: PCU Control Linkage, Kinematic Diagram

$$error = \frac{b}{a+b} \cdot X_i - \frac{a}{a+b} \cdot X_a \tag{3.7}$$

The angle ε (small angle) generated by the error is introduced such as:

$$\varepsilon \approx \sin \varepsilon = \frac{error}{c} \tag{3.8}$$

From the crank gain, we have the following relation:

$$X_v = f \cdot \sin \Phi \tag{3.9}$$

$$\Phi \approx \sin \Phi = \varepsilon \cdot \frac{d}{e} \tag{3.10}$$

Therefore,

$$X_v = \frac{error}{c} \cdot \frac{d}{e} \cdot f \tag{3.11}$$

The control valve displacement is:

$$X_v = \frac{1}{c} \cdot \frac{d}{e} \cdot f \cdot \left(\frac{b}{a+b} \cdot X_i - \frac{a}{a+b} \cdot X_a \right) \tag{3.12}$$

Introducing K_{in} the input link gain, K_f the feedback link gain and K_{sv} the servovalve static gain, as given respectively by:

$$K_{in} = \frac{b}{a+b} \tag{3.13}$$

$$K_f = \frac{a}{a+b} \tag{3.14}$$

$$K_{sv} = \frac{1}{c} \cdot \frac{d}{e} \cdot f \cdot \tag{3.15}$$

therefore, equation 3.12 can be written as:

$$X_v = K_{sv} \cdot \left(K_{in} \cdot X_i - K_f \cdot X_a \right) \tag{3.16}$$

Figure 3.14 presents the model of the PCU control linkage, which corresponds to equation 3.16.

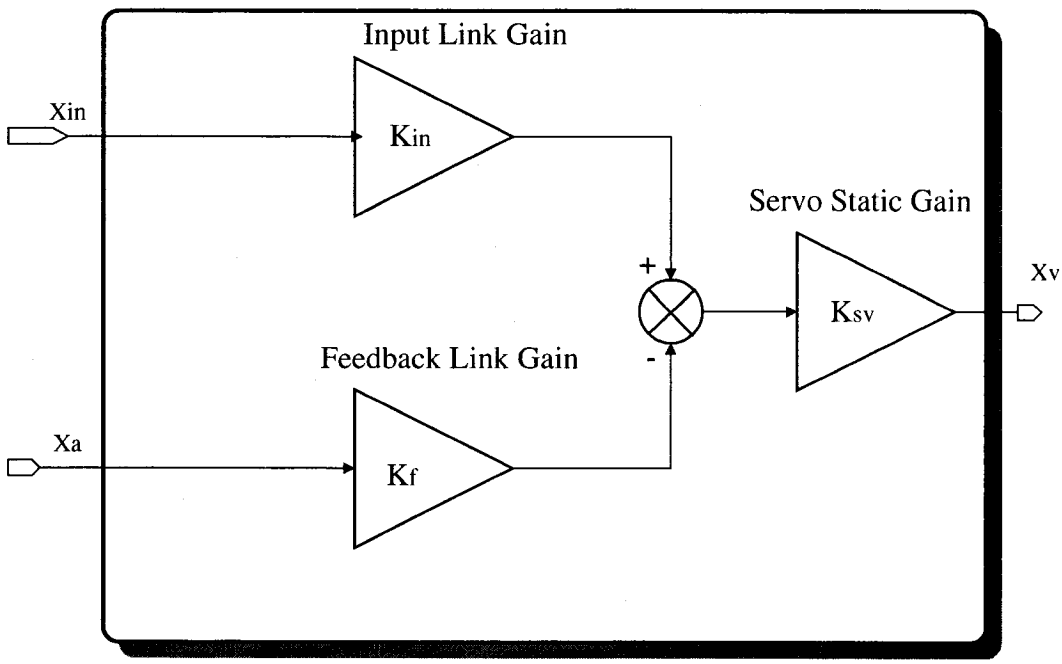

Figure 3.13: PCU Control Linkage Model

3.3.4.2 Control Valve

There are two methods that can be taken to model the flow and dynamics from the control valve. One method is a more detailed model of the control valve including the flow forces acting on the spool valve. A second simpler model is to use a static gain to define the flow as a function of the error generated by the differential lever (refer to section 3.3.4.1).

The equations for a detailed mathematical model of the control valve were developed and are presented in this section as a reference for the next phase of the project. From control theory, the bandwidth of the control valve is well beyond that of the actuator, thus the dynamics of the spool valve will be neglected in this thesis.

The flow forces applied on the spool valve are shown in the Figure 3.14.

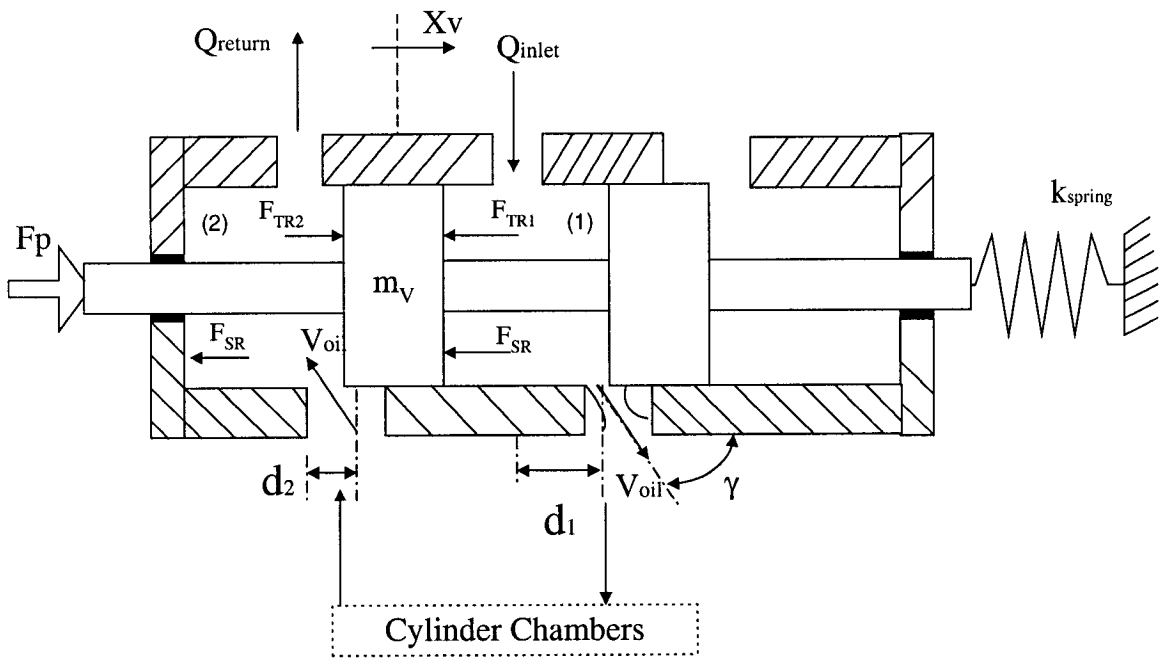

Figure 3.14: Forces Acting on the Spool Valve

The forces acting on the spool valve are the pilot input force (F_p), the spring force, the friction, the flow momentum forces and the transient reaction forces. The mass of the spool valve is considered and is denoted by m_v. The spring force is proportional to the deflection of the preloaded spring. The friction of the spool on the cylinder should be considered (refer to section 3.3.4.6 for friction modelling). The static friction, also called stiction is important in this case, because the radial clearance between the cylinder and the spool has very close tolerances.

The assumptions of the model are the following:

-The inlet and outlet port openings are large compared with the control orifices, therefore these velocities can be ignored.

- The flow is considered as ideal two dimensional flow for an ideal fluid.

- The radial forces are not considered in this model. These forces tends to push the valve spool sideways against the sleeve and cause sticking of the spool against the sleeve. However, it is compensated in practice by locating the valve ports symmetrically around the spool [37].

Considering the steady state flow of the oil through the valve, the fluid momentum force acts on the spool and is parallel to the spool axis, and is represented by F_{SR} [38,39]. This fluid force appears in the two chambers of the control valve, and is given by:

$$F_{SR} = -\rho * V_{oil} * Q_{oil} * \cos\gamma \qquad (3.17)$$

where V_{oil} is the velocity of the oil, and Q_{oil} is the volumetric flow rate and ρ the density of the fluid.

Assuming a constant control port pressure drop Δp and area A_{cv} per unit port opening X_v, F_{SR} can be expressed as:

$$F_{SR} = -\rho * C_d * A_{CV} * X_V * \frac{2 * \Delta p}{\rho} \cos\gamma \tag{3.18}$$

Considering the valve spool to be suddenly displaced to the open position. This will cause the liquid within the chamber to be accelerated and an additional reaction force (transient reaction force F_{TR}) on the spool valve will be created. The brutal displacement of the spool creates a transient force in both chambers of the control valve. In the inlet chamber, the transient force is opposite to the displacement of the control valve due to the compressibility of the fluid. In the return chamber, the transient force helps the spool valve to fully open.

$$F_{TR} = -\rho * A_C * d_v * \frac{dV_{oil}}{dt} \tag{3.19}$$

where A_C is the cross section area of the valve chamber and d_v the distance between the entry and exit ports of the flow. The relationship between the flow rate and the velocity of the flow is the the following:

$$Q_{oil} = A_C * V_{oil} \tag{3.20}$$

therefore,

$$\frac{dV_{oil}}{dt} = \frac{dQ_{oil}/dt}{A_C} = \frac{d\left[C_D * A_{VC} * Xv * \sqrt{\left(\frac{2*\Delta p}{\rho}\right)}\right]/dt}{A_C} \tag{3.21}$$

The transient reaction force (F_{TR}) is thus:

$$F_{TR} = -\rho * d_v * C_d * A_{VC} * \sqrt{\left(\frac{2*\Delta p}{\rho}\right)} * \frac{dX_v}{dt} \tag{3.22}$$

From Newton's Second Law, the spool valve equation of motion is the following:

$$m_v \frac{d^2 X_v}{dt^2} + f_{cv} \frac{dX_v}{dt} + k_{spring} X_v = 2F_{SR} + F_{TR1} - F_{TR2} - F_0 \tag{3.23}$$

where F_0 is the bias spring preload, and,

$$F_{TR1} = -\rho * d_{v1} * C_d * A_{CV} * \sqrt{\left(\frac{2*\Delta p_1}{\rho}\right)} * \frac{dX_v}{dt} \tag{3.24}$$

and,

$$F_{TR2} = -\rho * d_{v2} * C_d * A_{CV} * \sqrt{\left(\frac{2*\Delta p_2}{\rho}\right)} * \frac{dX_v}{dt} \tag{3.25}$$

where Δp_1 and Δp_2 are the pressure drops through their respective chamber. In this case, d_1 and d_2 are equal. The approach to model the control valve was to use a static gain and model the deadband of the overlapped valve and the stops of the spool valve. The next section presents the calculation of the flows through the control valve.

3.3.4.3 Flow equations

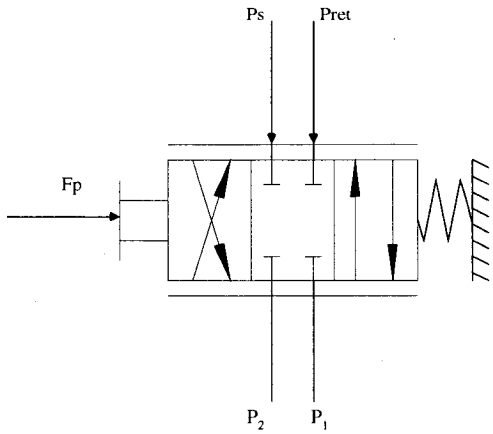

Figure 3.15: Principle Schematic of a Control Valve

The control valve (refer to Figure 3.15) has the important role to distribute the fluid in the cylinder and therefore to control the displacement of the actuator. The flow through the control valve is regulated by varying the size of the orifices. The control valve of a servoactuator usually have sharp edged metering lands and square ports so that the flow versus displacement curve can be linear as shown in Figure 3.16. For a certain position of the actuator to be maintained, the control valve must be closed and the internal leakages must be minimized. Theoretically, the control valve has to be a critically lapped valve to minimize the internal leakages and to improve the performance of the PCU [40].

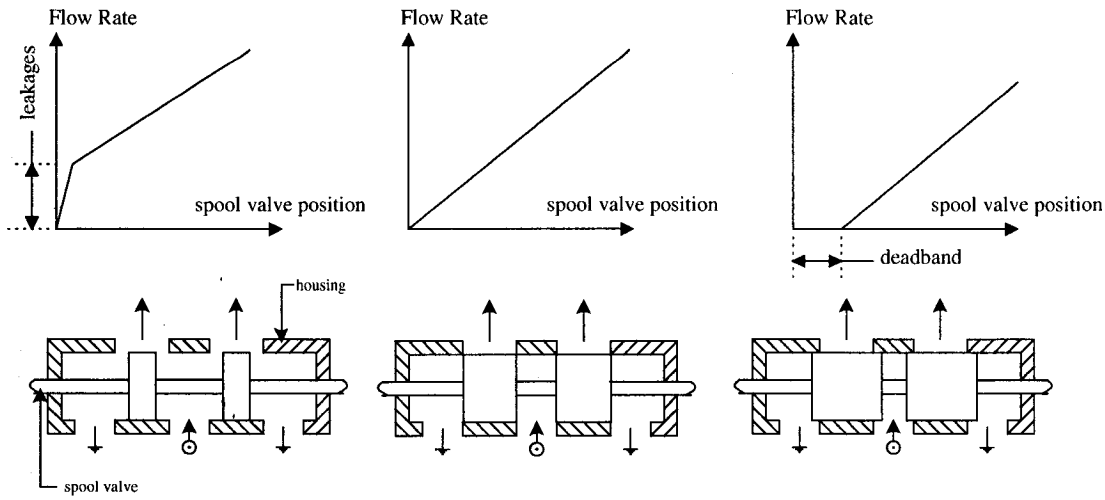

(a) underlapped (b) critically lapped (c) overlapped

Figure 3.16: Control Valve "Lapping" for a Constant Pressure Gradient

The control valve design is the most critical part of the servoactuator. Indeed, the spool valve has to perfectly fit (radially and axially) in the sleeve, and any imperfections can affect the system performance. The leakages of the control valve have to be minimum at relatively high pressure, therefore the geometrical and operational tolerances are important. Overlapped spool valves are often used to reduce leakages from a manufacturing point of view. Ideally, the critically spool valve will be used to drive the servoactuator. Since the design tolerances of the spool valve and the control valve cylinder are so close and difficult to achieve, overlapped valves are chosen. Unfortunately, the overlapped control valve can be a source of backlash in the system due to the deadband shown in Figure 3.16c. If the spool valve moves, and there is no reaction from the system, the distance of which the spool valve have to be moved until the system reacts is defined as the deadband.

A control valve is characterized by its pressure and flow gains when the valve is operating in the linear portion of its control motion.

The flow gain K_Q is defined as:

$$K_Q = \frac{\partial Q_L}{\partial X_v} \tag{3.26}$$

where Q_L is the load flow, and X_v is the control valve displacement.

As shown in Figure 3.16, the flow gain curve is a plot of load flow (Q_L) versus the spool valve stroke (X_v) for a given pressure drop across the servovalve. The flow gain is directly affected by the lap condition.

The pressure gain K_P is defined as:

$$K_P = \frac{\partial P_L}{\partial X_V} \tag{3.27}$$

where P_L is the load pressure.

The pressure gain is presented in Figure 3.17. When the deadband is passed, the pressure gain of an overlapped valve is higher than the underlapped valve because only a slight displacement creates full system pressure on the load port while opening the other to the return line.

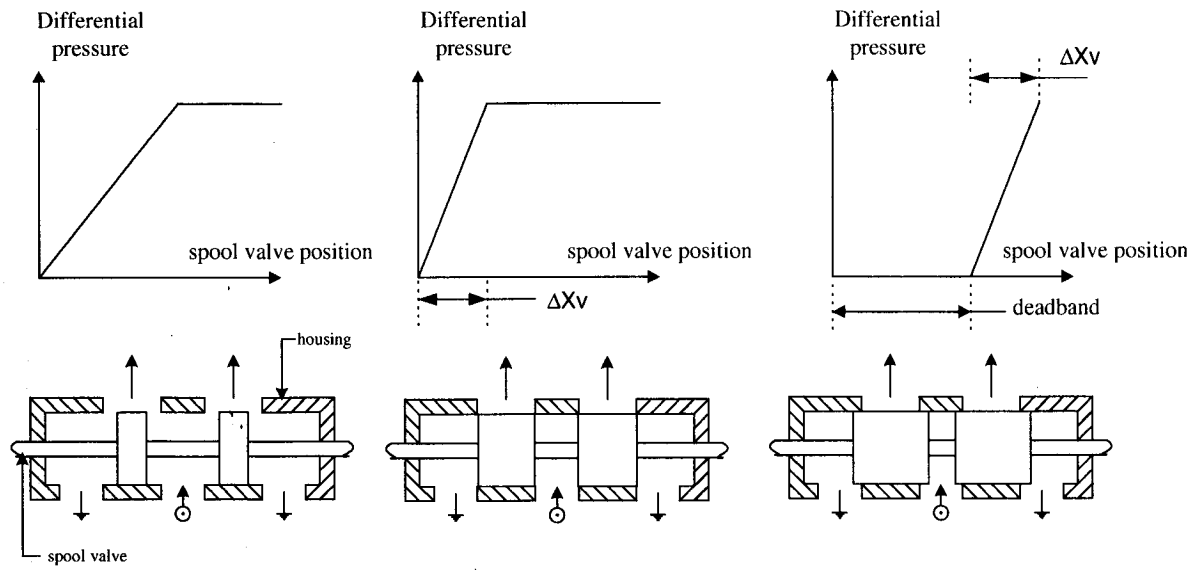

(a) underlapped (b) critically lapped (c) overlapped

Figure 3.17: Pressure Gain for Different Types of Valves

Since most orifice flows occur at high Reynolds numbers, the control valve flows are assumed turbulent, and the following set of equations is used [41]. The control valve displacement is denoted as X_v.

If $X_V \geq 0$

$$Q_{01} = (C_d \cdot w_p \cdot X_V)\sqrt{\frac{2 \cdot |p_S - p_1|}{\rho}} \cdot sign(p_S - p_1) \tag{3.28}$$

$$Q_{02} = (C_d \cdot w_p \cdot X_V)\sqrt{\frac{2 \cdot |p_2 - p_{ret}|}{\rho}} \cdot sign(p_2 - p_{ret}) \tag{3.29}$$

where ρ is the mass density of the fluid and is a temperature dependent factor, and w_p is the width of the ports.

If $X_V < 0$

$$Q_{01} = (C_d \cdot w_p \cdot X_V)\sqrt{\frac{2 \cdot |p_1 - p_{ret}|}{\rho}} \cdot sign(p_1 - p_{ret}) \tag{3.30}$$

$$Q_{02} = (C_d \cdot w_p \cdot X_V)\sqrt{\frac{2 \cdot |p_S - p_2|}{\rho}} \cdot sign(p_S - p_2) \tag{3.31}$$

Figure 3.18 presents the block diagram that calculates the net flow rates that enter (exit) into (from) the piston chambers. The legend is the following: j and k are equal to 1 or 2, but j must have a different value than k. Figure 3.19 also introduces the servovalve leakage and the pressure relief valves.

The internal leakage at the control valve must also be considered when analyzing servoactuators. Studies from Merritt [40] states that an overlapped valve under 0.001 inch of deadband may be considered as a critically lapped valve. As shown in Appendix B, the servovalve under consideration has an overlap less than 0.001 inch.

Figure 3.19 shows the typical internal leakage characteristics of a critical center spool valve. This curve is obtained by cycling the valve through its rated input range with output ports blocked. Leakage flow rate is maximum when the spool valve is at its neutral position.

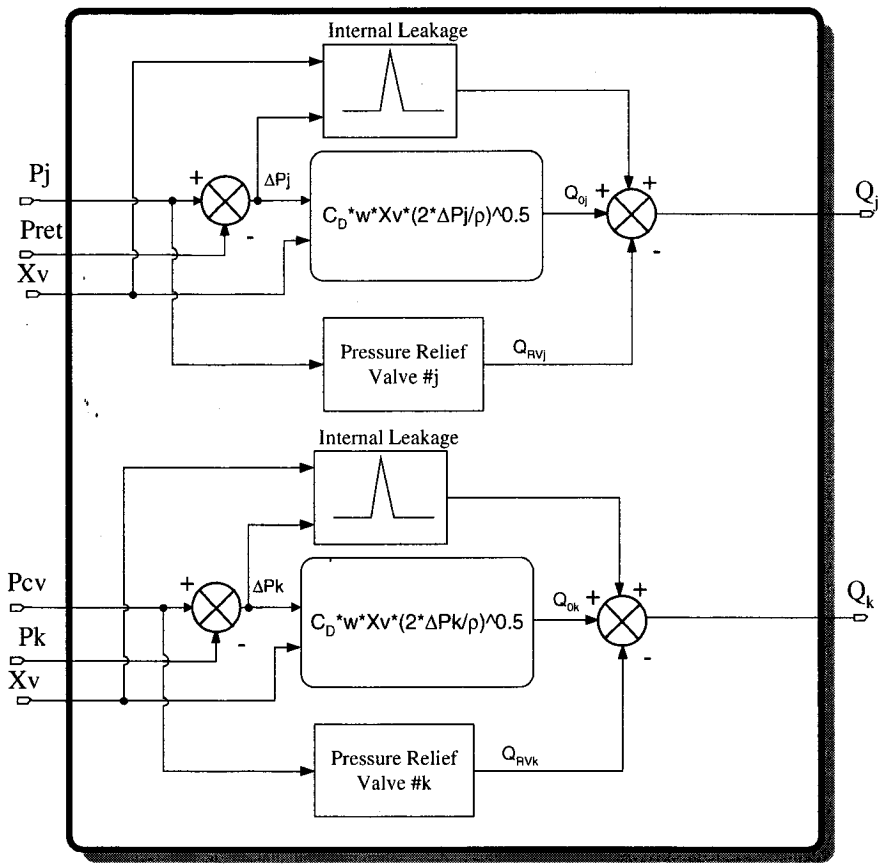

Figure 3.18: Flow Calculation Model

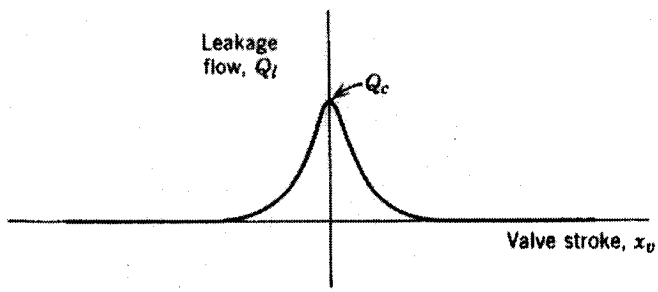

Figure 3.19: Spool Valve Internal Leakage [42]

Qc is called the center flow rate that corresponds to the flow through the valve with blocked load ports and centered spool, and its expression is given by [42]:

$$Q_c = \frac{\pi \cdot w_c \cdot r_c^2}{32\mu} P_s \tag{3.32}$$

where w_c is the area gradient of valve [in^2/in],

r_c is the radial clearance between the spool and the sleeve [in],

μ is the absolute viscosity [lb-sec/in^2],

Ps is the supply pressure [psi],

The internal leakages have to be well designed in order to get adequate static stiffness. The static stiffness is the ability of the PCU to contain external forces with a small actuator displacement. Static stiffness will be explained and developped in Chapter 4 when the performance validation of the PCU will be considered.

3.3.4.4 Pressure Relief Valves

One possibility was that the yaw kick (i.e rudder deflection step) could be the result of the opening or closure of the pressure relief valve. Pressure peaks occuring inside a chamber of the cylinder, would suddenly open the pressure relief valve, and cause a fast displacement of the piston. In fact, only pressure peaks can open the relief valve, thus, first, one may look at what kind of pressure peaks can be generated and in which situation they could occur. Once pressure peaks are understood and simulated, the effects of dynamics of this type of safety valve should be deeply investigated to determine if it could explain the observed yaw kicks. When the valve opens it behaves as a simple orifice with turbulent flow.

For the pressure relief valve linked to chamber i (i=1,2) of the actuator, the flow can be expressed as:

$$Q_{PRVi} = (C_d \cdot A_{PRV}) \sqrt{\frac{2 \cdot |p_i - p_{ret}|}{\rho}} \quad when\ p_i > p_{ret} \tag{3.33}$$

The relief valve is characterized by two important parameters; the cracking pressure (pressure at which the valve opens) and the return pressure (pressure at which the valve closes). Different types of pressure relief valves exist, but PCU manufacturers often use poppet relief valves as shown in Figure 3.20.

The pressure force acting on the poppet is equal to the poppet area (A_P) at its closed position times the pressure of the fluid acting on the poppet, given by:

$$F_{press} = A_P \cdot (P_i - P_{ret}) \tag{3.34}$$

The momentum force (F_m) acting on the relief valve poppet is:

$$F_m = \rho \cdot Q_{PRVi} \cdot V_{PRVi} \tag{3.35}$$

where Q_{PRVi} is the flow rate [in^3/sec], which is coming from the servoactuator cylinder chamber, V_{PRVi} is the velocity of the fluid [in/sec] and ρ is the density of the fluid (oil in this case).

The component of this force that acts parallel to the poppet axis is:

$$F_{mp} = \rho \cdot V_{PRVi} \cdot Q_{PRVi} \cdot \cos\theta_{PRV} \tag{3.36}$$

where the flow rate Q_{PRVi} is given by:

$$Q_{PRVi} = C_d A_{PRV} \sqrt{\frac{2 \cdot \Delta p_i}{\rho}} \tag{3.37}$$

with $\Delta p_i = p_i - p_{ret}$, p_i is the pressure inside one chamber of the cylinder and p_{ret} is the return pressure for the aircraft hydraulic system reservoir.

The force F_{mp} can be expressed as:

$$F_{mp} = 2 \cdot C_d \cdot A_{PRV} \cdot \Delta p_i \cdot \cos\theta_{PRV} \tag{3.38}$$

The momentum force is only active when the poppet starts to move. The spring is preloaded to constrain the valve to open at the given pressure called the cracking pressure. A typical model of the poppet type pressure relief valve is shown in Figure 3.20.

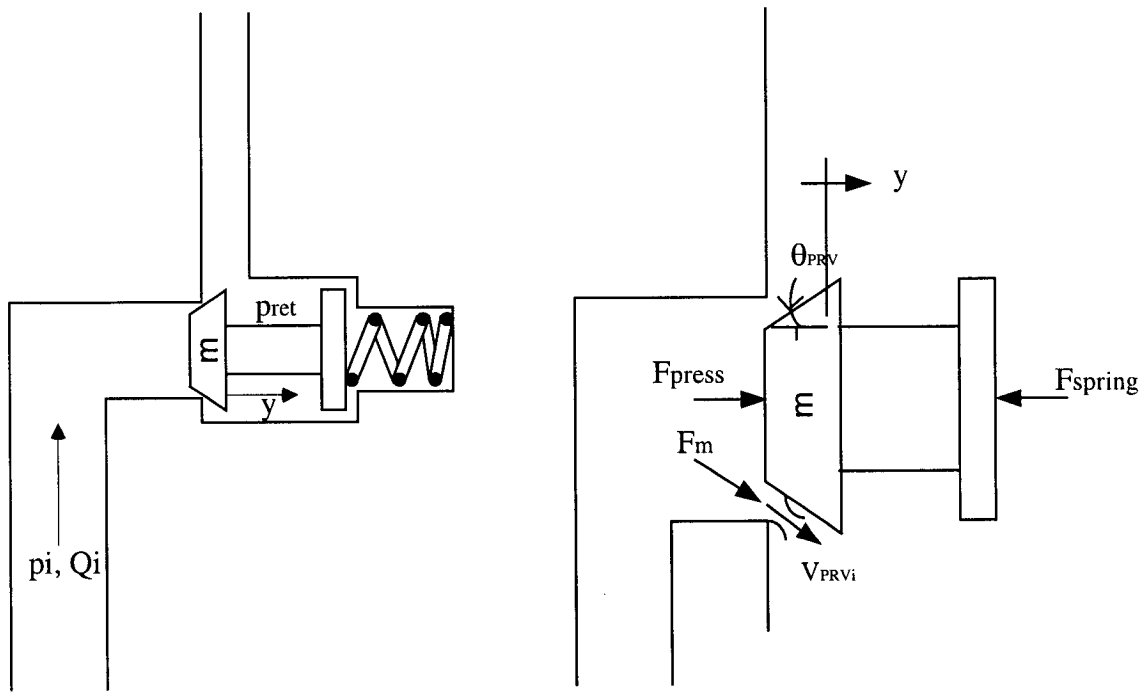

Figure 3.20: Typical Relief Valve Model

The equation of motion for the poppet is:

$$F_{press} + F_{mp} - F_{spring\ preload} = m \cdot \frac{d^2 y}{dt^2} + f_{PRV} \cdot \frac{dy}{dt} + k_{spring} \cdot y \tag{3.39}$$

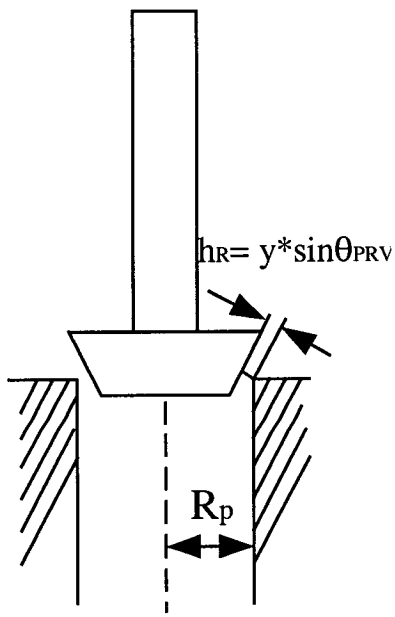

Figure 3.21: Poppet Schematic

The flow area provided by the open pressure relief valve is (Figure 3.21):

$$A_{PRV} = 2 \cdot \pi \cdot R_P \cdot y \cdot \sin\theta_{PRV} \cdot [1 - \frac{y}{2 \cdot R_P} \cdot \sin\theta_{PRV} \cdot \cos\theta_{PRV}] \tag{3.40}$$

$$A_{PRV} = 2 \cdot \pi \cdot R_P \cdot y \cdot \sin\theta_{PRV} \cdot [1 - \frac{y}{2 \cdot R_P} \cdot \sin\theta_{PRV} \cdot \cos\theta_{PRV}] \tag{3.40}$$

For small poppet angle (θ_{PRV}), equation 3.40 becomes:

$$A_{PRV} = 2 \cdot \pi \cdot R_P \cdot y \cdot \sin\theta_{PRV} \tag{3.41}$$

Finally, the force F_{mp} has the following expression:

$$F_{mp} = -C_d \cdot \pi \cdot y \cdot D_p \cdot \Delta p_i \cdot \sin 2\theta_{PRV} \tag{3.42}$$

where $D_p = 2 \cdot R_p$

Figure 3.22 presents the pressure-flow characteristics of the pressure relief valve, when the valve is modeled as a simple orifice. When modeled in more detail, pressure relief valves experience hysteresis because of the friction in the system and the momentum flow forces that are created during the opening and closing of the valve, as shown in Figure 3.23 [43].

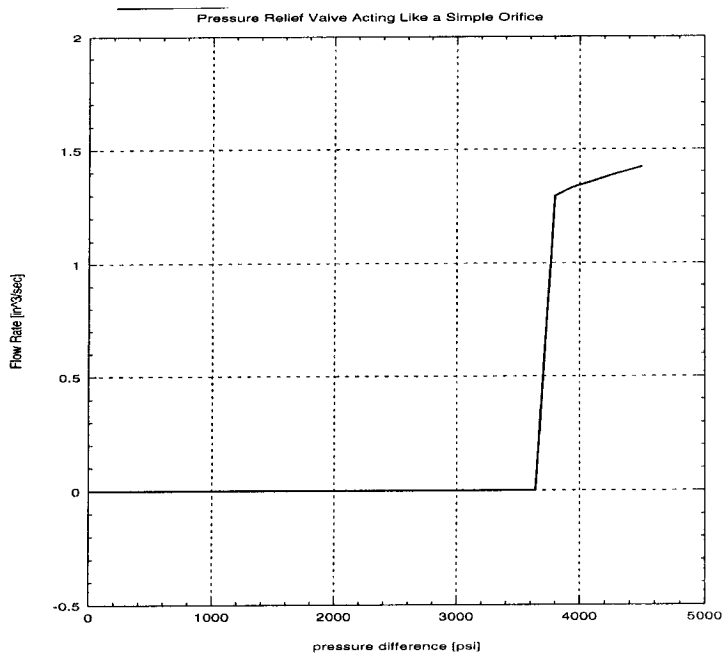

Figure3.22: Simple Pressure Relief Valve Simulation Results

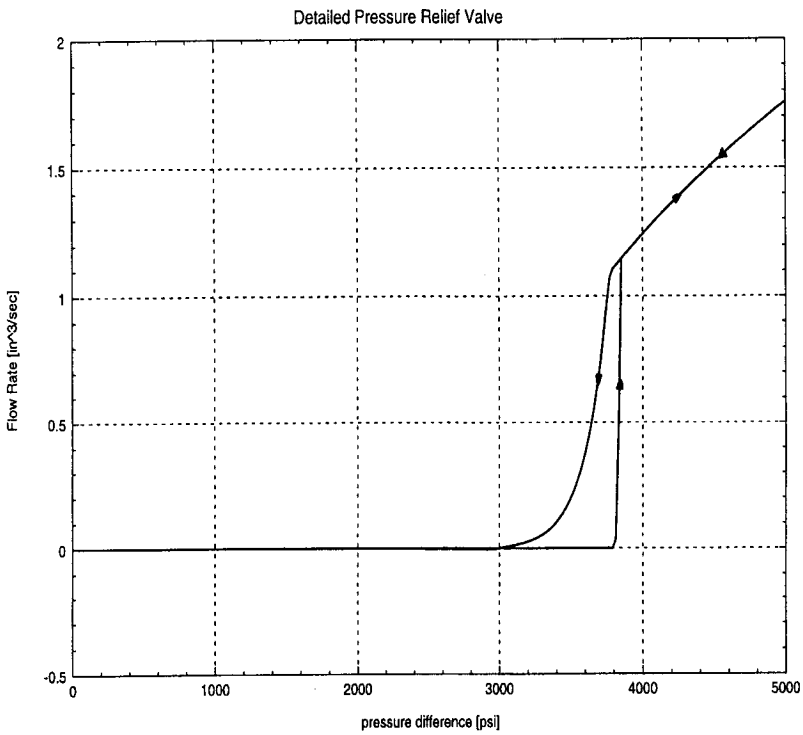

Figure 3.23: Detailed Pressure Relief Valve Simulation Results

3.3.4.5 Check Valve

Figure 3.24 shows the poppet-style check valve placed between the supply pump and the control valve. The check valve is considered wide open at a cracking pressure of 15 psi. The purpose of the check valve is to prevent reverse flow back into the hydraulic source if the PCU system becomes inoperative.

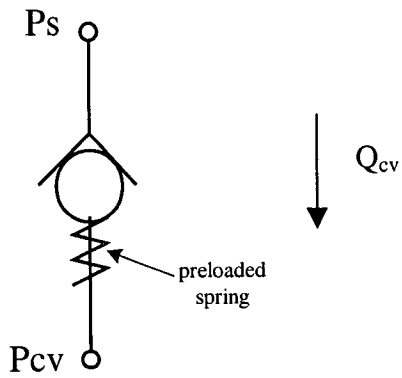

Figure 3.24: Check Valve Principle

The check valve is modelled as a simple switch. If the pressure drop is greater than the cracking pressure drop, then the resulting flow across the check valve (Q_{cv}) is :

$$Q_{CV} = C_d \cdot A_{Check} \cdot \sqrt{\frac{2 \cdot (p_s - p_{cv})}{\rho}} \tag{3.43}$$

However, if the pressure drop is less than the cracking pressure drop, the flow across the check valve is set to zero.

3.3.4.6 Actuator Equations of Motion

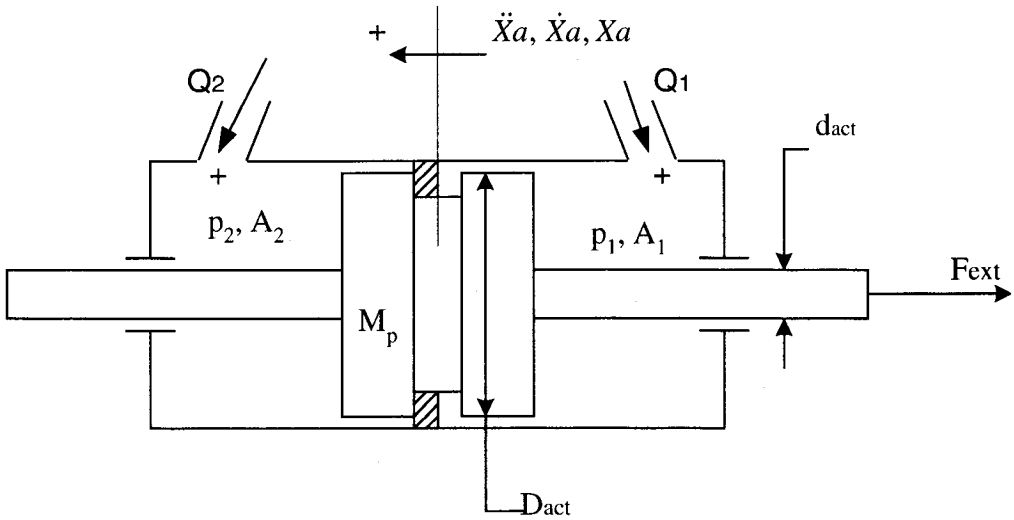

Figure 3.25: PCU Actuator Equations of Motion

From Figure 3.25, the acceleration of the PCU actuator is found from Newton's Second Law:

$$\sum \vec{F}orces = mass \cdot \vec{a}cceleration \tag{3.44}$$

$$A*(p_1 - p_2) - F_{ext} - F_{friction} = M_P \frac{d^2(x_a)}{dt^2} \tag{3.45}$$

For a balanced piston, A is the effective piston area since:

$$A_1 = A_2 = A \tag{3.46}$$

$$\text{where } A = \frac{\pi(D_{act} - d_{act})^2}{4} \tag{3.47}$$

F_{ext} is the external applied force by the rudder. F_{ext} depends on several rudder parameters such as the aerodynamic hinge moment and the weight and inertia of the control surface (refer to section 3.4). By double integration of the actuator acceleration, the displacement

of the PCU actuator is determined. Figure 3.26 presents the corresponding block diagram of the actuator position calculation.

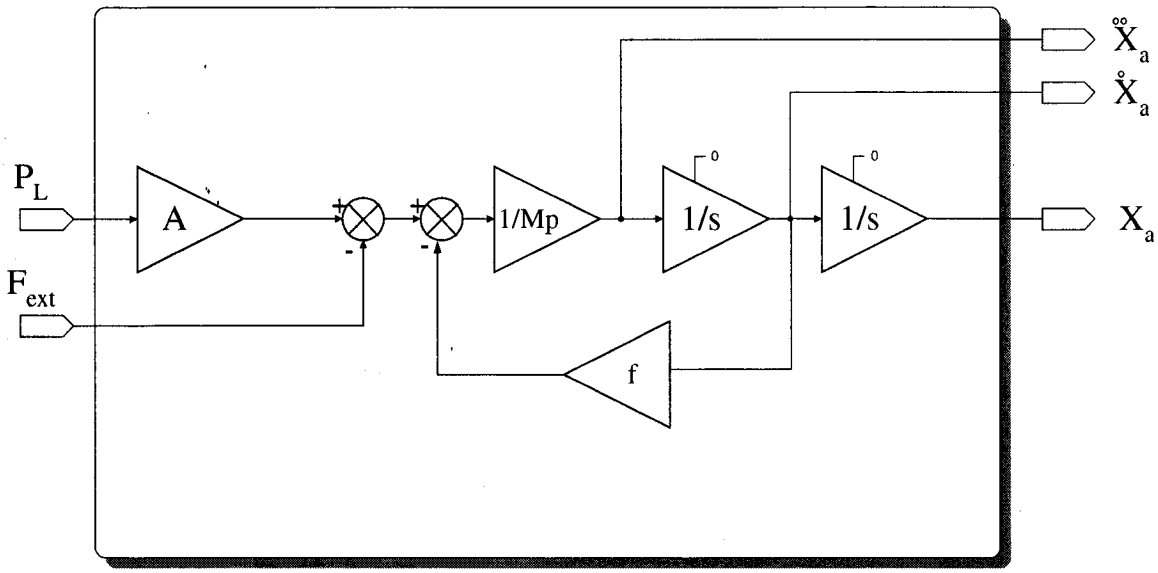

Figure 3.26: PCU Actuator Equations of Motion Model

The piston seal leakage was assumed to be negligible compared to the internal leakage of the control valve. Since during the apparition of yaw kicks, there was no record of PCU component degradation, it was assumed that the piston was working properly and that the leakage was too small to affect the performance of the power control unit.

When a body slides or tends to slide relative to another body or surface, a force tangent to the contacting surfaces is developed which resists the motion as illustrated in Figure 3.27. This force tangent to the contacting surfaces is defined as the friction force. The friction is proportional to the normal load, and its expression is :

$$F_{friction} = \mu \cdot N \tag{3.48}$$

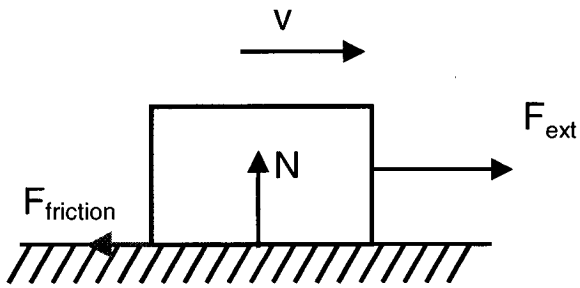

Figure 3.27: Principle of Friction

Friction of the piston on the cylinder is also an important factor and there are various ways to model the friction. A few people investigated and modeled the friction in detail such as Canudas de Vit and Dupont [44,45,46,47] as shown in Figure 3.28.

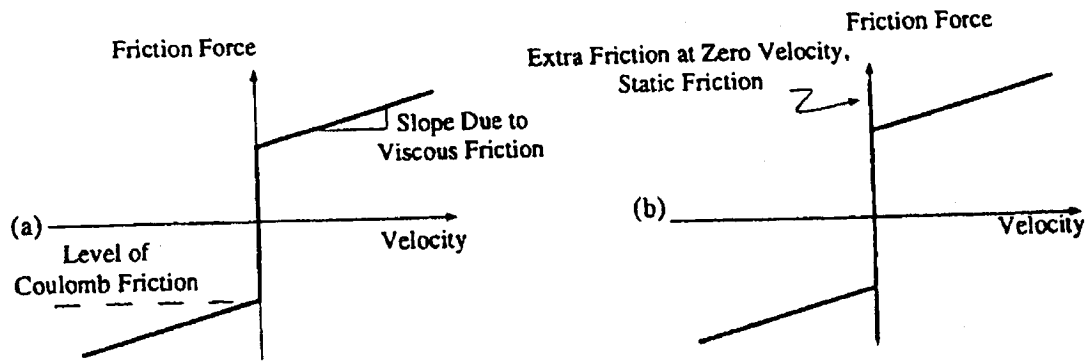

Figure 3.28: Detailed Friction Model [44]

As shown in Figure 3.28, Coulomb friction is the dry friction or the friction that exists between non-lubricated surfaces in contact as opposed to viscous friction, which exists between layers of a fluid moving at different velocities. When a body tends to slide relative to another body or surface, a force tangent to the contacting surfaces is developed

which resists the motion. When no relative motion occurs the friction is called as static friction.

For the present study, only Coulomb and viscous frictions are modelled. The static friction, also called stiction, can be neglected compared to the hydraulic pressure differential. The friction model is shown in Figure 3.29, and the equations can be expressed as:

$$F_{friction} = Fc + \sigma * \dot{x}_a \quad if \quad \dot{x}_a > 0 \tag{3.49}$$

$$F_{friction} = -Fc + \sigma * \dot{x}_a \quad if \quad \dot{x}_a < 0 \tag{3.50}$$

$$F_{friction} = 0 \quad if \quad \dot{x}_a = 0 \tag{3.51}$$

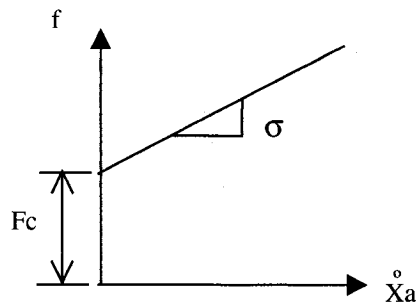

Figure 3.29: Friction Model

3.3.4.7 Actuator Pressure Equations

Applying the continuity equation and considering the compressibility of the fluid to the piston chamber 1 yields (refer to Figure 3.25):

$$\frac{dp_1}{dt} = \frac{\beta_{f1}}{V_1} \cdot \left[Q_1 - A \cdot \frac{dx_a}{dt} \right] \tag{3.51}$$

with the volume of the piston chamber 1, given by:

$$V_1 = V_{O1} + A \cdot x_a \tag{3.52}$$

Thus,

$$\dot{p}_1 = \frac{\beta_{f1}}{V_{O1} + A \cdot x_a} \cdot [Q_1 - A \cdot \dot{x}_a] \tag{3.53}$$

Similarly, the time rate of change of pressure in chamber 2 is:

$$\frac{dp_2}{dt} = \frac{\beta_{f2}}{V_2} \cdot \left[Q_2 + A \cdot \frac{dx_a}{dt} \right] \tag{3.54}$$

with the volume of the piston chamber 2, given by:

$$V_2 = V_{O2} - A \cdot x_a \tag{3.55}$$

However, it is assumed that the initial volumes of the return and forward chambers are equal,

$$V_O = V_{O1} = V_{O2} \tag{3.56}$$

therefore,

$$\dot{p}_2 = \frac{\beta_{f2}}{V_{O1} - A \cdot x_a} \cdot [Q_2 + A \cdot \dot{x}_a] \tag{3.57}$$

When considering the compressibility of the fluid, the bulk modulus coefficient is introduced. It is assumed constant in each piston chamber.

$$\beta_f = \beta_{f1} = \beta_{f2} \tag{3.58}$$

At a constant temperature, the bulk modulus β is the change in pressure divided by the fractional change in volume. It can decrease sharply with small amounts of air entrained in the liquid and mechanical compliance in the system. The natural frequency of the

servomechanism is defined by the bulk modulus (spring effect of the liquid) and the mass of the mechanical parts. However, the effective bulk modulus has to be introduced to represent a more realistic fluid behavior, it depends on the fluid type, the working temperature and pressure, the entrained air amount and the cylinder material. [48,49]

Figure 3.30 presents the block diagram for the calculations of cylinder pressures.

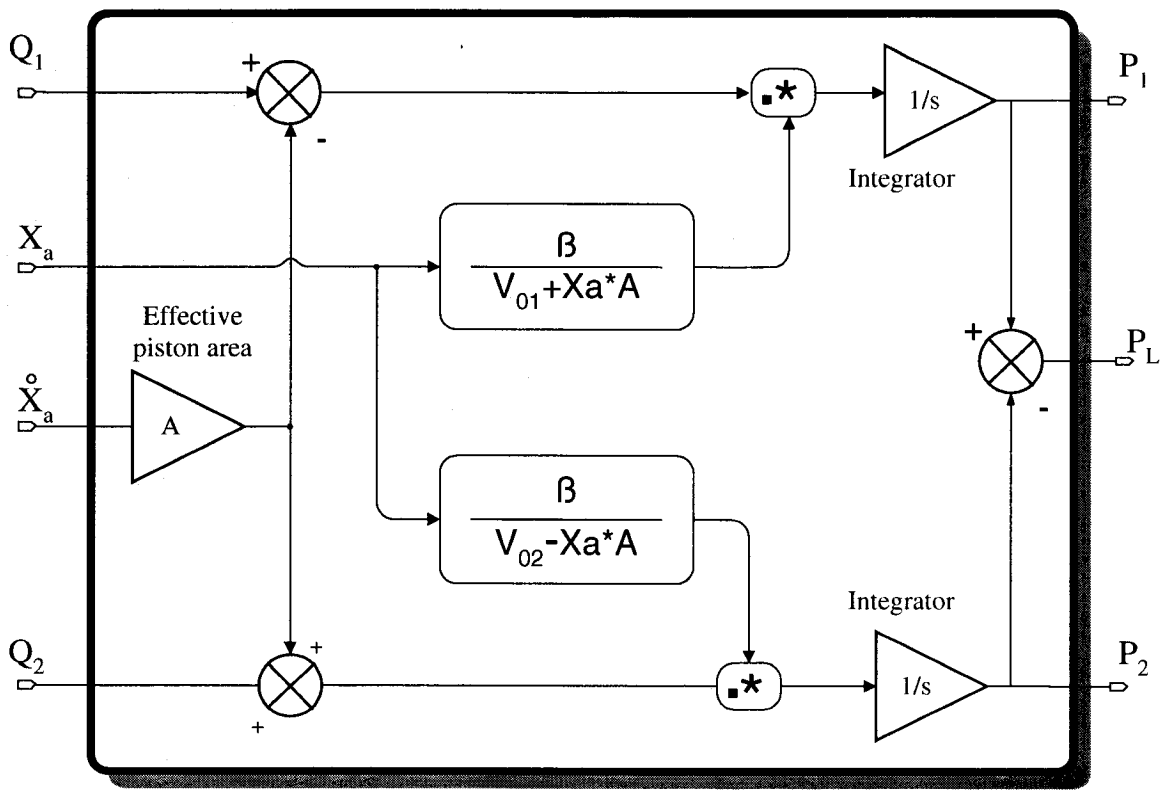

Figure 3.30: Pressure Calculation Block Diagram

3.4 Rudder Control Surface

3.4.1 Power Control Unit Kinematics

The mechanical linkage between the PCUs and the rudder surface has to be analyzed and modeled in order to determine their interactions for the possibilities of "force fight"

between the servo-actuators. The aerodynamic loads applied on the rudder control surface may be shared inadequately by the three servo-actuators, because of deadband, backlash or friction in the mechanical assembly. Therefore, each servo-actuator may respond differently to the pilot input, and they may start to "fight" when reaching the commanded position.

The aerodynamic moment is applied to the rudder surface, and the moment arm between the PCU and the surface is not constant. As shown in Figure 3.31 and from the cosine law, the kinematic relationship between the PCU displacement and the commanded rudder angle can be determined as:

$$L_1^2 + R_{PCU}^2 - L_3^2 = 2 \cdot L_1 \cdot R_{PCU} \cdot \cos\alpha \tag{3.58}$$

$$L_1^2 + R_{PCU}^2 - L_3^2 = 2 \cdot L_1 \cdot R_{PCU} \cdot \cos(\theta_{crank} - \delta_{xa}) \tag{3.59}$$

Therefore,

$$\delta_{xa} = \theta_{crank} - a\cos\left(\frac{L_1^2 + R_{PCU}^2 - L_3^2}{2 \cdot L_1 \cdot R_{PCU}}\right) \tag{3.60}$$

Where $L_3 = L_2 - Xa$, and θ_{crank} is constant defined when the rudder is at its neutral position.

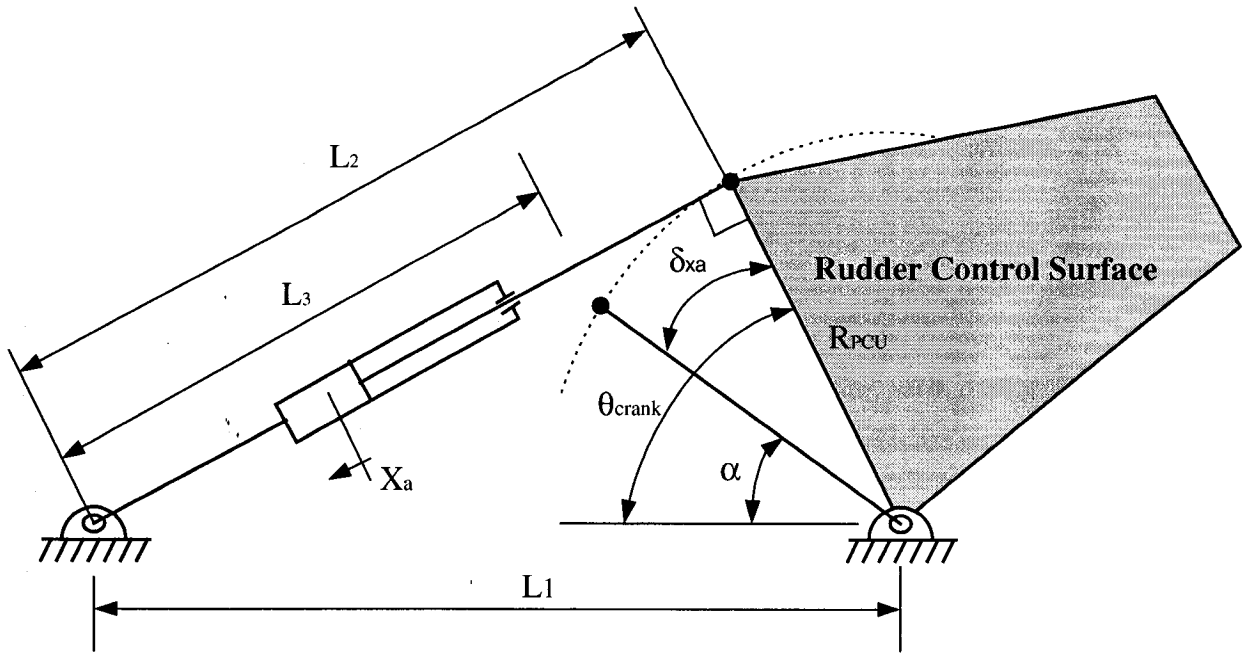

Figure 3.31: PCU to Rudder Surface Kinematics

The kinematic relation (equation 3.58) between the actuator position (X_a) and the commanded rudder angle (δ_{xa}) can be rewritten as:

$$X_a = L_2 - \sqrt{L_1^{\,2} + R_{PCU}^{\,2} - 2 \cdot L_1 \cdot R_{PCU} \cdot \cos(\theta_{crank} - \delta_{xa})} \tag{3.61}$$

The moment arm $R(X_a)$ is given by the relation between the actuator rate and the rudder angular velocity (method of virtual work) [50]:

$$R(X_a) = \frac{dX_a}{d\delta_{xa}} \tag{3.62}$$

Then, from equations 3.61 and 3.62, $R(X_a)$ has the following expression:

$$R(X_a) = \frac{L_1 \cdot R_{PCU} \cdot \sin(\theta_{crank} - \delta_{xa})}{\sqrt{L_1^2 + R_{PCU}^2 - 2 \cdot L_1 \cdot R_{PCU} \cdot \cos(\theta_{crank} - \delta_{xa})}} \tag{3.63}$$

Therefore, this moment arm will be used to transform the hinge moment applied on the rudder into a force in the PCU actuator.

3.4.2 Rudder Panel Motion Equation

When looking at the moments applied on the rudder, the equation of motion of the rudder control surface is (refer to Figure 3.32):

$$I_R \ddot{\delta}_R = K_H \cdot (\delta_{xa} - \delta_R) - M_{aero} - B \cdot \dot{\delta}_R \tag{3.64}$$

where I_R is the moment of inertia of the rudder control surface at the hinge line. K_H is the attachment stiffness from the attachment joint between the rudder panel and the PCU. B is the structural damping coefficient. δ_R is the actual rudder angle.

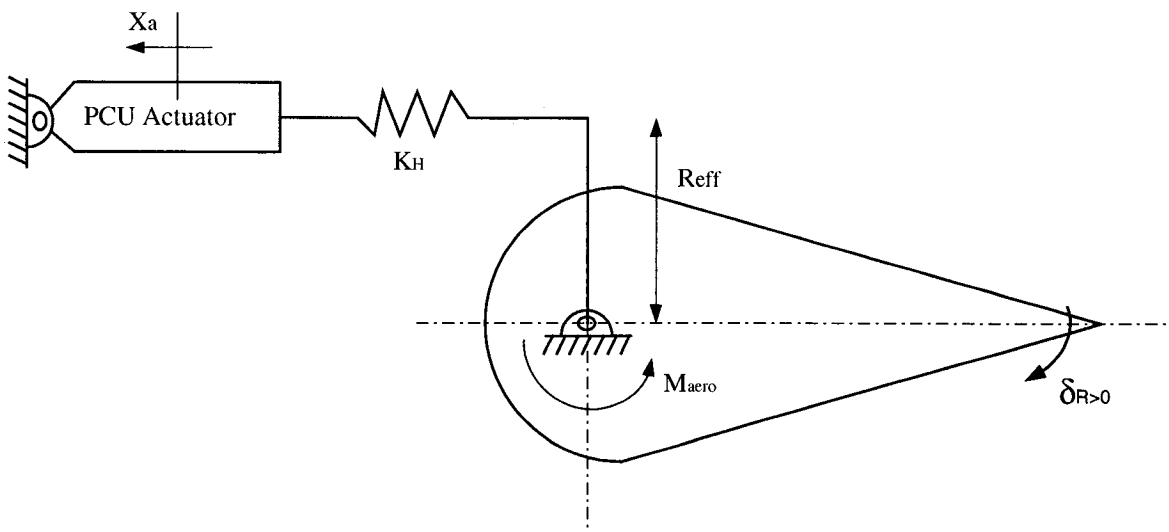

Figure 3.32: Rudder Panel Motion Equations

Due to the inclination of the rudder control surface on the vertical stabilizer, the weight of the rudder tends to center the surface to its neutral position. This damping effect of the weight is lumped in the model to the backup structural damping (B).

When considering three PCUs, equation 3.64 becomes:

$$I_R \ddot{\delta}_R = K_H \cdot [(\delta_{xa}(up) - \delta_R) + (\delta_{xa}(mid) - \delta_R) + (\delta_{xa}(low) - \delta_R)] - M_{aero} + B \cdot \dot{\delta}_R \quad (3.65)$$

Practically, the three servoactuators do not have the same performance. The torsion of the surface between the points of attachment of the PCU have to be considered. The torsion stiffness of the rudder control surface is introduced, and this leads to the analysis of force fight of the PCUs when they do not have the same performance (refer to section 3.4.4).

Figure 3.33 presents the model of the PCUs and rudder assembly:

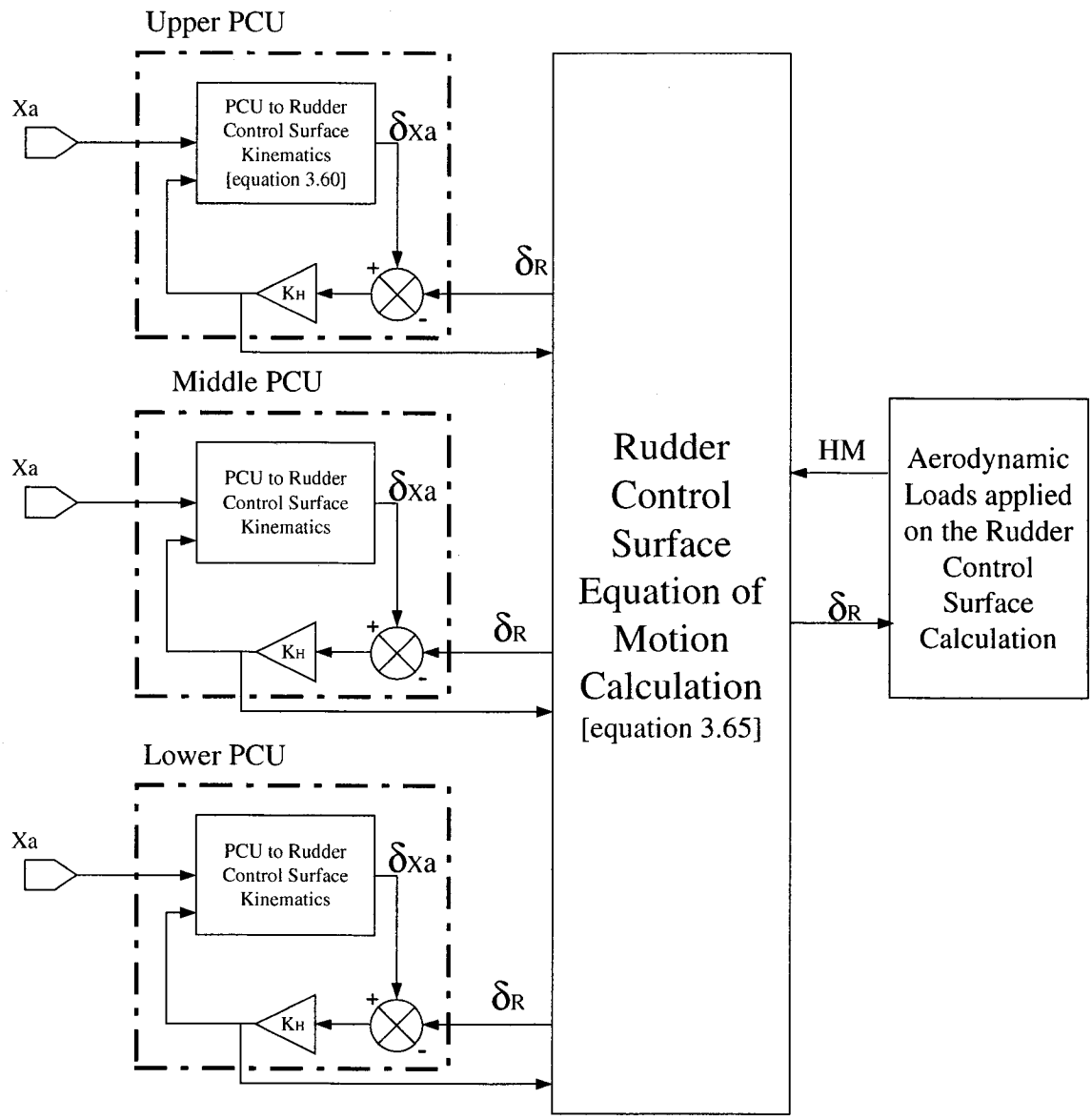

Figure 3.33: PCUs – Rudder Assembly

3.4.3 Aerodynamic Loads Applied on the Rudder Control Surface

Aerodynamic loads (also called "Hinge Moments") are applied on the rudder control surface when it deflects. The hinge moment is acting at the hinge line of the rudder control surface. It is the moment the pilot has to overcome by exerting a force on the

rudder pedal. The hinge moment depends on different factors such as the dynamic pressure (airspeed of aircraft and ambient air density) and sideslip angle.

The expression for the aerodynamic hinge moment (M_{aero}) is [51]:

$$M_{aero} = \frac{1}{2} \cdot \rho_{air} \cdot V^2 \cdot C_{hR} \cdot S_R \cdot C_R \tag{3.66}$$

Where C_{hR} is the hinge moment coefficient that is mainly a function of the sideslip angle, the rudder deflection and the airspeed of the aircraft. S_R is the area aft of the hinge line, and C_R is the chord measured from the hinge line to the trailing edge of the control surface as shown in Figure 3.34.

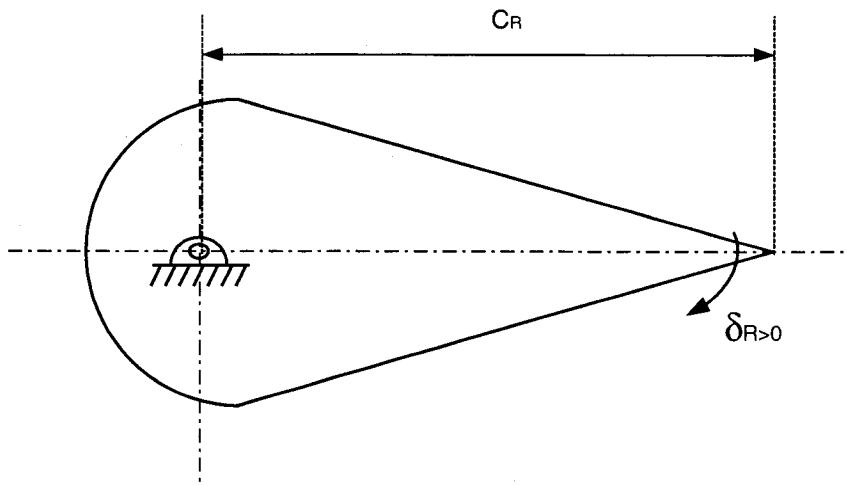

Figure 3.34: Rudder Control Panel

3.4.4 Force Fight between PCUs

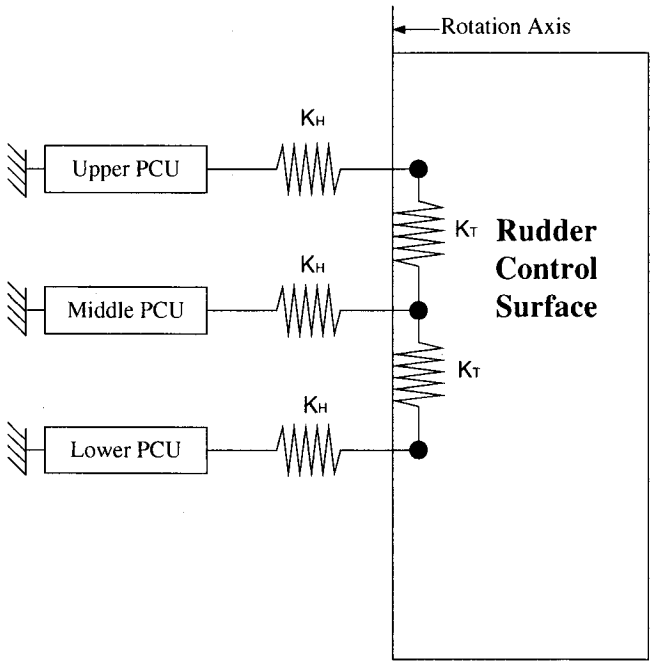

Figure 3.35: Force Fight Analysis

When acting on the rudder pedals, the pilot commands a PCU displacement that results in a force applied to the rudder surface. Together, the three PCUs apply a resulting force to the rudder surface that fights the control surface aerodynamic hinge moment. Because of the mechanical system compliance, manufacturing tolerances and PCU assembly, all three PCUs do not give the same input force on the rudder surface. This phenomenon may result in pressure increase that are different for each of the three PCU hydraulic cylinder chambers. The force fight between the servoactuators can create also a small torsion of the rudder attachment. The torsion is taken into account to reflect the small deformation of the rudder control surface as shown in Figure 3.35. The purpose of this analysis is to see the effect of the force fight on the PCU performance. The simulation results are presented in Chapter 4, section 4.8.

3.5 Integration of Flight Controls in Flight Model

3.5.1 Flight Model Architecture

Figure 3.36 presents the model architecture. Detailed PCU models were introduced in the aircraft rudder control system. The implementation of the PCUs in the full flight model is done in order to investigate the possible source of yaw kicks.

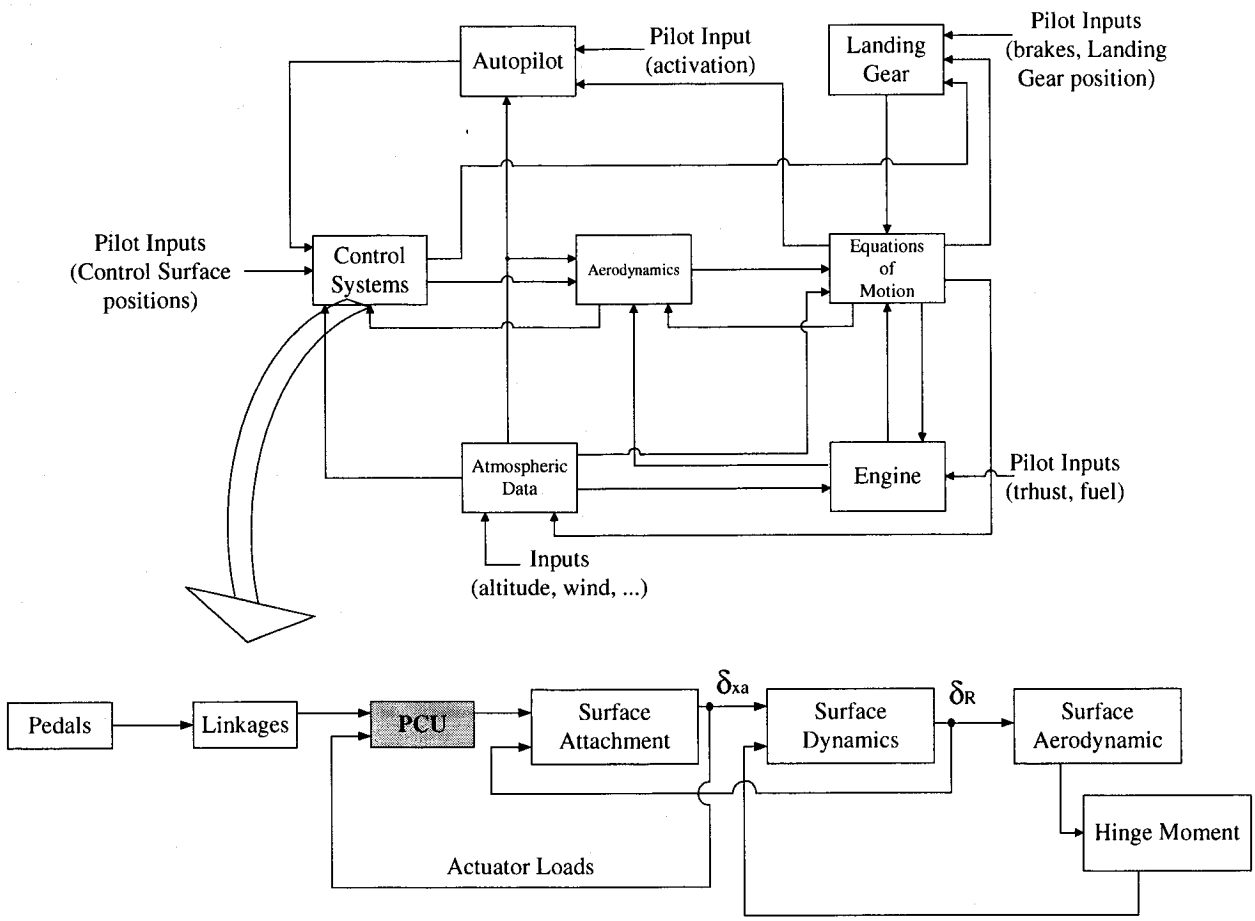

Figure 3.36: Aircraft Model Architecture

The integrated model can predict the behavior of the aircraft in flight or on ground for different configurations and different types of PCU failure in the rudder control system. The aircraft model must replicate the flight test with sufficient accuracy. For the present

study, the aerodynamic aircraft model is used as a research tool to investigate yaw kicks, with the objective to reduce the number of flight tests so as to reduce the cost of the investigation.

3.5.2 Integration of Flight Controls

The integration of the three detailed servoactuators in the flight model is necessary to see the impact of the fluid mechanics, friction and backlash on the rudder flight control system and hence on the aerodynamic behavior of the aircraft. First, the existing aircraft model is defined as a discrete system, whereas the three detailed PCUs and the rudder surface models were defined as a continuous system. Hybrid models (continuous and discrete systems) are supported by MATRIXx, but it is impossible "to trim" the aircraft. A trim condition includes both steady state and dynamic initial conditions. A simulation may be initialized with initial rates and accelerations. Trimming the aircraft to a certain state means to completely define the state values so that all equations are satisfied initially. Therefore, the simulation could start in arbitrary flight condition, and there is no need to bring the aircraft to this state. Trimming will therefore reduce considerably the simulation time, but the standard MATRIXx trim function only applies to a discrete system.

When converting a PCU continuous model into a discrete model, the compressibility of the fluid plays a major role. The bulk modulus is the stiffness of the system and is very high for this type of oil. Thus, the natural frequency of the PCU is high, and the response of the PCU is very fast. The different MATRIXx solvers are not able to capture this PCU

fast response and do not converge to acceptable trimmed values. MATRIXx provides its own integrator blocks, however, they seem inefficient in this case because the user cannot have access to the internal logic. New integrators were developped and "limiter blocks" were reshaped (replaced by splines) to avoid or reduce the effect of the discontinuities. The detailed PCUs model was able to run at 10,000 Hz with a 300 Hz flight model. The signal input is in discrete, therefore using the Z-transform of the signal, the new integrators will have the following logic as shown in Figure 3.37:

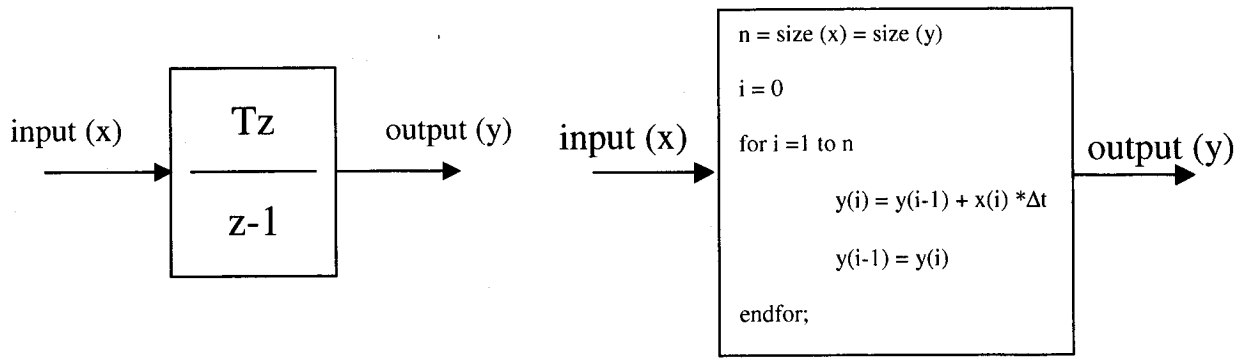

Figure 3.37: Integrator Block

For the limiter blocks, the discontinuity when for example the control valve reaches the stops is reshaped as shown in Figure 3.38.

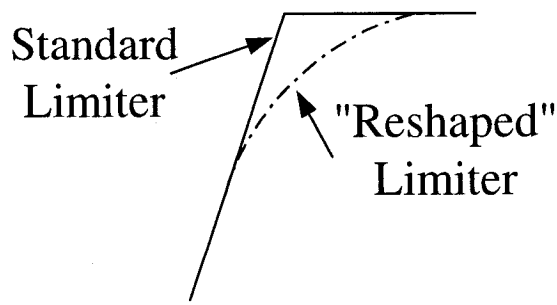

Figure 3.38: Limiter Block

CHAPTER 4

SIMULATION RESULTS

In this chapter, the analysis of the PCU model will be compared to the available test results. The static and dynamic stiffnesses of the PCU model will be performed to complete the validation of the PCU model. Then, the yaw kick will be investigated. The objective is to verify if the PCU may be the root cause of the yaw kicks. Therefore, the PCU hydraulic components or characteristics that may be the source of these non-linearities will be studied. The internal leakage through the control valve will be varied to see their effects on the PCU performance. The three PCUs will be attached to the rudder control surface, and force fight of the three servoactuators will be analyzed.

4.1 PCU Model Architecture and MATRIXx Implementation

MATRIXx allows users to define superblocks and blocks [33]. Each superblock corresponds to one part of the system or has the function to calculate parameters such as pressures in the piston chambers or flow rates passing through the control valve. Figure 4.1 presents the model of three servoactuators attached to the rudder surface. In Appendix C, all the block diagrams of the model are collected. The input to the servoactuator is a commanded position. For this model, the dynamics of the spool valve was not taken into account as previously stated in section 3.3.4.2.

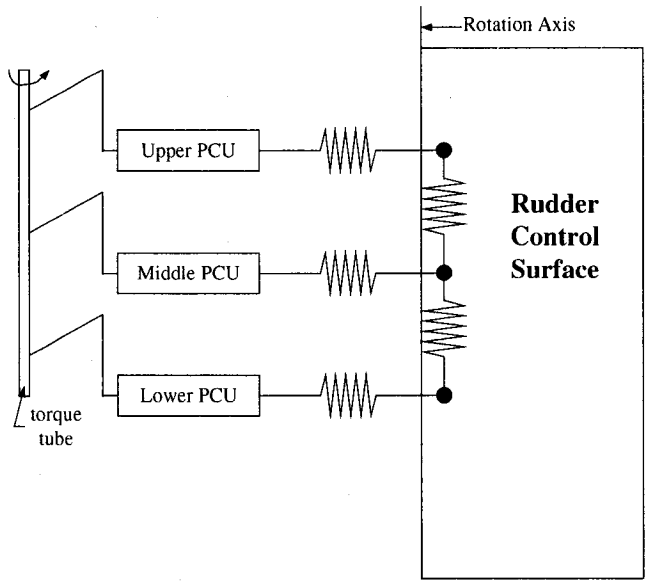

Figure 4.1: Model of three PCUs attached to the rudder surface

4.2 Acceptance Test Procedure

An acceptance test procedure (ATP) is clearly defined by the PCU supplier and Bombardier Aerospace to check the validity of the components. Before being installed in the aircraft, each servo-actuator has to be tested by the manufacturer on a test bench and show compliance with the ATP tolerances. Therefore, the first step in this investigation of the yaw activity was to compare the ATP results for the aircraft that experienced yaw kicks and for aircraft that did not in order to collect clues about what can generate the yaw kicks. Table 4.1 presents some results of this investigation.

Aircraft that experienced yaw kicks

	(a)	(b)	(c)	(d)	(e)	(f)	(g)	(h)
PCU Number	**Output Stroke – Retract [in]**	**Output Stroke - Extend [in]**	**Static Leakage, 300 psig, Extend [cc/min]**	**Static Leakage, 300 psig, Retract [cc/min]**	**Static Leakage, 300 psig, Neutral [cc/min]**	**Piston Velocity - Extend [in/sec]**	**Piston Velocity - Retract [in/sec]**	**Input Lever Force - Retract [lbs]**
1	1.164	1.164	8	12	13	2.7	2.72	2.25
2	1.164	1.165	17	11	10	2.68	2.68	2
3	1.165	1.163	26	10	14	2.73	2.76	2
4	1.163	1.164	17	10	12	2.83	2.95	2.25

Aircraft that did not experience yaw kicks

PCU Number	**Output Stroke - Retract [in]**	**Output Stroke - Extend [in]**	**Static Leakage, 300 psig, Extend [cc/min]**	**Static Leakage, 300 psig, Retract [cc/min]**	**Static Leakage, 300 psig, Neutral [cc/min]**	**Piston Velocity - Extend [in/sec]**	**Piston Velocity - Retract [in/sec]**	**Input Lever Force - Retract [lbs]**
5	1.162	1.16	25	2	3.5	2.94	2.92	2.3
6	1.161	1.16	9	6.5	2.5	2.75	2.87	2.25
7	1.162	1.16	15	2.5	5	2.78	2.91	2.2

Tolerances

record	record	**90 max**	**200 max**	**95 max**	**range: 2.3 to 3.0**	**range: 2.3 to 3.0**	**2.5 max**

Table 4.1: ATP results

Column (a) of Table 4.1 presents the output stroke test when retracting. This test measures and records the output stroke from null to full retract using the input lever of the servo-actuator. This is the same test, but in the opposite direction for column (b). Columns (c), (d) and (e) present the static leakage of the servo-actuator for different positions of the input lever (retract, neutral and retract). Columns (f) and (g) present the piston velocity when extending and retracting the input lever up to the PCU rate stops. Column (h) presents the input lever force required to drive the actuator to full retract from the full extend position.

From Table 4.1, it is very difficult to compare the PCU characteristics and to conclude on these results. Moreover, the calculated values for each PCU are within the specified tolerances of the manufacturer. However, the servo-actuator for aircraft that experienced yaw kicks have more leakage than the aircraft that did not experienced the phenomenon. The only conclusions that can be made from the ATP tests are, considering also the tolerances of the manufacturer:

- the acceptance test procedure tests are not appropriate to track the yaw activity

or

- the problem of yaw oscillations does not come from the PCU by itself.

However, the internal leakage of the servo-actuator has to be investigated to see its effect on the servo-actuator performance.

The characteristics of a PCU vary when a load is applied on it. The tolerances given by the supplier and Bombardier Aerospace can be too large which may overshadow the supposed PCU problem, or they do not cover other characteristics and behavior. Or the PCU itself may not be the problem, and only the arrangement of the three servomechanisms may introduce some discrepancies into the flight control system such as PCU force fight. The force fight will be addressed in the section 4.8.

4.3. Single PCU at no load

The simulation results were compared to the design data and ATP test data. The latter are limited data but are the only available ones for all the PCUs. Only a few important parameters have to be verified to match the static behavior of the servoactuator such as

position and rate of the rudder surface and the position and rate of the PCU actuator. The pressures in the chambers guarantee a good PCU model; a model error will generate a huge pressure discrepancy with test data.

To stay consistent with the ATP results, the simulation of the PCU model was done at no load. Figure 4.2 presents the simulation results of a unit step position input of the differential lever (Xi). The step position input starts at one second. The actuator position reaches the commanded position and when attained, the control valve closes. The rate of the actuator is about 2.75 inch per second, and this value corresponds to the one measured during acceptance test (refer to Table 4.1).

Figure 4.3 presents the pressure time response in the hydraulic cylinder chambers. As soon as the control valve closes, the pressures in the PCU chambers become equal, and no more hydraulic force is generated. The PCU actuator motion stops. The rated flow rate for a no load case is 0.691 in^3/sec (Figure 4.4). The model predicts the same value as the supplier data (Bombardier data are not included in this thesis).

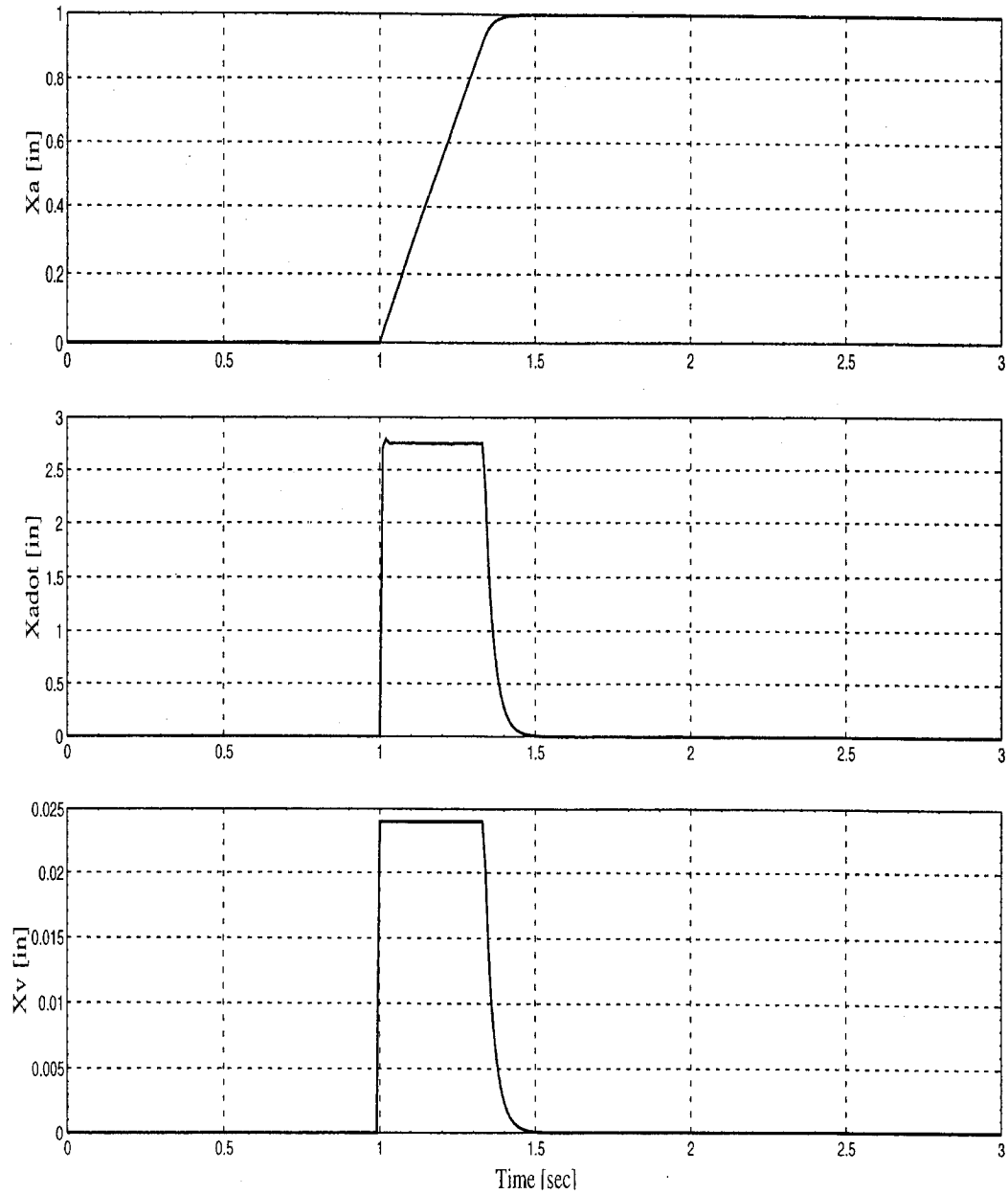

Figure 4.2: Simulated PCU response for a PCU unit step input (continued)

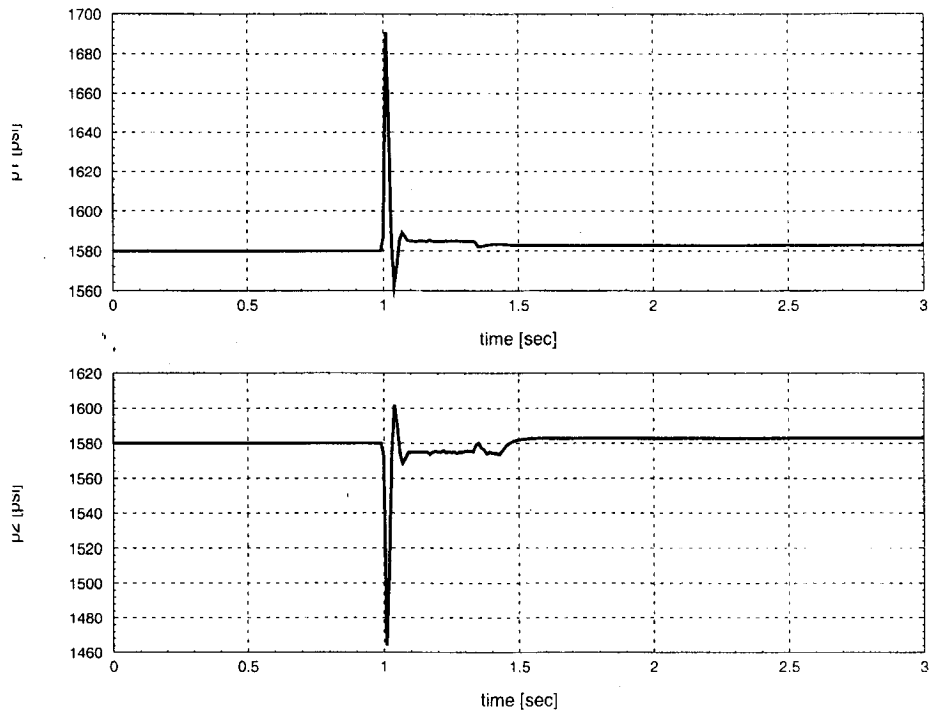

Figure 4.3: Simulated PCU response for a PCU unit step input

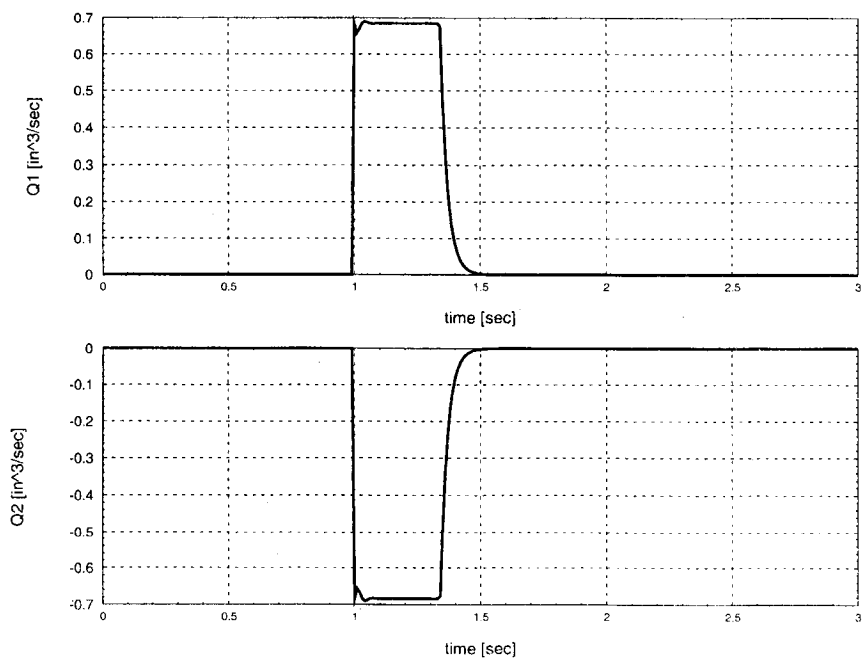

Figure 4.4: Simulated PCU response for a PCU unit step input (continued)

4.4 Static Stiffness Analyses

This section is necessary to verify the stability of the PCU model. The qualification test report written for the rudder system certification by the authorities and the ATP are the only sources of test data for the validation of the PCU model. The static stiffness analyses must be performed to comply with the authority requirements.

When designing a power control unit, two basic performance requirements must be complied with [52]:

1) The surface must be actuated in a stable manner

2) The PCU has to be stiff enough to meet flutter resistance requirements.

These two requirements are unfortunately not always compatible. Compliance with the first requirement tends to lower either the actuator static stiffness, or even the structural stiffness. However, to satisfy the second requirement, the actuator and the structural stiffnesses must be high. The next section presents the modifications of the detailed PCU model that were made to the previous model to perform static analysis when the rigidity of the PCU is taken into account.

The mathematical equations of the PCU system described in Chapter 3 must be slightly modified for dynamic analysis to include the attachment of the PCU to the aircraft structure. As previously stated, the attachment of the servo-actuator on the aircraft structure was considered as rigid. Therefore, to perform dynamic analysis, the position of the servo-actuator relative to the aircraft structure has to be taken into account (refer to Figure 4.5).

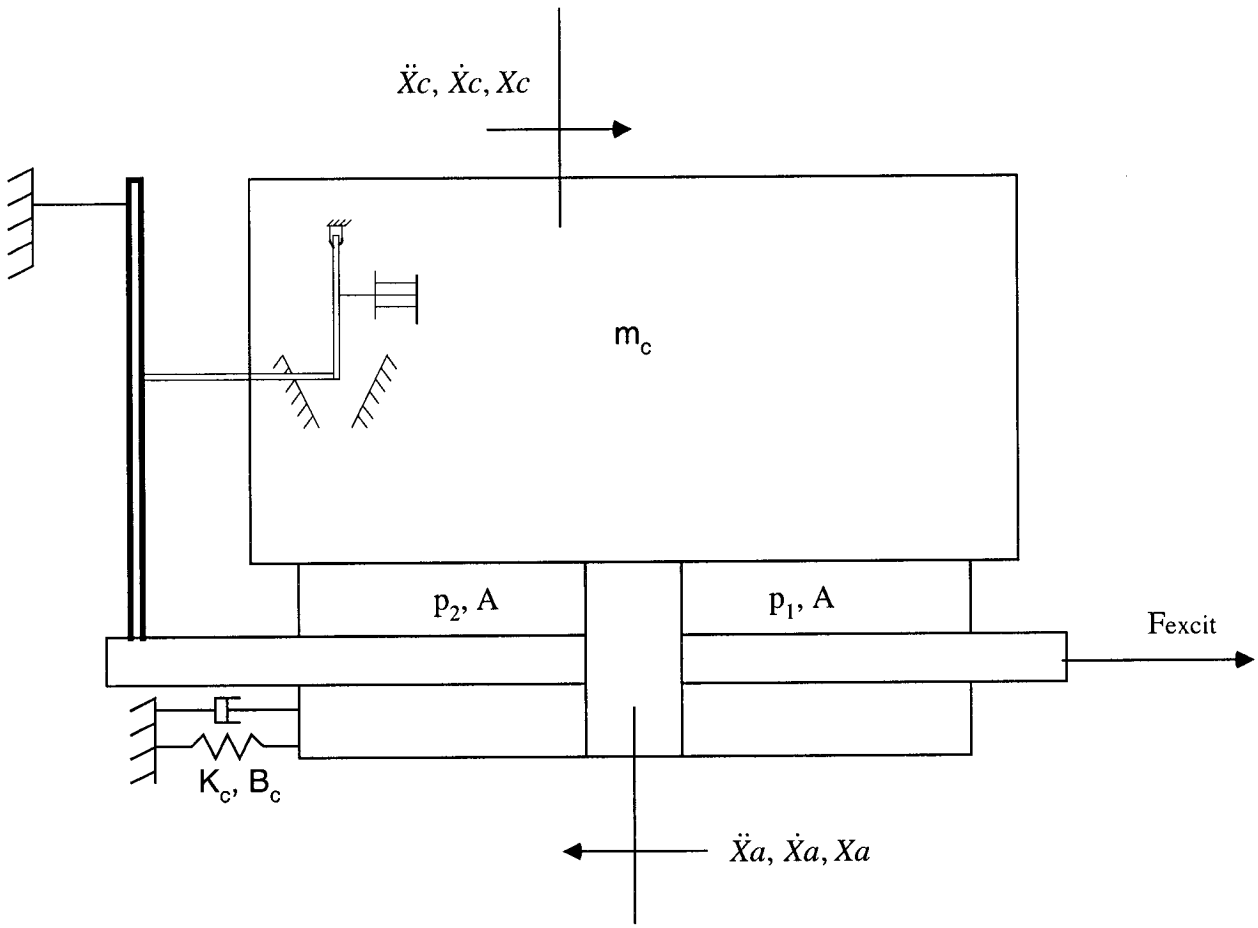

Figure 4.5: PCU Model Considering Casing Displacement

The following is the new set of dynamic equations for the PCU system:

The control valve position equation is the following:

$$X_v = \frac{1}{c} \cdot \frac{d}{e} \cdot f \cdot \left(\frac{b}{a+b} \cdot X_i - \frac{a}{a+b} \cdot X_a + X_c \right) \tag{4.1}$$

where X_c represents the motion of the servoactuator casing relative to the aircraft structure, and is given by:

$$(p_1 - p_2) \cdot A - B_c \cdot \dot{X}_c - K_c \cdot X_c = m_c \cdot \ddot{X}_c \tag{4.2}$$

The piston equation of motion is the same as equation 3.45:

$$(p_1 - p_2)\cdot A - F_{excit} - F_{friction} = M_p \cdot \ddot{X}_a \tag{4.3}$$

As shown in Figure 4.6 for a second order system:

$$m^*\cdot\ddot{X} + B^*\cdot\dot{X} + K^*\cdot X = F^* \tag{4.4}$$

where m* is the mass, K* is the stiffness of the spring, B* is the damping, and F* is the external forces. The equation can be re-written such that the natural frequency and damping term can be extracted:

$$\ddot{X} + \frac{B^*}{m^*}\cdot\dot{X} + \frac{K^*}{m^*}\cdot X = \frac{F^*}{m^*} \tag{4.5}$$

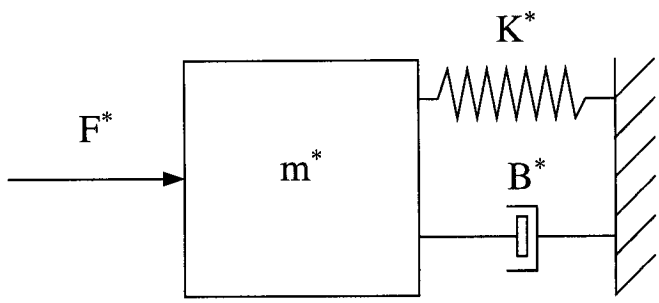

Figure 4.6: Typical Second Order System

The natural frequency of the system is therefore:

$$\omega_n = \sqrt{\frac{K^*}{m^*}} \tag{4.6}$$

and the damping term is:

$$2\zeta\omega_n = \frac{B^*}{m^*} \tag{4.7}$$

Therefore, equation 4.5 can be written as:

$$\ddot{X} + 2\zeta\omega_n\cdot\dot{X} + \omega_n^2\cdot X = \frac{F^*}{m^*} \tag{4.8}$$

Applying the definition of the natural frequency and the damping term of a second order system to the equation 4.2, the backup structural damping of the casing is defined as:

$$B_c = 2 \cdot \xi \cdot \sqrt{K_c \cdot m_c} \tag{4.9}$$

F_{excit} is the excitation force (input force) used to generate a vibrating behavior of the control surface. For the test, the PCU is installed on a rig and a device with a motor is connected to the differential lever to generate the oscillatory force input. The internal PCU hydraulic circuit does not change, therefore the flow equations stay the same as developed in Chapter 3.

The actuator chamber pressures are computed from the net flow rate to the actuator chambers accounting for fluid compressibility, as well as a function of the relative piston position to the casing position, given as (refer to Figure 4.7):

$$\dot{p}_1 = \frac{\beta_{f1}}{V_{O1} + A \cdot (x_a + x_c)} \cdot [Q_1 - A \cdot (\dot{x}_a + \dot{x}_c)] \tag{4.10}$$

$$\dot{p}_2 = \frac{\beta_{f2}}{V_{O1} - A \cdot (x_a + x_c)} \cdot [Q_2 + A \cdot (\dot{x}_a + \dot{x}c)] \tag{4.11}$$

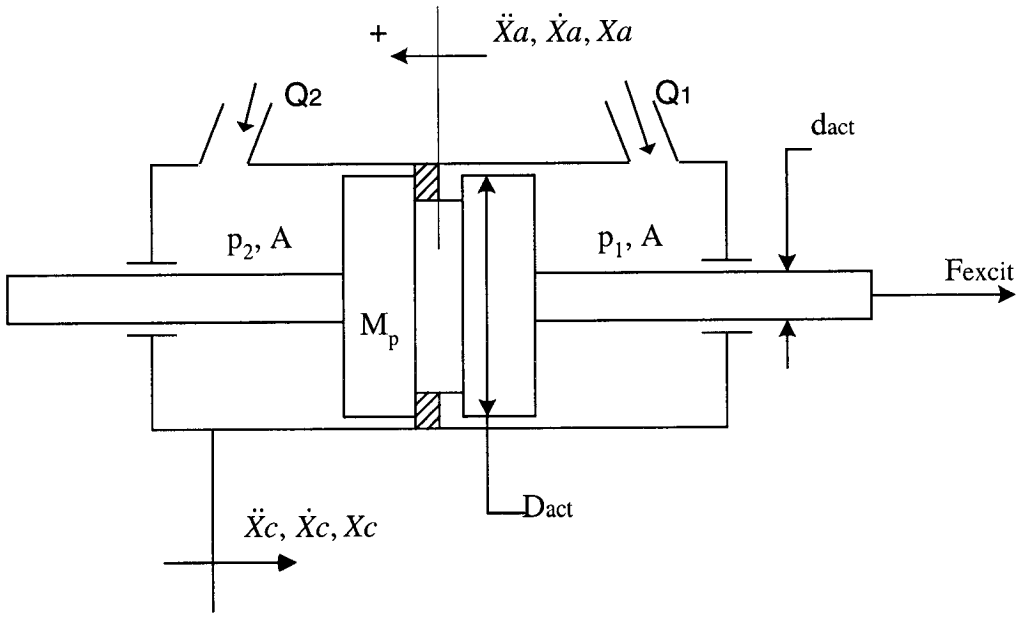

Figure 4.7: PCU Motion Equations Considering Casing Displacement

These equations lead to a model that is used to evaluate the effective PCU stiffness at various frequencies, since the stiffness of the power control unit is frequency dependent. For low frequencies, below say 3 Hz, there is a static stiffness regime. The static stiffness is the ability of the PCU actuator to maintain a force applied on it with a small displacement of the actuator. The static stiffness is a function of the effective area of the piston, the feedback ratio and the pressure gain. Therefore, the static stiffness is influenced by the internal leakage of the control valve when the control valve is at its neutral position [52]. It has to be noted also that the compressibility of the fluid does not significantly affect the stiffness at low frequency.

With the model, a force F_{excit} is applied on the actuator rod and no input command is given to the PCU (Xi = 0). The applied force (F_{excit}) divided by the displacement of the actuator (X_a) is the static stiffness of the PCU. This test is performed to evaluate the

ability of the PCU to withstand large loads. As shown in Figure 4.8, the more internal leakage the PCU has, the less is its ability to absorb large loads.

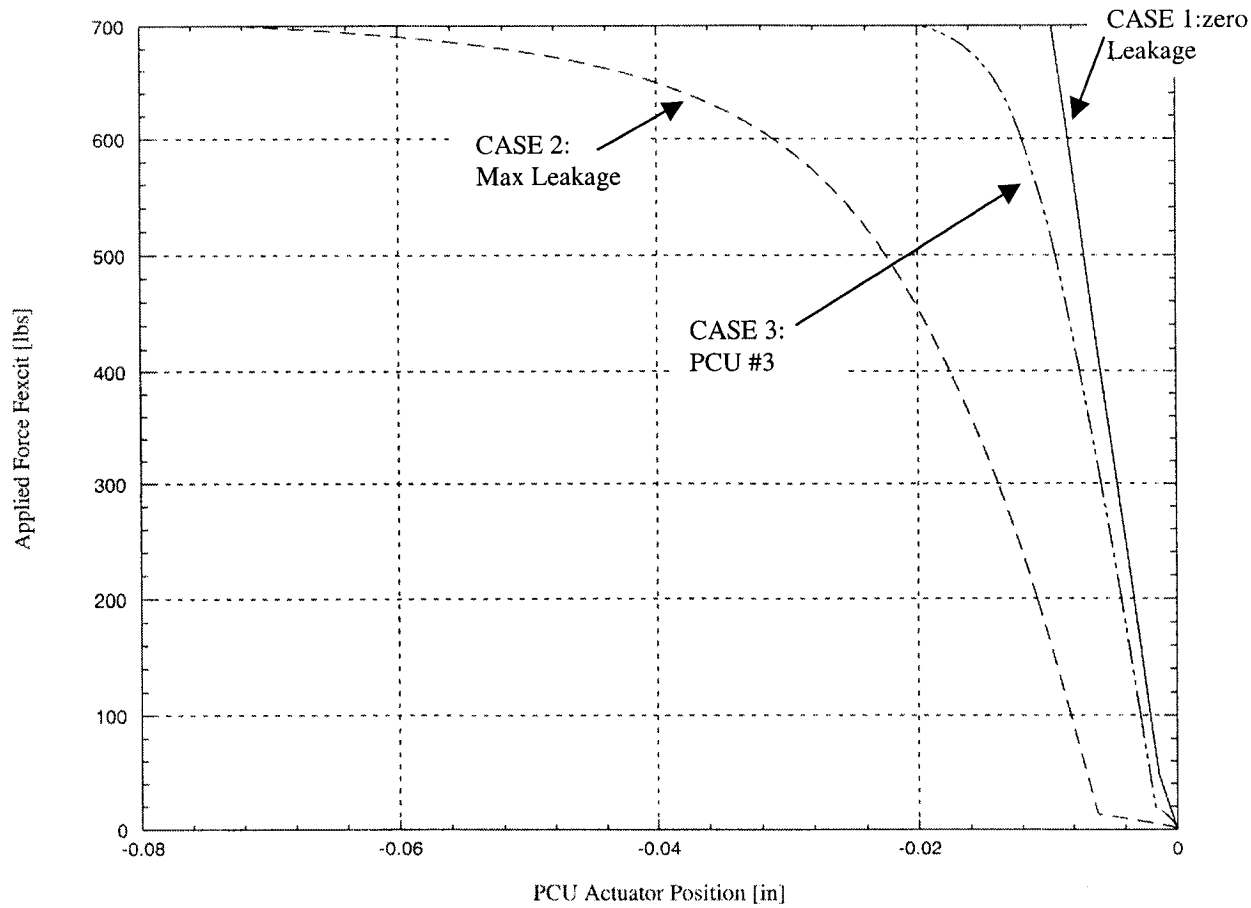

Figure 4.8 : Simulation Static Stiffness Results

Figure 4.8 shows the simulation results for the static stiffness of the PCU actuator when applying a force in tension. The force F_{excit} is ramped until it reaches the PCU actuator stall force. The stall force is the maximum force the actuator can generate (i.e. the actuator effective area times the maximum differential pressure across the actuator). Three conditions were simulated. Case 1 represents the case where there is no internal leakage in the servovalve. Case 2 is the maximum permissible internal leakage through

the control valve condition, and case 3 is the PCU # 3 from Table 4 (PCU that experienced yaw kicks). The internal leakages in the servovalve are introduced in the model by a lookup table as a function of the control valve position [42]. The stiffness for PCU #3 is about 40,000 lb/in, which is consistent with the data provided by the supplier (30,000 to 50,000 lb/in). Therefore the PCU static stiffness varies with the internal leakage of the servovalve. The internal leakage affects directly the pressure gain of the PCU actuator. Therefore, when designing the servovalve, the internal leakage has to be as low as possible. However, an overlapped valve is not desirable either, because overlapped valve creates deadband and backlash in a hydro-mechanical system. This is the reason why the servovalve of the PCU is the most difficult part to manufacture.

From Figure 4.8, the closer the applied force is to the stall force, the more the static stiffness starts to decrease. Above the stall force of the actuator, the excitation force will be able to backdrive the PCU actuator, and the performance of the PCU will be affected. The stiffness (K_{oil}) due to the oil compressibility in the actuator chambers and the structural backup stiffness (K_c) define the static stiffness. The stiffness of the cylinder, the piston and the bearings are much higher than the stiffnesses K_c and K_{oil}, therefore were not considered in the model. The spring rate of the actuator oil column is defined as [52]:

$$K_{oil} = \frac{4 \cdot A^2 \cdot \beta}{V} \tag{4.12}$$

where V is the volume is one of the actuator chambers.

4.5 Internal Leakages

From reference [42], theoretically and experimentally the internal leakage flow rate in the control valve decreases when moving the spool valve; this is illustrated in Figure 4.8. From the ATP test results, the behavior of the internal leakage flow rate increases as the spool valve is moved out of the zero position. Internal leakage usually damps the system more than excites it; therefore they may not be the cause of the yaw oscillations.

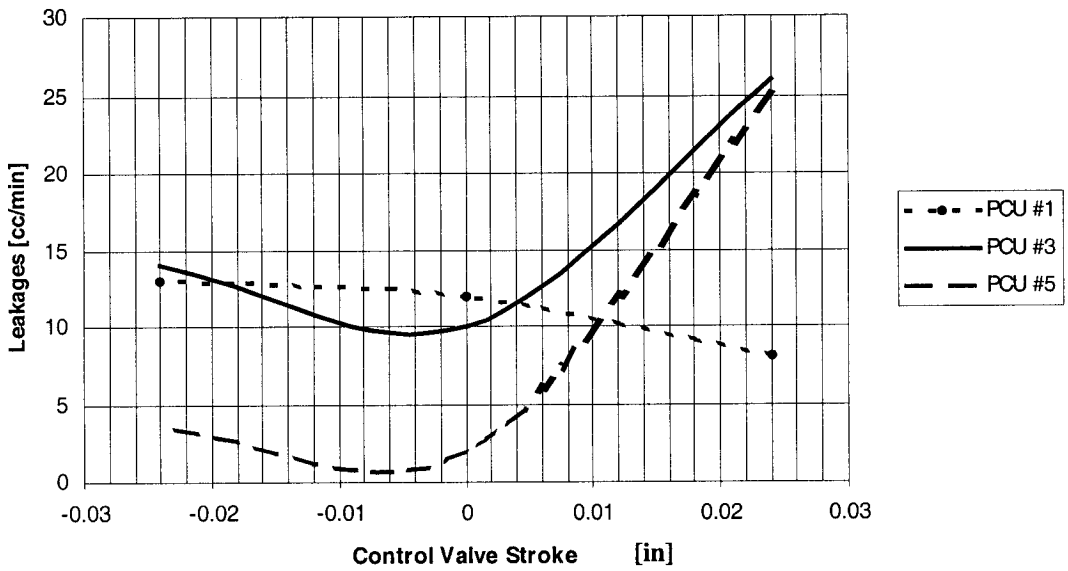

Figure 4.8: Leakages Experimental Results

From Figure 4.8, ATP tests give only three points to describe the internal leakage curve. However, the resulting curves are different from the expected behavior of leakage flow (refer to Figure 3.19). The hydraulic overlap of the servo-valve is greater than expected because, when the valve is at neutral, the internal leakage is not maximum. By trying to

manufacture a critically lapped valve (the one expected), because of tolerances, the actual final product maybe a small overlapped value.

Dynamic simulation of the PCU system was performed for two cases: with servo-valve leakage (maximum permissible leakage) and without leakage. Figure 4.9 presents the simulation results of the internal leakage investigation at no load. A displacement step input was commanded to the servo-actuator. The solid line refers to the PCU without internal leakage and the dotted-line refers to the PCU model with maximum permissible internal leakage. As shown in Figure 4.9b-c, the response of the actuator is faster when there is no leakages. At no load, the maximum difference in velocity is 0.2 in/sec. After moving, the control valve does not return to its original position as shown in Figure 4.9a. Due to internal leakage, the equilibrium point of the PCU actuator and control valve has changed.

In flight, aerodynamic loads are applied on the PCU actuator. Therefore, a force was applied to the actuator and the same investigation was performed. The purpose of this simulation is to see if the characteristics of internal leakage seen from the previous simulation with no load are the same as when the actuator is loaded. Figure 4.10 presents the simulation results for one single PCU with and without internal leakage, and a constant force of 150 lbs (about 20% of maximum load) applied on the actuator. The force direction is the opposite of the PCU actuator displacement. As illustrated in the Figure 4.10b-c, when applying a constant load on the actuator, the internal leakage slows down the response of the servo-actuator. As shown in Figure 4.10a, the control valve

position, in the case of maximum internal leakage, has an offset generated by the small movement of the actuator position. The control valve position is the error of the position input and the actuator position (refer to section 3.3.4.1).

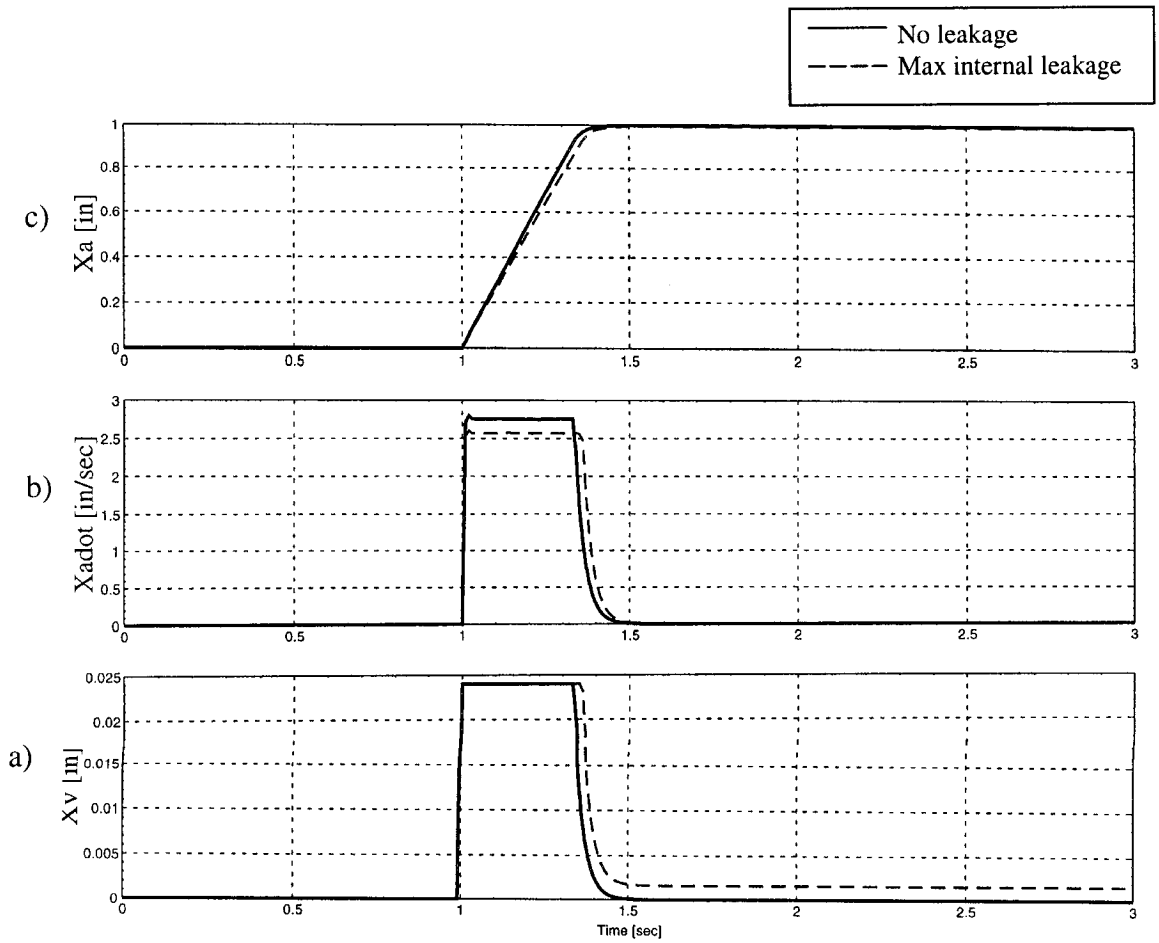

Figure 4.9: Simulation results of PCU at No Load; With and Without Internal Leakage

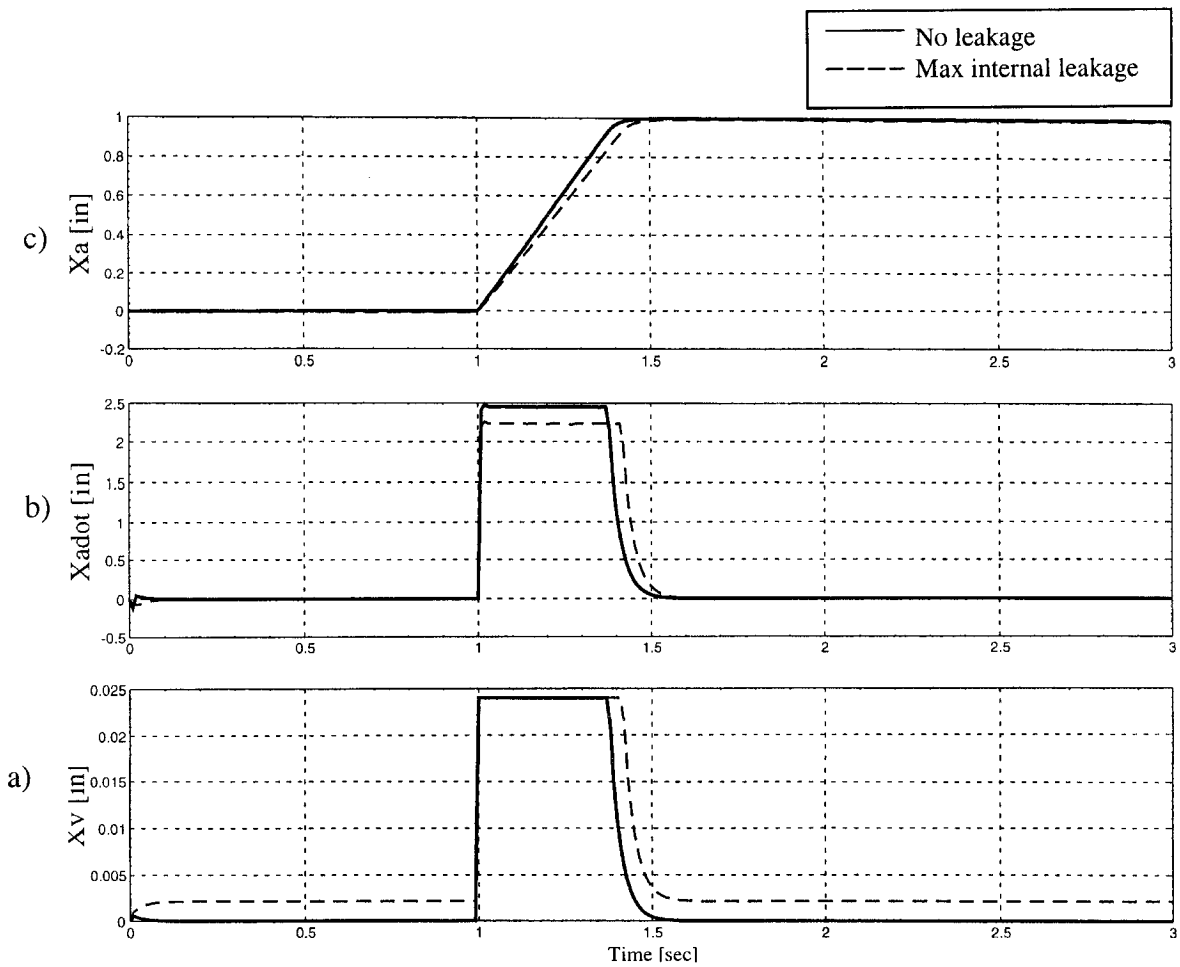

Figure 4.10: Simulation Results of PCU with Constant Load; With and Without Internal Leakage

4.6 Pressure Relief Valve Investigation

The objective of this analysis is to understand the effect of the pressure relief valve in the system. However, there is no record that shows a problem with the pressure relief valves during the apparition of yaw kicks.

Figures 4.11 to 4.13 show the effect of the pressure relief valves on one PCU for different loading conditions. Figure 4.11 shows the actuator position and rate for a no load condition. With the failed pressure relief valve #1 and a command input of 1 inch, the response of the PCU actuator is slower. In fact, most of the flow coming from the servovalve goes through the relief valve and reduce the amount of flow in chamber 1. Figure 4.12 shows the case where 20 percent of the stall force is applied, and the force goes against the piston motion. Figure 4.13 shows the opposite case where the 20 percent of the stall force (143.1 lbs) assists the actuator to reach the commanded position. In each case, the actuator rate is reduced because of the failed pressure relief valve. For the case with the opposing force acting on the PCU: since the pressure relief valve has failed and stayed wide open, the stiffness of the oil inside the actuator chamber is affected, and the actuator moves slightly as shown in Figure 4.12.

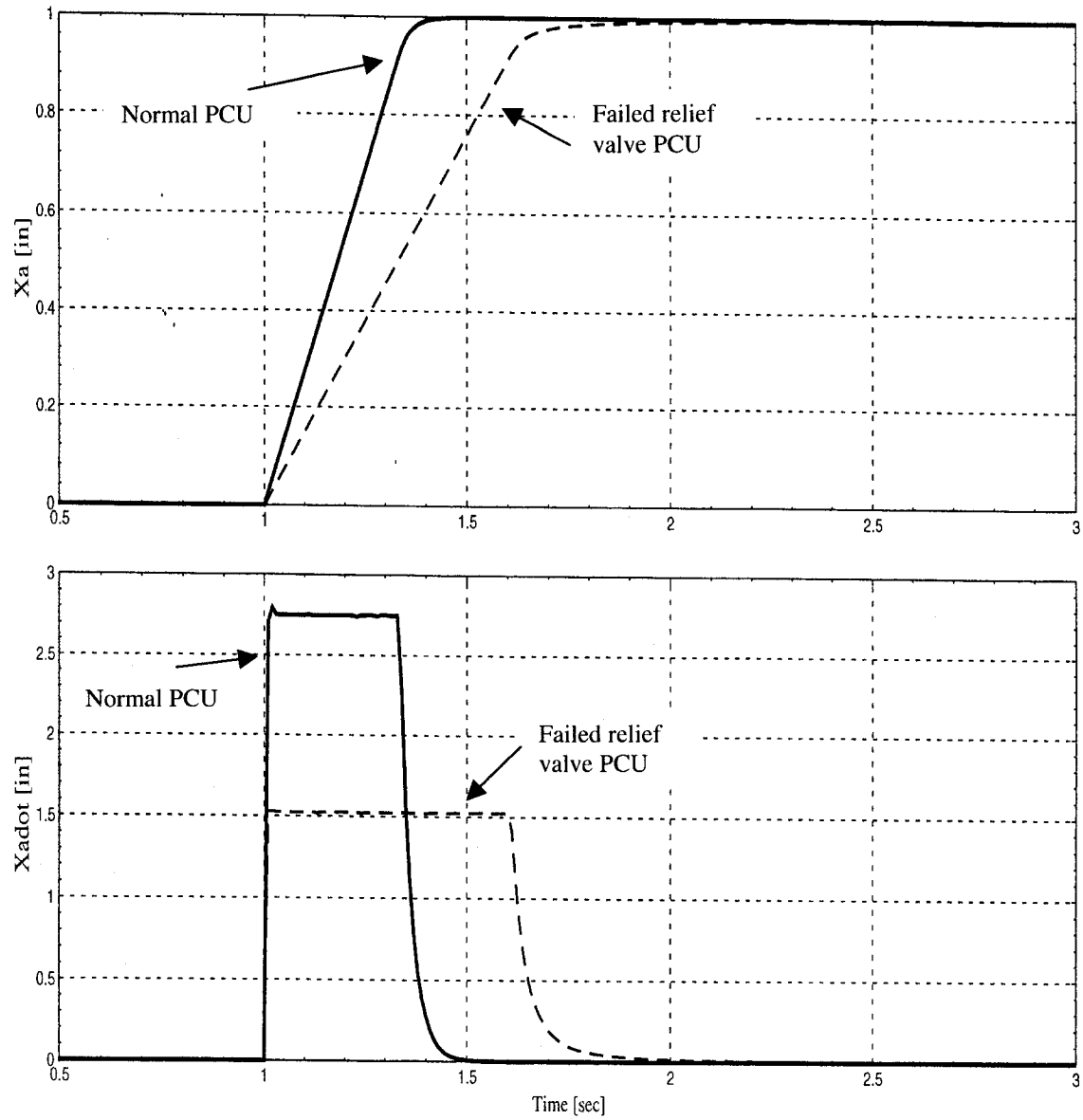

Figure 4.11: Failed Pressure Relief Valve #1 at no Load

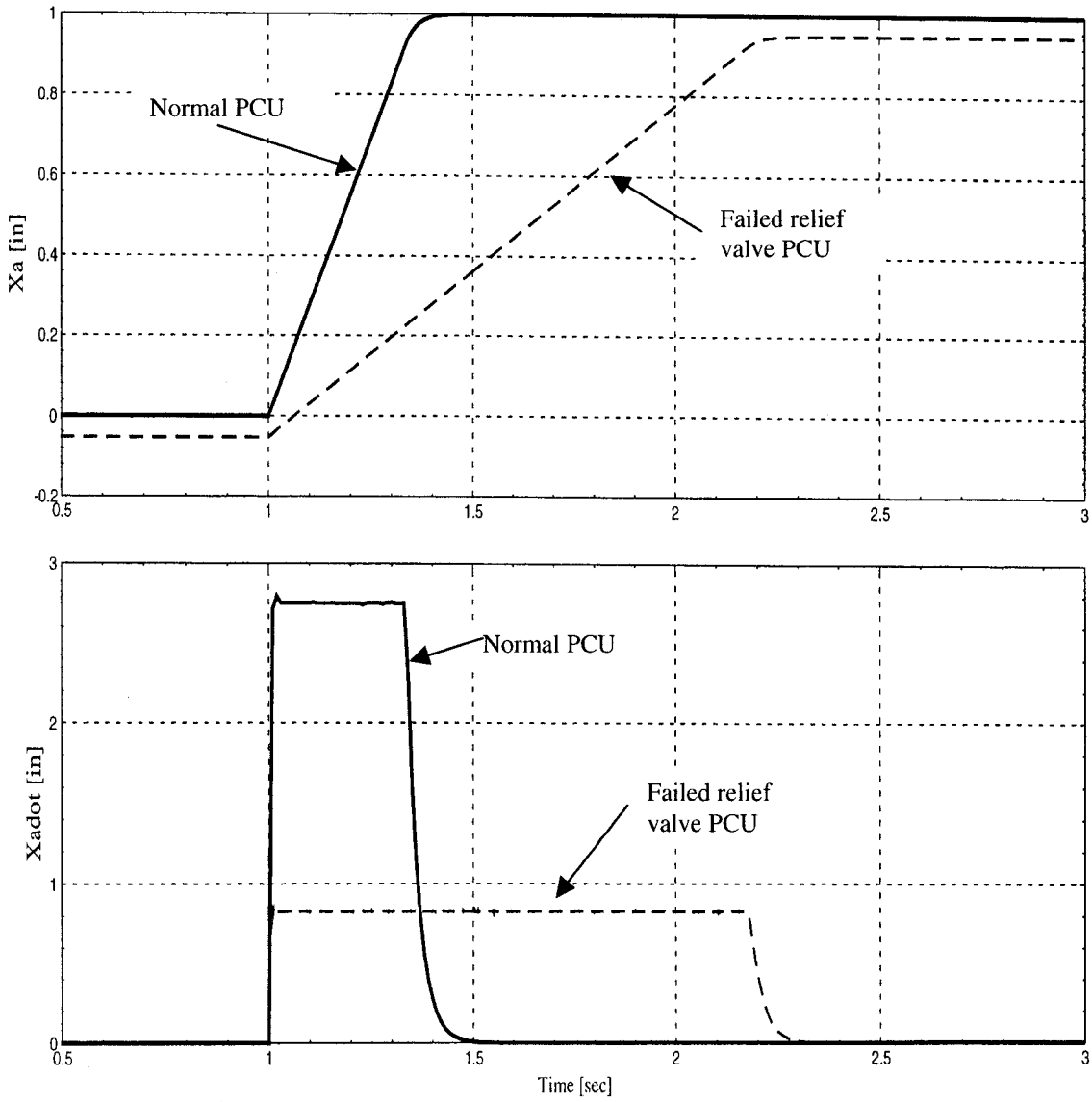

Figure 4.12: Failed Pressure Relief Valve #1 with Opposing Force

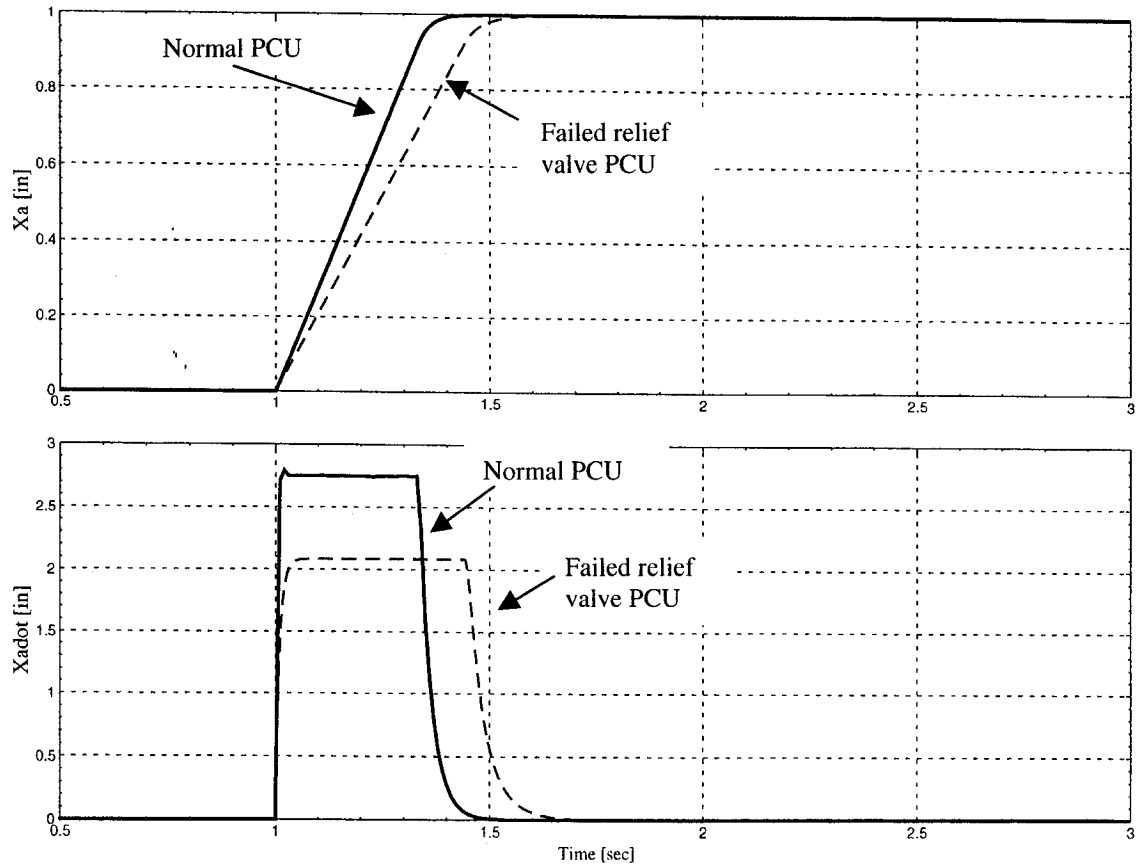

Figure 4.13: Failed Pressure Relief Valve #1 with Helping Force

The case where there are three PCUs attached to the rudder, and one pressure relief valve of one PCU failed open was also analyzed. As shown in Figure 4.14, the pressure relief valve #1 of the upper PCU failed and stayed open. A step load (500 lb.in) is applied on the rudder control surface, to see the effect of the failed pressure relief valve on the other PCUs when there is no pilot command (i.e. $X_i = 0$). As discussed in Chapter 1, the environmental conditions of the apparition of yaw kicks are: altitude of 20,000 feet and aircraft airspeed of 275 knots. At these conditions, the hinge moment is about 500 lb.in (this value was extracted from a BA flight test memo [53]).

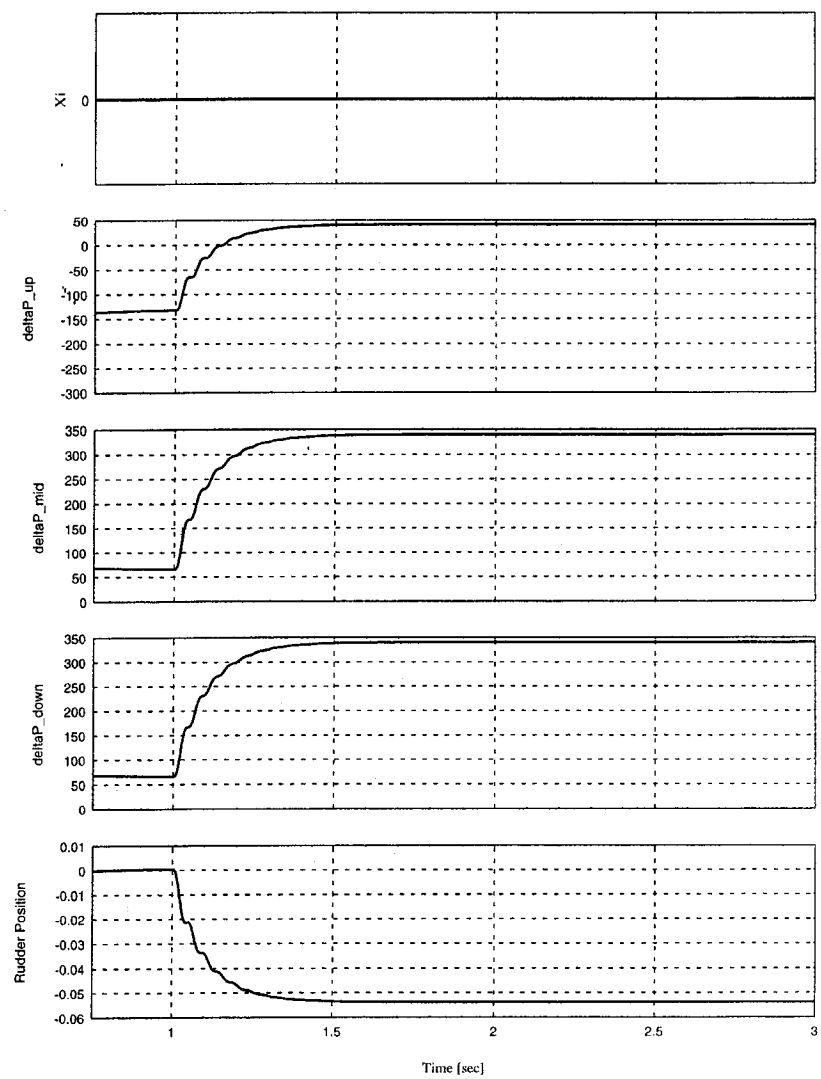

Figure 4.14: Failed Pressure Relief Valve #1 – PCUs & Rudder Assembly

The delta_P_up label corresponds to the differential pressure (psi) of the upper PCU. The same nomenclature is used for the middle and lower PCUs (refer to Figure 4.14).

The maximum deflection the rudder control surface is 0.06 degrees. The pressure deltas were plotted versus time for the upper, middle and lower PCUs to provide an understanding of the load sharing amongst the three PCUs. The upper PCU lost its stiffness, and the two other PCUs are able to maintain the rudder centered. Therefore, a failure of one pressure relief valve in one of the PCU will not affect the rudder control system performance.

The performance of the three servoactuators attached to the rudder control surface has to be investigated, and then the force fight between the PCUs.

4.7 Three PCUs – Rudder Assembly

Figures 4.15 and 4.16 present the simulation results for the actuator position and rate when one, two or three actuators are attached to the rudder control surface, and are commanded to a step input position of one inch travel. The response of the actuator is fastest when three PCUs actuate the rudder control surface, since the torque at the hinge line required to move the rudder control surface is shared by all three PCUs. This analysis is assuming that the PCU do have the same performance. If they do not, each will command a different position to the rudder and they will start to "force fight".

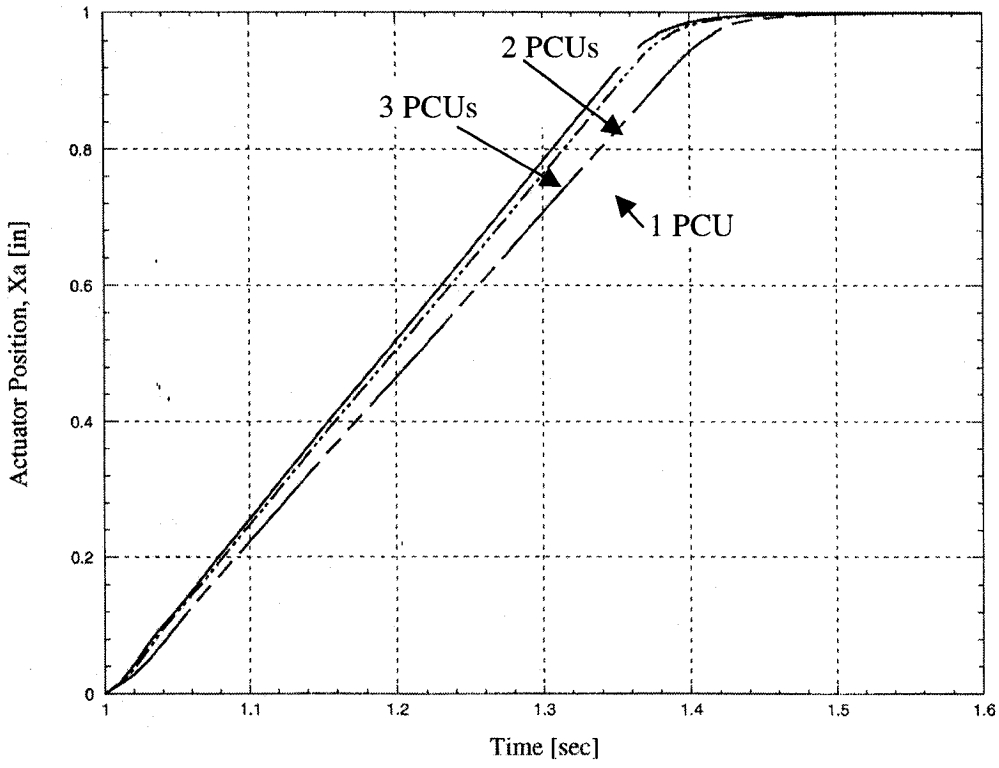

Figure 4.15: Actuator(s) Position Response to a Step Position Command at no Load

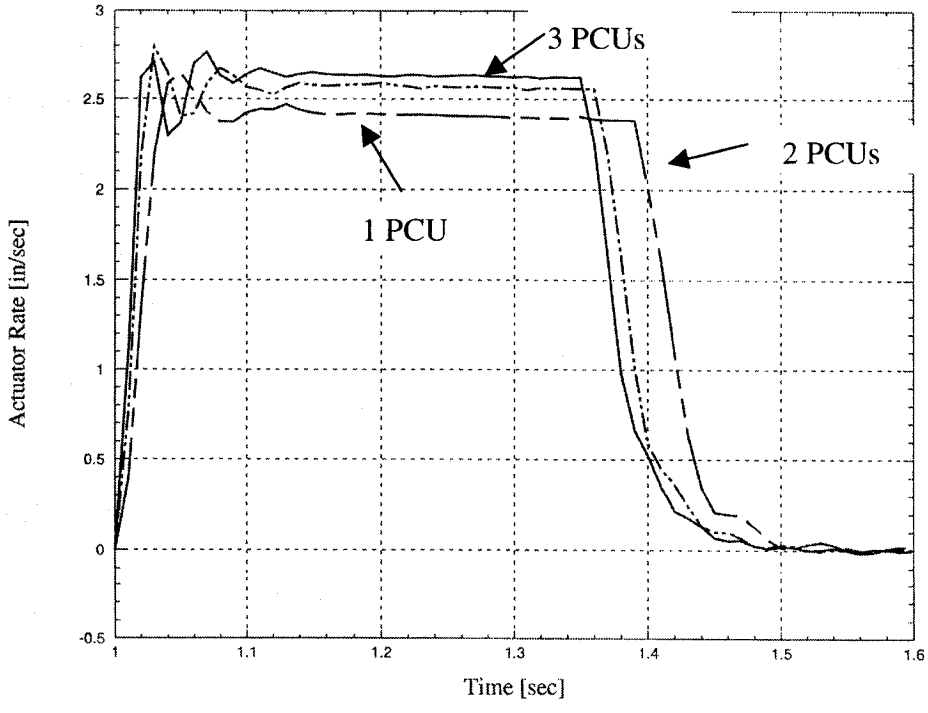

Figure 4.16: Actuator(s) Rate at no Load

4.8 PCU Force Fight

The force fight between PCUs is verified during the functional test of the aircraft prior to flight (+/- 0.25 degrees of rudder is tolerated). As previously stated, the PCUs are hydraulically independent, therefore the force fight test consists of switching on the three hydraulic systems one after the other, and then verify the maximum deflection difference of the rudder. This section presents the analysis done with the three PCUs and rudder system model to evaluate the amount of rudder deflection when yaw kicks appear.

Figure 4.17 presents the simulation of force fight between the three PCUs. The torsional stiffnesses between the PCUs were also taken into account and combined to the attachment stiffnesses (refer to Figure 3.33). With aerodynamic loads being applied on the rudder surface, the PCUs were commanded to slightly different positions (variation of positions within Bombardier tolerances (0.01 inch at neutral for the upper PCU and 0.005 in for the lower PCU)). The two PCUs, at the extreme ends of the hinge axis, are fighting and the other one is following the commanded position without producing a large force (compared to the others). The conditions are the same as when yaw kicks appear during a flight (the altitude is 20,000 feet and the airspeed is 275 knots). At these conditions, the hinge moment is about 500 lb.in. Force fight appears because of the forces generated by the PCUs. The sum of PCU forces and the applied hinge moment applied on the rudder surface is equal to zero at static equilibrium. At steady state, the force fight is between the three PCUs with more load applied on the upper PCU (more deadband). The aerodynamic loads are distributed amongst the three PCUs until steady state. The force

fight between the PCUs is a force balance with the aerodynamic loads applied on the rudder control surface panel. The rudder reaches its commanded position without any kicks.

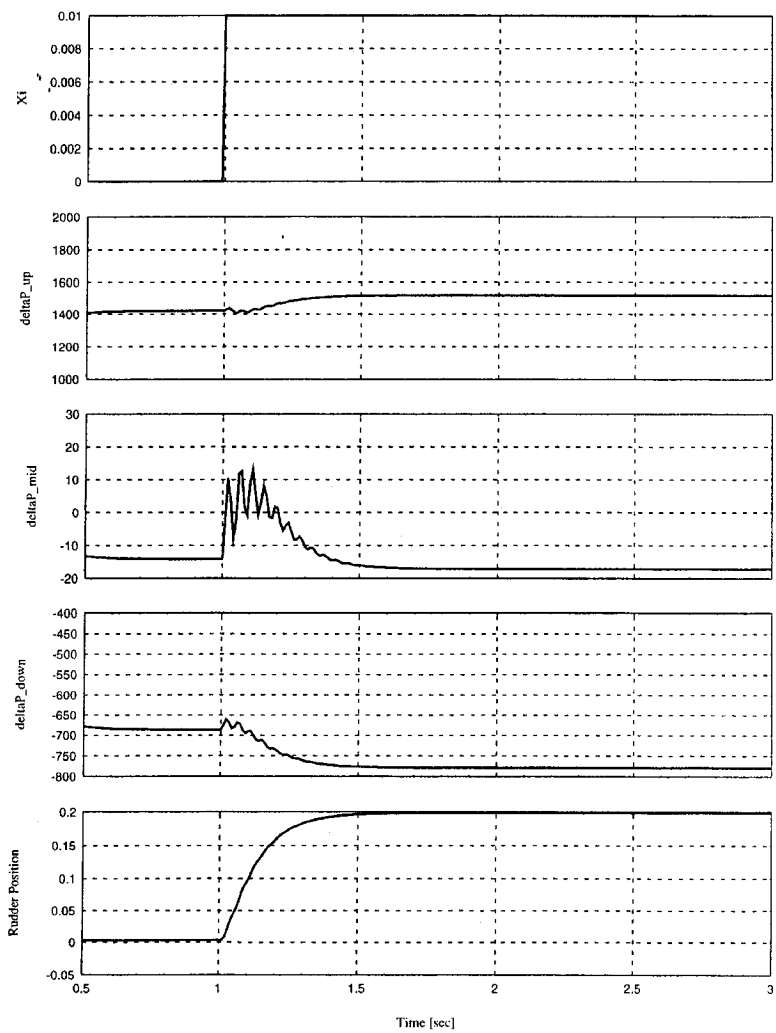

Figure 4.17: PCU Force Fight Analysis

CHAPTER 5

CONCLUSION

5.1 Conclusion

The objectives of this thesis were twofold. One goal was to produce a computerized model of the power control unit that is compliant with Bombardier Aerospace standards, while still presenting all the features necessary to pursue the main goal of this thesis, that is to find the root cause to the yaw kick phenomenon. The simulation PCU model was also integrated to the Bombardier flight model to adequately simulate the yaw kick phenomenon.

The steps leading to the development of the model were presented in Chapter 3, and the results of the analyses are presented in Chapter 4. Development involved the detailed modeling in MATRIXx of a power control unit and it appears to be a success. Lessons learned gained by Concordia were transferred to Bombardier Aerospace, and the expertise of Bombardier Aerospace was a great help in the analysis phase of the lateral phenomenon and the simulation results. This model is now part of the Bombardier Systems Simulation Group's library of models, ready to be used as a tool for evaluating future design changes, or to investigate possible failure cases of the hydro-mechanical system. This work therefore perfectly fulfills the requirements of the first objective.

The second objective was then to carefully investigate the possible causes of the yaw shudders or "kicks". The yaw kick was investigated to see the parameters that may induced the phenomenon such as hydraulic system component failure (relief valve opening during a phase of flight), PCU internal leakage, overlapped valve (deadband) and friction during motion of the actuators. Then, the yaw kick phenomenon was reproduced by simulation using the flight model. A step of 0.5 degrees displacement of the rudder control surface reproduced the same aircraft characteristics as seen on the flight tests. The servo-actuator was the main possible cause of the phenomenon as explained in Chapter 1. Analysis of the flight model shows the need to include a detailed model of the servo-actuators. The flight model did not include the compressibility of the fluid, the hysteresis generated by the overlapped valve, and the rudder panel attachment stiffness.

Limited experimental data was available, therefore the validation of the model was limited. However, validation against theoretical values from the supplier was successful. Different components of the servo-actuator were modeled at different complexities. The pressure relief valves were modeled in detail because the opening and the closure of this valve created non-linearities in the hydraulic system. However, it was shown that the servo-actuator has a fast response that reduces the assumptions of a large pressure surge in the cylinder chambers. The performance of a PCU with a pressure relief valve that failed and stayed open was evaluated through simulation. The rate of the actuator slows down because of this type of failure. Moreover, the test with three PCUs attached to the rudder with one failed pressure relief valve shows that two PCUs are able to maintain the rudder control surface relatively centered.

The control valve was modelled as a simple valve, but theoretical equations were written for the next phase of the project. The next phase of the project should contain test data to make sure all the components are validated accordingly such as a detailed control valve. For this analysis, a simple valve was enough since the bandwidth of the control valve is well beyond that of the actuator.

The internal leakage of the PCUs were the only noticeable difference between PCUs that experienced yaw kicks and those that did not in the ATP tests. However, simulation results show that the internal leakage have a tendency to slow down the actuator rather than exciting it.

The static stiffness was also simulated to reproduce the theoretical values produced by the supplier. The internal leakage has a pronounced effect on the static stiffness of the PCU. The more the leakage, the less stiff is the system, therefore the servo-valve should be well manufactured to provide the expected performance of the servo-valve.

The suspected components of the servo-actuator were investigated to lead to the analysis of the "force fight" between the servo-actuators that could have produced yaw kicks. The rudder - PCUs assembly was analyzed to see how the servo-actuators react when they do not have the same performance. The "force fight" was performed using the manufacturing acceptable tolerances between the PCU and the rudder. The pressure

differentials in the cylinder chambers did not generate enough displacement of the rudder control surface to generate a yaw kick as seen in the Chapter 1.

The second objective was also a success, since at the beginning of the project, the assumed culprit was the PCU assembly. This analysis permits to understand the behavior of the servo-actuator assembly, then to validate its performance against flight test data. Various cases were investigated to lead to the conclusion that the PCU does not generate yaw kicks by itself, therefore the mechanical system from the rudder pedals to the PCU input torque tube had to be investigated in detail. A parallel work from Concordia University demonstrates that under certain conditions (combination of backlash and friction), the system can self-initiate a rudder deflection of the order of magnitude expected. The contribution to the rudder deflection of the PCU assembly non-linearities is negligible compared to the complete flight control system non-linearities [7].

5.2 Future Work

The first step of the future work is to develop an appropriate flight test procedure to validate the simulation findings. Flight testing should be performed to gather enough experimental data to validate the tests performed with the simulation model. In parallel two ways should be taken. First, the mechanical system before the servo-actuators, consisting of backlash and friction in the joints between the mechanical components should be modeled and analyzed [7]. A detailed mechanical model should be created, and sensitivity analysis has to be performed to see the effects of each component of the mechanical system. Another aspect that the next project should consider is the

temperature effect on the different parts of the rudder control system. This task can be handled successfully only if experimental data is available.

Another approach is to analyze the yaw dampers. Even if it seems to have no effect on the yaw kick, the logic of the yaw dampers should be understood and modeled. One major assumption of this project was that the yaw dampers were turned off during the apparition of yaw kicks, however yaw dampers have a passive mode that could generate oscillations or kicks along the vertical axis of the airplane. The flight test should be well defined to make sure that it covers all the components of the rudder control system.

REFERENCES

1 ISO 2631-4: Mechanical vibration and shock – evaluation of human exposure to whole-body vibration – Part 2: Guidelines for the evaluation of the effects of vibration and rotational motion on passenger and crew comfort of fixed guide-way transport systems, International Standards Organization, 1997

2 Thibaudeau J., "A proposal for Yaw Activity Production Specification", Bombardier Flight Operations, Montreal, January 2000

3 ISO 2631-1: Mechanical vibration and shock – Evaluation of human exposure to whole-body vibration – Part 1: General Requirements 2nd Edition, International Standards Organization, 1997

4 Harris C.M., "Shock and Vibration Handbook", 3rd Ed., McGraw-Hill, New York, USA, 1988, pp.44_20-44_58

5 ISO 2631-2: Mechanical vibration and shock – Evaluation of human exposure to whole-body vibration – Part 2: Vibration in buildings (1 to 80 Hz), International Standards Organization, 1997

6 ISO 6897-1984: Guidelines for the evaluation of the response of occupants of fixed structures, especially buildings and off-shore structures to low frequency horizontal motion (0.063 to 1 Hz), International Standards Organization, 1984

7 Ulysse N., "Investigation of Aircraft Yaw Motion Control", M.A.Sc. Thesis, Concordia University, Montreal, August 2003

8 http://pespmc1.vub.ac.be/ASC/Limit_cycle.html

9 Ananthkrishnan N., Sudhakar K, "Characterization of Periodic Motions in Aircraft Lateral Dynamics", Journal of Guidance, Control and dynamics (0731-5090), Vol. 19, no. 3, May-June 1996, pp. 680-685

10 Kooi S.B.L, Svoboda J., "Dynamic Recurrent Neural Networks for Stable Adaptive Control of Wing-Rock Motion", IFAC Symposium on Automatic Control in Aerospace, 14th, Seoul, Korea, August 1998

11 Arena A.S., "An Experimental and Computational Investigation of Slender Wings Undergoing Wing Rock", Ph.D. Dissertation, Department of Aerospace and Mechanical Engineering, Notre Dame, April 1992

12 Hsu C.H., Lan C.E., "Theory of Wing-Rock", Journal of Aircraft, vol. 12, no 19, Oct. 1985, pp. 920-941

13 Morris S.L., Ward D.T., "A Video-Based Experimental Investigation of Wing-Rock", IN: AIAA Atmospheric Flight Mechanics Conference, Boston, MA, Aug. 14-16, 1989, Technical Papers (A89-49051 21-01). Washington, DC, American Institute of Aeronautics and Astronautics, 1989, pp. 25-35

14 Levin D., Katz J., "Self-Induced Roll Oscillations of Low Aspect-Ratio Rectangular Wings", IN: AIAA Atmospheric Flight Mechanics Conference, Portland, OR, Aug. 20-22, 1990, Technical Papers (A90-45134 20-08). Washington, DC, American Institute of Aeronautics and Astronautics, 1990, pp. 165-172

15 Gao N., Wang Z.J., and Zhang S.G., "A Study of Wing-Rock", IN: ICAS, Congress, 17th, Stockholm, Sweden, Sept. 9-14, 1990, Proceedings. Vol 2 (A91-

24301 09-01). Washington, DC, American Institute of Aeronautics and Astronautics, 1990, pp. 1984-1989

16 Ericsson L.E., "Slender Wing-Rock Revisited", AIAA, Aerospace Sciences Meeting, 29th, Reno, NV, Jan. 7-10, 1991

17 Suarez C.J., Kramer B.R., and Ong L.Y, "Forebody Vortex Control for Wing-Rock Suppression", Journal of Aircraft (0021-8669), vol. 31, no. 2, Mar.-Apr. 1994, pp. 298-305

18 Ericsson L.E., Mendenhall M.R., "On Forebody-Induced Wing-Rock", AIAA, Aerospace Sciences Meeting & Exhibit, 32nd, Reno, NV, Jan. 10-13, 1994.

19 Dietz P., "Coordination MEMO ECM-604-BA/CU-AERO-001", Coordination Memo from Bombardier Flight Science Group to Concordia University, 26 of July 2002, pp.4

20 http://history.nasa.gov/SP-367/appendc.htm

21 Pallett E. H., Coyle S., "Automatic Flight Control", 4th Edition, Blackwell Scientific Publications, Cambridge, MA, 1993, p.39

22 Shevell R. S., "Fundamentals of Flight", 2nd Edition, Prentice Hall, Englewoods Cliffs, N.J., 1989, pp. 54-57

23 Dommasch D. O., Sherby S. S., and T. F. Connolly, "Airplane Aerodynamics", 4th Edition, Pitman Publishing Corporation, New York, 1967, pp 65-66

24 http://www.glenbrook.k12.il.us/gbssci/phys/Class/newtlaws/u2l3a.html

25 Asselin M., "An Introduction to Aircraft Performance", American Institute of Aeronautics and Astronautics, Inc, Reston, VA, 1997, pp.141-143

26 Nelson R. C., "Flight Stability and Automatic Control", 2nd Edition, McGraw-Hill, New York, 1998, p.78

27 Roskam J., "Airplane Flight Dynamics and Automatic Flight Controls, Part I", Roskam Aviation and Research Corporation, 1994, p. 21

28 Pallett E. H., Coyle S, "Automatic Flight Control", 4th Edition, Blackwell Scientific Publications, Cambridge, MA, 1993, p.31

29 Raymond E. T., Chenoweth C., "Aircraft Flight Control Actuation System Design", Society of Automotive Engineers, 1993, p. 43

30 Bombardier Aerospace, "Challenger Maintenance Training Manual", 1995, p 11

31 Raymond E. T., Chenoweth C., "Aircraft Flight Control Actuation System Design", Society of Automotive Engineers, 1993, pp. 27-30

32 Shevell R. S., "Fundamentals of Flight", 2nd Edition, Prentice Hall, Englewoods Cliffs, N.J., 1989, pp. 177-178

33 Raymond E. T., Chenoweth C., "Aircraft Flight Control Actuation System Design", Society of Automotive Engineers, 1993, pp 9-53

34 http://www.ni.com/support/matrixsupp.htm

35 Raymond E. T., Chenoweth C., "Aircraft Flight Control Actuation System Design", Society of Automotive Engineers, 1993, pp 243-249

36 Straub H. H., Creswell R., "The Boeing 747-400 Upper Rudder Control System with Triple Tandem Valve", pp. 31 – 40

37 Bombardier Aerospace, "Challenger PCU Maintenance Training Manual", 1980, p 13

38 Merritt H. E., "Hydraulic Control Systems", John Wiley & Sons, Inc., New York, 1967, pp. 101 - 118

39 Goodwin A.B., "Fluid Power Systems", Macmillan Press LTD, 1976, pp. 100-103

40 Merritt H. E., "Hydraulic Control Systems", John Wiley & Sons, Inc., New York, 1967, pp. 76-88

41 Keller G. R., "Hydraulic System Analysis", Hydraulics and Pneumatics Magazine, 2nd Edition, 1969, pp. 107-110

42 Merritt H. E., "Hydraulic Control Systems", John Wiley & Sons, Inc., New York, 1967, pp.89-91

43 Lee Company, Technical Hydraulic Handbook, "Section F: Pressure Relief Valves", Lee Company, 2000

44 Armstrong, B., Canudas de Vit, C., "Friction Modeling and Compensation", The Control Handbook, 1996, pp. 1369 - 1382

45 Canudas de Vit, C., Olsson, H., Aström, K.J., and Lischinsky, P., "A New Model for Control Systems With Friction", IEEE Trans. Autom. Control, in press, 1994

46 Dupont, P. E., "The Effect of Friction on the Forward Dynamics Problem", The International Journal of Robotics Research, vol. 12, No 2, April 1993

47 http://www-lag.ensieg.inpg.fr/canudas/

48 Merritt H. E., "Hydraulic Control Systems", John Wiley & Sons, Inc., New York, 1967, p 34

49 Lee Company, Technical Hydraulic Handbook, Lee Company, 2000, p. M-24

50 Shigley J.E., Uicker J.J., Jr, "Theory of Machines and Mechanisms", 2nd Edition, McGraw-Hill, New-York, 1995, pp. 476-480

51 Nelson R. C, "Flight Stability and Automatic Control", 2nd Edition, McGraw-Hill, New York, 1998, p.68

52 Raymond E. T., Chenoweth C., "Aircraft Flight Control Actuation System Design", Society of Automotive Engineers, 1993, pp.243-249

53 Bombardier Aerospace, "Rudder Hinge Moment Due to Sideslip and Rudder Deflection - Analysis of Flight Data", Oct. 1979, p.4